36
Human Eye

Handbook of Optical Systems: Vol. 4 Survey of Optical Instruments. Edited by Herbert Gross

ISBN: 978-3-527-40380-6

36.1 Introduction

This chapter deals with the optical system of the human eye and the correction of its defects by means of spectacles. Primarily, the optical properties of the eye will be discussed. This representation does not intend to go into the biological or medical details of the eye.

36.1.1 Basic Structure of the Eye

Figure 36-1 shows a picture of the human eye. From the optical point of view, the black central circle, which is the pupil area, and the structured iris diaphragm are the most interesting parts. From the reflected light it can be seen that the front surface of the cornea is smooth and glossy.

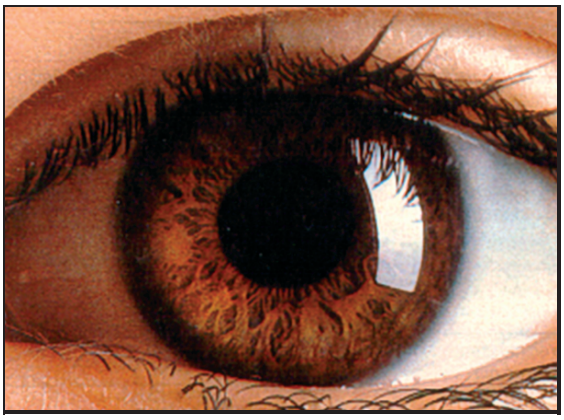

Figure 36-1: The human eye.

The shape of the eye approaches a spherical ball. Figure 36-2 gives details of its geometry. In figure 36-3 the geometrical lengths and sizes are indicated. The pure spherical ball model is of limited accuracy. The light enters the eye through the cornea, which is a layer 0.5 mm thick, and which has a refractive index of $n = 1.377$. Then passes through the anterior chamber, which has a lower index of refraction of approximately $n = 1.336$. The thickness of this aqueous front part is 3.04 mm and ends at the iris plane and the eye lens. The iris is a diaphragm of variable diameter, which controls the numerical aperture and the radiance entering the eye.

The lens is of a variable shape and changes its refractive power so that the eye can accommodate to an object a certain distance away. The lens is built from several nested shells. In a first approximation, only one optical medium is assumed, while more refined models distinguish a crystalline core lens and a surrounding lens cap-

sule. Behind the lens, the light passes through the vitreous humor and is received at the retina where the detection of light takes place.

The retina consists of different regions. It contains a central part, where the resolution is maximized, which is a small area called the fovea and which has a diameter of 1.8 mm. The fovea is not located centrally, around the geometrical axis of the eye, but usually lies 2.5 mm towards the human temple (temporal region). Another part of the spherically curved retina is the blind spot, which has a diameter of 1.8 mm or 5° equivalent and is located at a distance of 15° towards the nose (nasal region). In the blind spot, no light can be detected, because the nerve enters the eye in this region.

The eye-ball can be rotated inside its socket around the centre point C, which lies 13.5 mm behind the front vertex of the eye. Figure 36-4 shows the distribution of the refractive index within the eye. This is a simplified representation where the lens is divided into a crystalline lens and a lens capsule, and the refractive indices are considered as constant in each part.

The eye has a finite speed of response and image gathering. Fluctuating and oscillating fast signals above a time frequency of 30 Hz give the impression of a constant signal and are detected as one integrated signal.

Figure 36-4 shows the distribution of the refractive indices in the eye as a function of the axis coordinate z. It can be seen that a significant index difference occurs only at the anterior cornea surface. The differences around the eye lens are quite small and lie in the range $\Delta n = 0.08$.

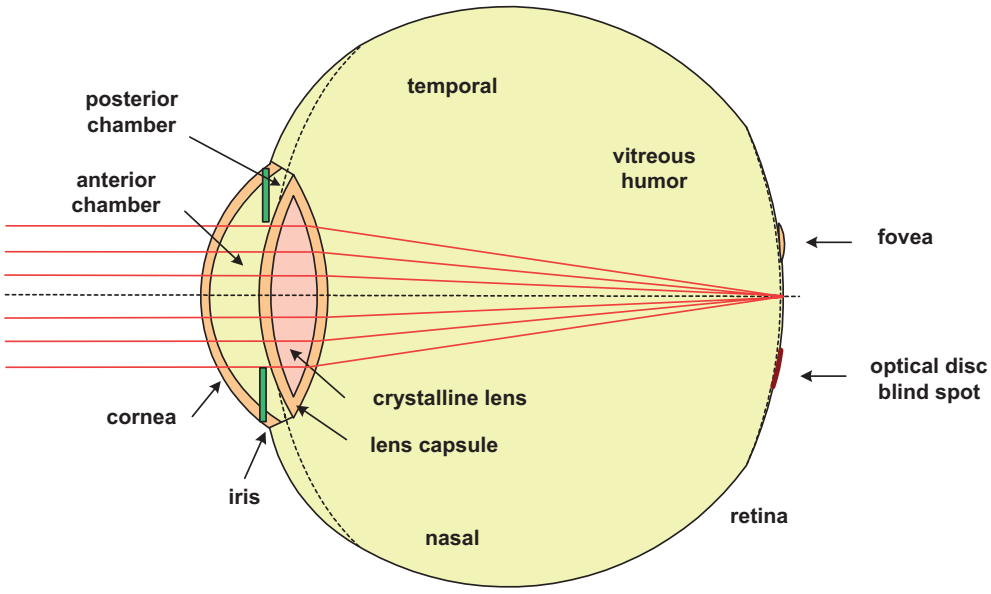

Figure 36-2: Details and geometry of the human eye.

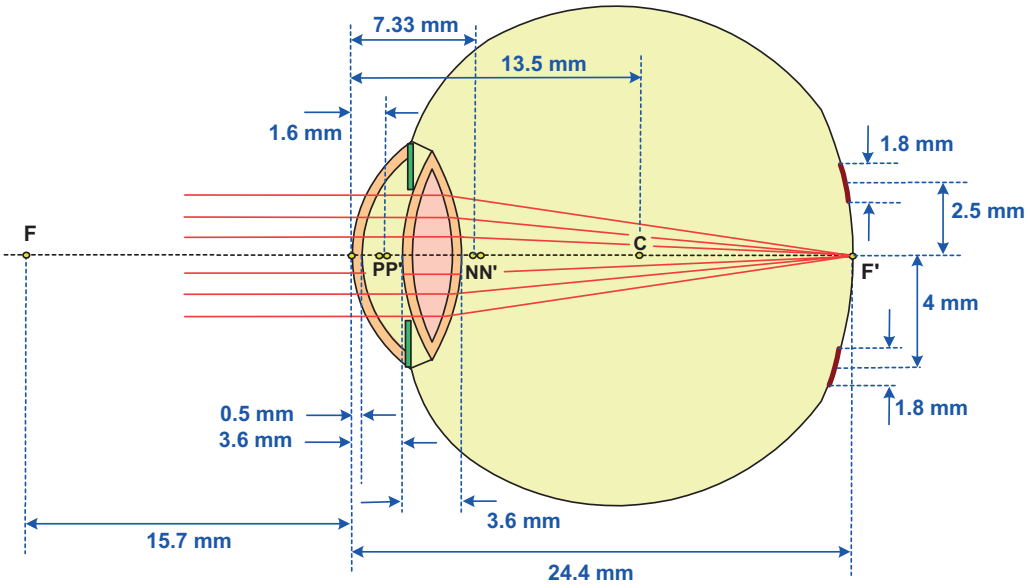

Figure 36-3: Dimensions and lengths of the human eye. N and N′ are the nodal points, P and P′ indicate the position of the principal planes.

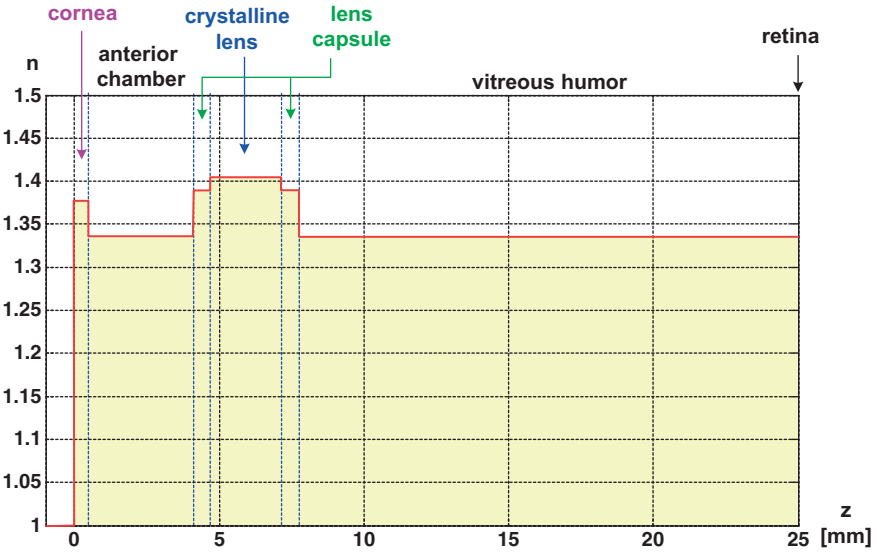

Figure 36-4: Simplified distribution of the development of the index of refraction in the eye.

36.1.2 Optical Data of the Eye

Table 36-1 contains the most important optical data of the human eye. A distinction is made between the relaxed eye, for objects at infinity, and the accommodated (or focused) status.

Table 36-1: Major optical parameters of the human eye.

Property	Relaxed	Accommodated
Refractive power	58.63 dpt	70.57 dpt
Focal length in air	17.1 mm	14.2 mm
Refractive power of the crystalline lens	19 dpt	33 dpt
Field of view – maximum	108°	
Field of view – fovea	5°	
Pupil diameter	2–8 mm	
F-number	6.8–2.4	
Diameter of the eye-ball	24 mm	
Distance of the front vertex from the rotation point C	13.5 mm	
Wavelength of largest sensitivity for photopic sight	555 nm	
Distance of the nodal point N from the front vertex	7.33 mm	
Distance of the principal plane P from the front vertex	1.6 mm	
Distance of the entrance pupil from the front vertex	3.0 mm	

In the optics of the eye, the refractive power is usually considered and is measured in diopters (1 dpt = 1/m).

Approximately 2/3 of the refractive power of the human eye is located in the front surface of the cornea, which has a difference in refractive index of 0.377 against air on the front side and approximately 1/3 of the crystalline lens, which has only a difference of 0.08 against the vitreous chamber and the vitreous humor. If the eye is put into water with $n = 1.33$, the relative refractive index of the cornea to the environmental medium is reduced by a factor of 7. Therefore, the image distance lies far from the retina position and only a rather fuzzy image can be seen. A fish has a crystalline lens, which has much more strongly curved surfaces; the lens geometry is in fact nearly spherical.

The cornea contributes the greater part of the refractive power to the optical system of the eye. It is aspherically shaped in the outer zone to reduce the spherical aberration for a larger pupil diameter. Sometimes the central part of the anterior

surface is conically shaped. If this topology is particularly marked, a keratoconus problem occurs. The exact shape of the cornea is built by the stroma, which has a microstructure. The size of the periodic detail is less than $\tilde{\omega}/2$ and this structure is therefore diffractive and has an anti-reflecting effect. This helps to reduce the generation of stray light in the eye.

The lens system inside the eye has a shell structure. It can be considered as a gradient lens with a structure formed from a finite number of shells. Corresponding models for the eye have been proposed in the literature [36-1], [36-2]. Figure 36-5 shows the measured distribution of the refractive index along the optical axis of the eye lens as a function of the location z. It can be seen that the value changes smoothly without steps. The gradient structure of the eye lens helps to avoid reflections of the incoming light inside the eye.

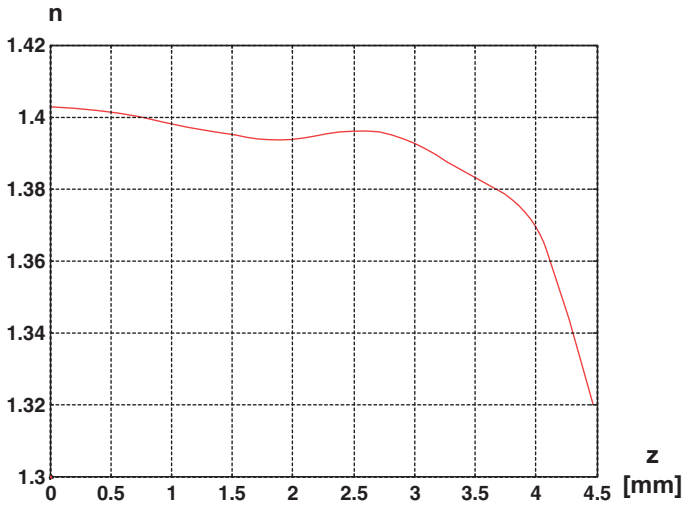

Figure 36-5: Distribution of the refractive index in the crystalline lens.

The depth of focus depends on the form of the caustic and is therefore strongly influenced by the diameter of the iris diaphragm. Typically, the depth of focus lies in the range 0.1 dpt to 0.5 dpt. The natural uncertainty of the focusing mechanism is in the region of 0.25 dpt.

The optical surfaces of the cornea enlarge the iris image for an outside observer by a factor of $m = 1.13$. The position of the iris diaphragm relative to the front vertex of the eye is $s = -3.04$ mm.

If optical instruments are adapted for the eye, it is necessary to match the diameter and location of the system pupil to the eye pupil. Otherwise, a reduced field of view results which gives a key-hole effect.

36.1.3 Neuronal Structure

The human retina serves as a light-detecting surface. There are different types of sensor elements within the retina and the underlying tissue, which is called the sclera. In the central part, the cones detect the light with high resolution and color sensitivity and, in the peripheral region, the rods detect the light for larger field sizes without color sensitivity and lower resolution, but with a higher sensitivity to brightness. Table 36-2 compares the major properties of these sensors.

Table 36-2: Comparison of the light sensors within the human eye.

Property	Cones	Rods
Location	in the fovea	outside the fovea
Covered field of view	small, 5°	large, 108°
Resolution and visual acuity	large	small
Brightness sensitivity	small, for daylight vision	large, for night vision
Color sensitivity	yes	no
Total number of elements	5 million	120 million
Limiting brightness	683 lm W^{-1}	1699 lm W^{-1}
Spectral sensitivity maximum	555 nm	507 nm

The distribution of the sensor elements in a cross-section through the retina is shown in figure 36-6 [36-3]. Table 36-3 shows some additional data for the fine structure of the retina.

Table 36-3: Data and regions of the retinal structure.

	Range	Diameter [mm]	Cones	Rods
Macula lutea	Foveola	0.35	number: 3500 density: 190000 mm^{-2} pitch: 2.3 µm	no rods
	Fovea	1.85	density: 100000 mm^{-2} pitch: 3.2 µm	a few rods
	Prafovea	2.85		
	Perifovea	5.85		density: 160000 mm^{-2} pitch: 2.5 µm
Periphery			density: 5000 mm^{-2} pitch: 14.0 µm	density: 50000 mm^{-2} pitch: 4.5 µm
Papille, blind spot	4 mm off-axis nasal	1.8	no cones	no rods

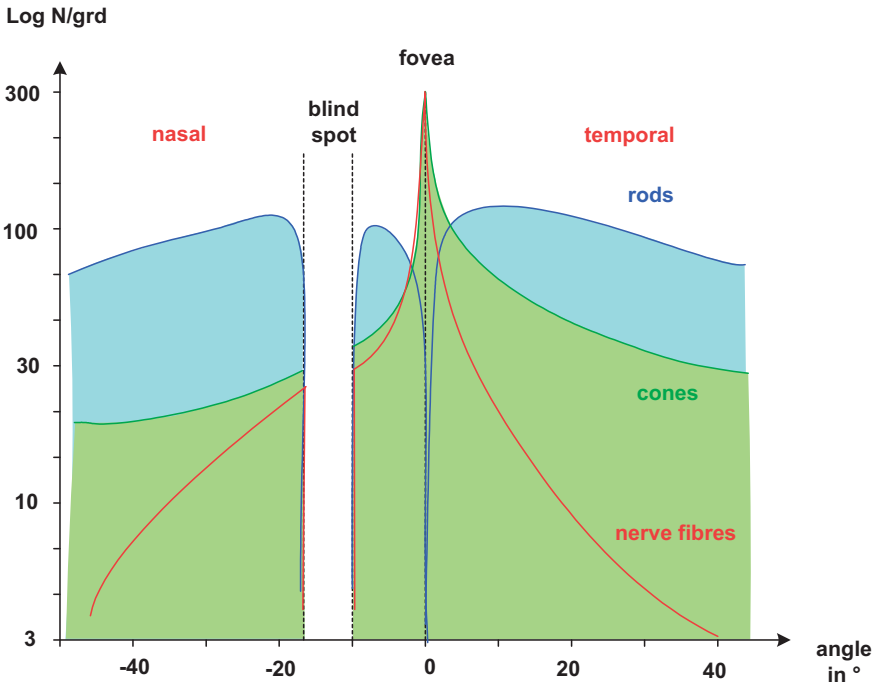

Figure 36-6: Distribution of rods, cones and nerve fibres in the human eye. The central location of the fovea is used as a reference for the field angle. The logarithm of the number *N* of receptors per degree of the field angle is taken as vertical axis.

There are three different types of cone in the eye, and these are responsible for different spectral ranges of visible light. The corresponding properties are summarized in table 36-4. The chromatic sensitivity distributions are discussed in section 36.5 in more detail.

Table 36-4: Properties of the different cone sensors.

Property	S-cones	M-cones	L-cones
Spectral sensitivity	blue	green	red
Wavelength of largest sensitivity	440 nm	535 nm	565 nm
Relative contribution to the cone number	12%	55%	33%
Special	only >3° outside fovea		

Figure 36-7 shows the density of the distribution of cones around the fovea. The density decreases with increasing angle *w* of the field of view. It should be noticed that the density of the S-type cones also decreases directly in the neighborhood of the fovea. They are responsible for the detection of blue light. There is a yellow pigment around the fovea within an approximate 5° diameter which absorbs the blue light and prevents the fovea from damage. Furthermore, this yellow color helps to correct color aberrations in the fovea, since eye correction is worse for blue light.

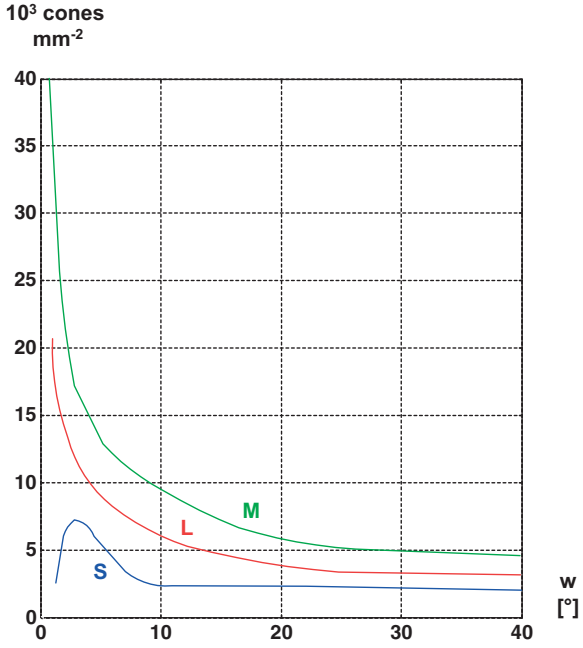

Figure 36-7: Distribution of various types of cones as a function of the field angle *w*.

In the sclera, the 130 million rod and cone receptors summarize the information into 1 million nerve fibres, which guide the signals to the brain. This concentration of signal channels is illustrated in figure 36-8 [36-3].

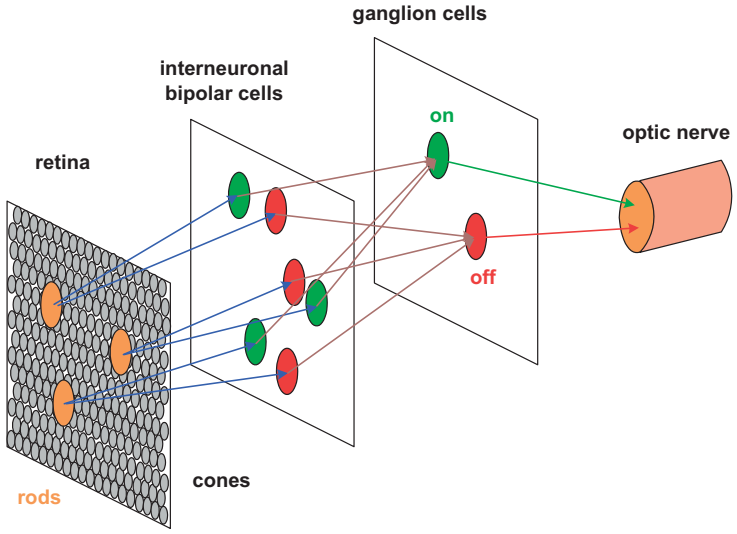

Figure 36-8: Sensor system with receptors, neuronal cells and nerves in the human eye.

36.1.4
Threshold Sensitivity

The absolute threshold of the eye for light signal differences lies in the range of 10^{-9} Lux. The threshold depends on the absolute radiance of the background of the scene. If the intensity is low, the threshold is higher. This behavior is shown in figure 36-9 [36-4]. In the range of approximately 50 cd m^{-2} to 10 000 cd m^{-2}, the relative

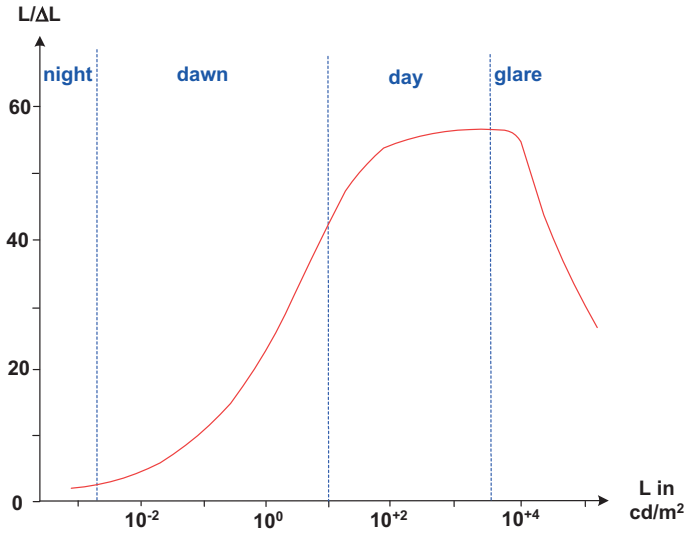

Figure 36-9: Variation in the inverse threshold sensitivity $L/\Delta L$ of the eye with the absolute radiance.

sensitivity ″ L/L is nearly constant. This behavior of the sensitivity for daylight conditions corresponds to the law of Weber, in eq. (36-7) below. Signal differences below the threshold are not detected. Furthermore, there is a strong dependence of the threshold on the size or the spatial frequency of the signal.

36.1.5 Movements of the Eye

There are several movements of the human eye which are essential for the various functions of visual perception and optical function [36-5]. There are slow drift movements in the range of 2′, which prevent the retinal image from fading. These statistical movements are uncorrelated between the two eyes. This helps to avoid saturation of the chemical processes in the cones. Tremor and micro saccades are highly dynamic movements of the eye, which are still there during the active fixation of an object point. These movements are necessary to give an active feedback signal to the eye in order to stabilize the operation. Tremors are more regular oscillations while saccades are statistically distributed with an amplitude of approximately 2′ to 50′. The vergence movements are used to relate the relative position of the eyes accurately in order to obtain correct stereoscopic vision. Typically, these movements take 0.2 to 0.8 seconds of time.

A regular tracking movement corresponds to a simultaneous rotation of both eyes in order to fix the details of a common object. The brain tries to locate the interesting detail in the fovea. This movement is done with a maximum speed of 30° per second.

36.1.6 Stiles–Crawford Effect

The cone receptors in the retina have a shape of long conical rods or tapers. The light which falls on these elements is guided towards the end of the cell by total internal reflection. If the incidence angle is large, this total internal reflection is perturbed and not all of the rays enter the end of the cell with the absorbing receptor. Therefore, the cones are less sensitive for larger angles. This means that the rays through the outer zones of the pupil are effectively damped and the pupil seems to be apodized. This is an advantage for the quality of the imaging process, since the spherical aberration for large pupil diameters has a lower energy weighting. This is called the Stiles–Crawford effect of the first kind. It is illustrated in figure 36-10 [36-6]. The Stiles–Crawford effect has almost no influence on the vision for high brightness. In this case, the pupil diameter is small and the outer zones of the pupil do not contribute to the imaging process.

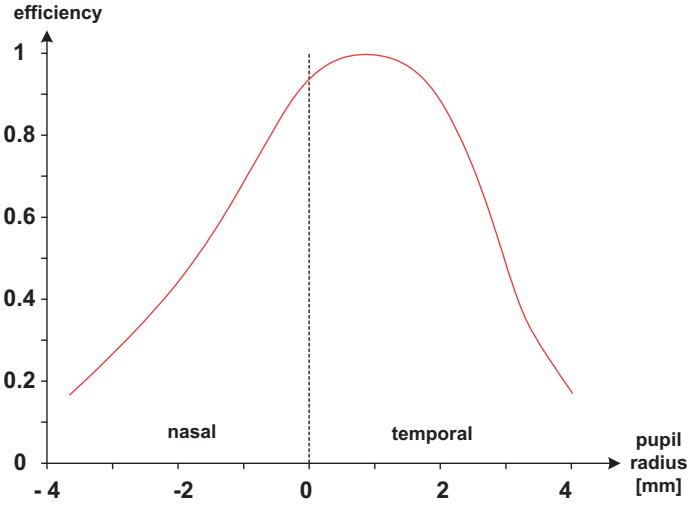

Figure 36-10: Apodization of the pupil due to the Stiles–Crawford effect.

There is another observation, which is called the Stiles–Crawford effect of the second kind. The color sensitivity is also a function of the incident ray angle on the retina. Green light seems to be shifted to the blue side, yellow light shifts to red and blue shifts to green, if it traverses the pupil in the outer zone.

In practical calculations of the performance of schematic eye models, it is possible to incorporate the influence of the Stiles–Crawford effect in a first approximation by introducing a Gaussian apodization of the form [36-7]

$$I(r) = 10^{-p \cdot r^2}, \tag{36-1}$$

where the parameter $p = 0.066$ and the radius of the pupil r is measured in mm. The Stiles–Crawford effect of the second kind can be described when the parameter p has a spectral dependence.

36.1.7 Image Processing in the Brain

The quality of the optical system of the human eye is remarkable, but indicates many defects and problems. Some of them are discussed in section 36.6 and concern residual aberrations. But the human brain has a very powerful image-processing capability. Figure 36-11 shows the image of a scene as it is projected onto the retina and the subjective image impression, for comparison.

One of the consequences of the work of the brain is the existence of optical illusions. The image impressions are influenced by neighboring signals and experience. Figures 36-12 to 36-15 show some examples of optical illusions. Figure 36-12 shows an example where the crossing point which is fixed is white, while the others seem to be dark, apart from those of the direct neighbors.

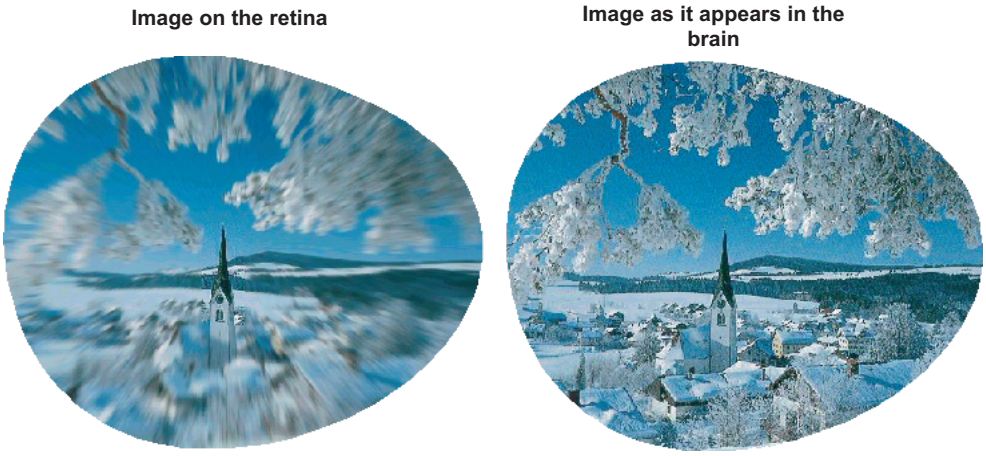

Figure 36-11: Image on the retina and corresponding processed image in the brain.

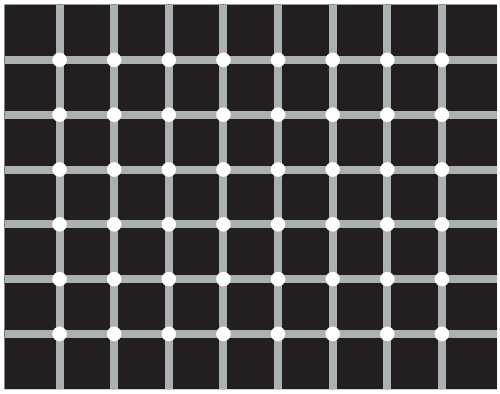

Figure 36-12: Optical illusion: the crossing points, apart from the points neighboring the fixed point, appear to be grey in color.

In figure 36-13, the impression of color and brightness is influenced by the surrounding colors. In diagram a) on the left side, the left violet bars seem to be darker than those on the right. In part b), the left grey square seems to be darker than the right one. In both cases, the colors are identical.

In figure 36-14, the influence of peripheral sight on shape recognition is demonstrated. In part a) of the figure, the red lines are of equal length, but the upper one seems to be longer. In part b), the effect of the background causes the impression of spiral curves while, in reality, the lines are closed circles.

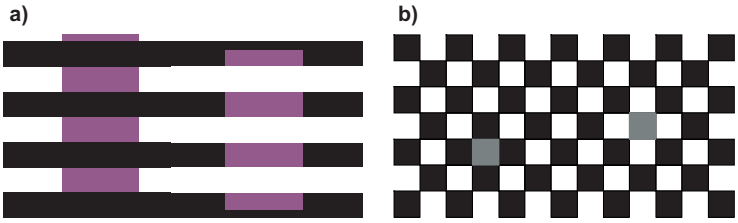

Figure 36-13: Optical illusion, in a) the violet and in b) the grey colored areas on the left side appear to be darker.

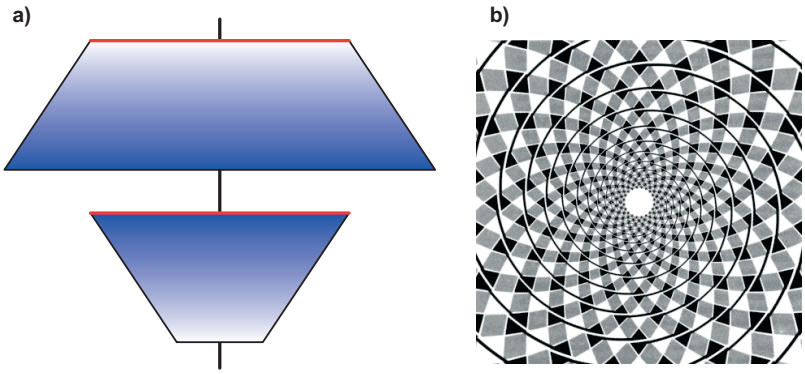

Figure 36-14: Optical illusion: in a) the upper red line seems to be longer, and the circles in b) seem to have a spiral shape.

In figure 36-15, the observer cannot decide about the depth relation. It is not clear whether the inner part of the picture represents a concave corner in a convex cube or a convex corner in a concave cube.

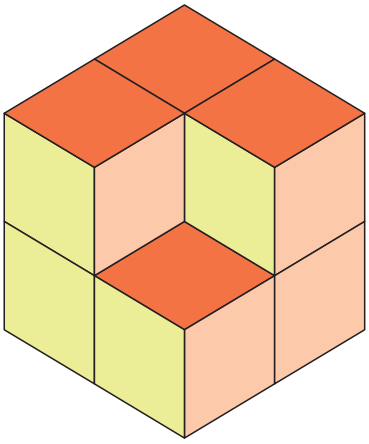

Figure 36-15: Optical illusion, the inner part can be imagined to be either convex or concave.

36.2 Optical System of the Eye

36.2.1 Accommodation

The eye is able to refocus and sharpen the image in a certain range when the distance from the object changes. The crystalline lens can be shaped in its geometry by the ciliar muscle and therefore is a variable refractive element. This effect is known as accommodation of the eye. The accommodation is performed by the signal from the cones and is not coupled to the rods outside the fovea region. The refractive power of the eye lens can be changed in the range between 22 dpt and 31 dpt. The accommodation difference therefore varies from approximately 9 dpt to 14 dpt and decreases with age.

The stimulus for accommodation occurs in the cones. If the absolute value of the radiance is below approximately 0.01 cd m^{-2}, there is no accommodation stimulus. In this case, the eye takes a point of immobility, which lies between the relaxed and the almost-accommodated position. A complete accommodation takes 1 second of time. The eye shows a fluctuation around the optimal accommodation of approximately 0.25 dpt with a 5 Hz frequency to obtain a feedback signal for adjustment.

The accommodation is defined as the difference in refractive power between the actual and the far-field case:

$$D_{\mathrm{acc}} = \frac{1}{s_{\mathrm{far}}} - \frac{1}{s} \tag{36-2}$$

where s is the intersection length. The nearest point which the eye can accommodate with a sharp image, defines the width of accommodation

$$''D_{\mathrm{acc}} = \frac{1}{s_{\mathrm{far}}} - \frac{1}{s_{\mathrm{near}}}. \tag{36-3}$$

For young people, the value $s_{\mathrm{near}} = 70\,\mathrm{mm}$ is assumed and this corresponds to an accommodation width of 14 dpt. During adaptation it is primarily the front surface of the eye lens which will have the stronger curvature.

The eye is relaxed when it is focused onto an infinitely distant object point. If an eye demonstrates a defect, the correction by glasses or other means is satisfactory when this is achieved. The lens changes its shape during accommodation. A model eye with two aspherical surfaces can be used to demonstrate the geometry of the lens as a function of the accommodation [36-8].

The accommodation interval $''D_{\mathrm{acc}}$ depends on the elasticity of the eye lens and decreases with age. This is illustrated in figure 36-16 and 37-17, where a range of uncertainty is shown. If the value of $''D$ is smaller than 4 dpt, one speaks of age-generating farsightedness or presbyopia.

The ability for accommodation reduces with increasing age. Figure 36-16 shows the range of accommodation as it changes with age. Figure 36-17 shows the position of the point for the relaxed eye, the near point with maximum accommodation and

the point of immobility of the eye, as it changes with increasing age. At greater ages, the relaxed eye has no sharp real imaging distance, which corresponds to a positive vergence relative to the far point in this diagram.

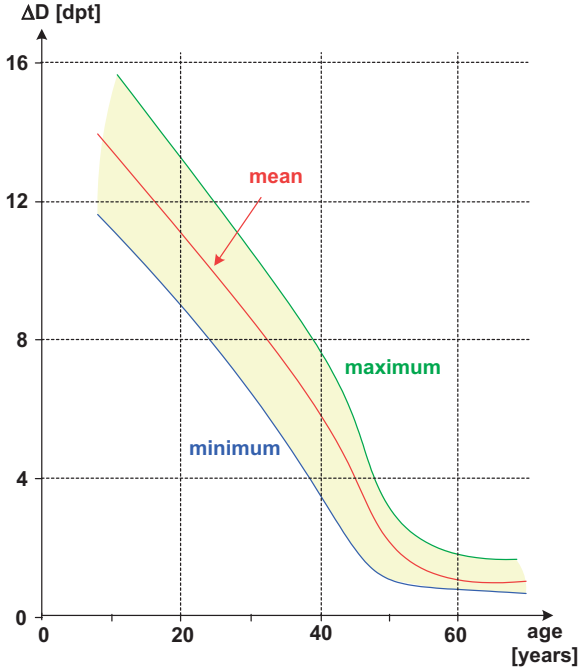

Figure 36-16: Decrease in the accommodation range with age.

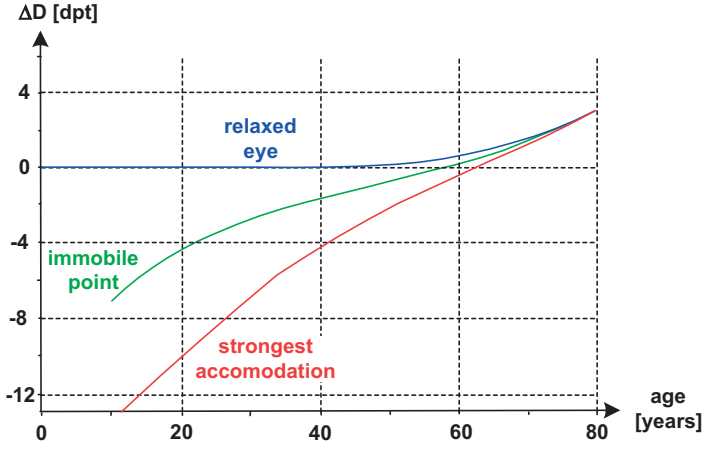

Figure 36-17: Change of the accommodation with age.

The following empirical formula gives the relationship between wavelength, diameter of the pupil, defocusing and error of refractive power ″ D. The corresponding units have to be taken into account,

$$''D[\mathrm{dpt}] = 2 \cdot 10^{-3} \cdot \frac{\tilde{\omega}[\mathrm{nm}] \cdot {}'' z[\mathrm{Ru}]}{D_{\mathrm{iris}}[\mathrm{mm}]}. \tag{36-4}$$

If the pupil has a diameter of 3 mm and green light at 550 nm is considered, the depth of focus according to the Rayleigh criterion, with $'' z = 1$ Ru, corresponds to a difference in the refractive power of $'' D = 0.12$ dpt.

The near and the far points of accommodation depend on the radiance of the scene. Figure 36-18 shows this relationship. If the object scene is rather dark, the distance of the near point increases and the far point decreases. In the case of scotopic vision with a radiance below 0.01 cd m^{-2}, the eye accommodates in the range between 0.5 and 2 m and remains in an immobile position, since the stimulus for accommodation is too small.

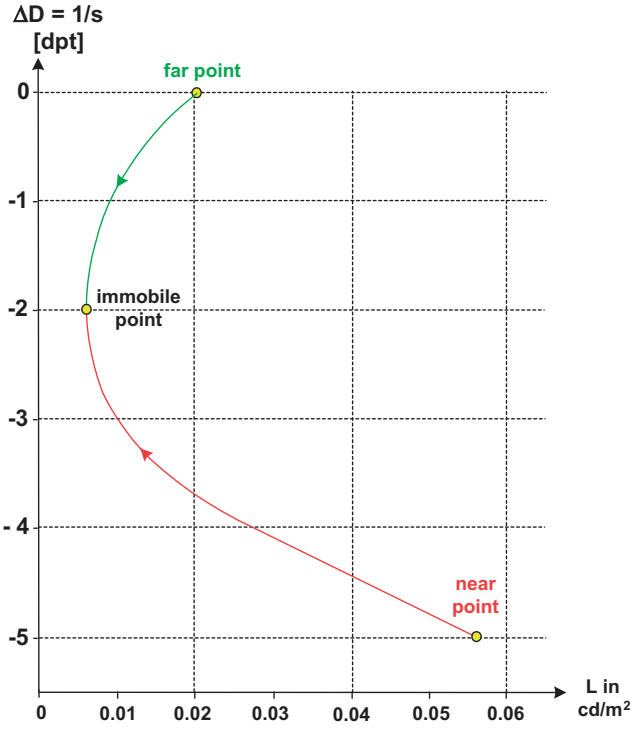

Figure 36-18: Limits of the refraction of the eye as a function of the radiance.

36.2.2
Axes of the Eye

There are several different axes, which can be distinguished in the eye. They are shown in figure 36-19. The four axes are:

1. The visual axis, which goes through the fixed object point and the nodal point N of the eye. If the function of the nodal points is taken into account, the ray, which represents the visual axis, passes to the retina through the fovea.
2. The optical axis, which is perpendicular to the cornea surface and passes the iris pupil at the midpoint. Since the fovea is not located central to the eye-ball, the optical axis differs from the visual axis. The optical axis is the geometrical symmetry axis of the eye-ball system and is different from the optical central ray, which reaches the central point of the fovea and passes obliquely through the eye system.
3. The line of sight is the axis, which goes through the object point and the centre of the entrance pupil. It is the ray, which passes through the centroid of the light bundle and is the axis of the ray cone, which enters the eye. Typically, the angle between the line of sight and the optical axis lies in the range between 3° and 8°. The centre of the entrance pupil is shifted towards the nasal side due to the asymmetrical imaging through the cornea system and the off-axis position of the fovea.
4. The pupillary axis, which passes through the centre of the entrance pupil and is perpendicular to the front surface of the cornea.

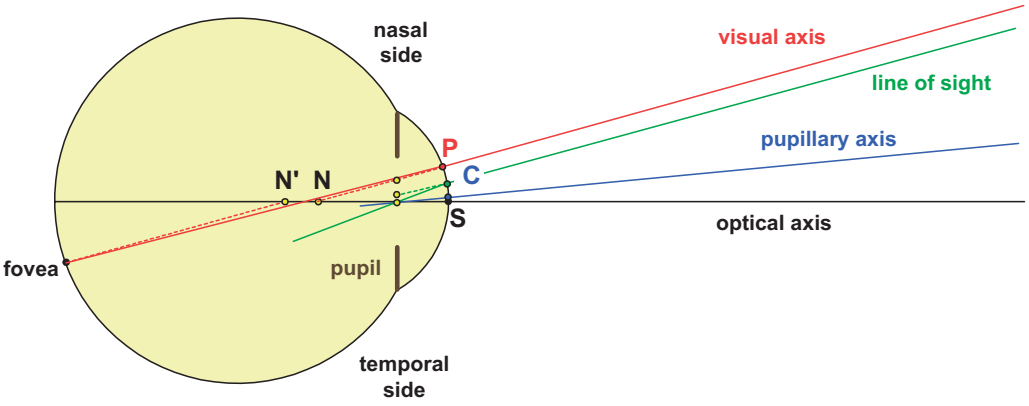

Figure 36-19: The axes of the human eye. N and N′ indicate the nodal points.

The field of view for monocular sight covers the whole retina without the small portion of the blind spot. Usually humans tend to rotate the eye to the most favourable position where the image is generated in the fovea. If the eye is moved in this way into a position of optimal orientation so that the image is in the central part of the fovea, the optical system of the eye is not used as a centered system. Nevertheless, the tilt is small and spherical aberration and astigmatism are the dominating aberrations of the eye.

36.3
Photometry and Adaptation

36.3.1
Iris

The iris works in the same way as the pupil of the eye. It is located in front of the crystalline lens and its size can be changed from 1.5 mm to 8 mm in diameter. These changes are made in order to adapt the energy for image formation and to prevent the retina from damage. The eye can accept a very large range in radiance of the object scene, which varies between 10^{-6} and 10^{5} cd m^{-2}. The radiance incident upon the retina is limited by an adaptive regulating mechanism, in order to avoid damage. The partial range from 10^{+2} to 10^{+4} cd m^{-2} of this adaptation is performed within the width of the iris diaphragm. Below this range, neuronal and chemical processes in the pigments within the retina help to reduce its sensitivity.

The exact adaptation also depends on the accommodation. The aging of the human eye reduces the nominal size and the dynamic range of iris changes. This is shown in figure 36-20, where size reduction of the larger size with rod imaging and the smaller size with cone imaging are shown.

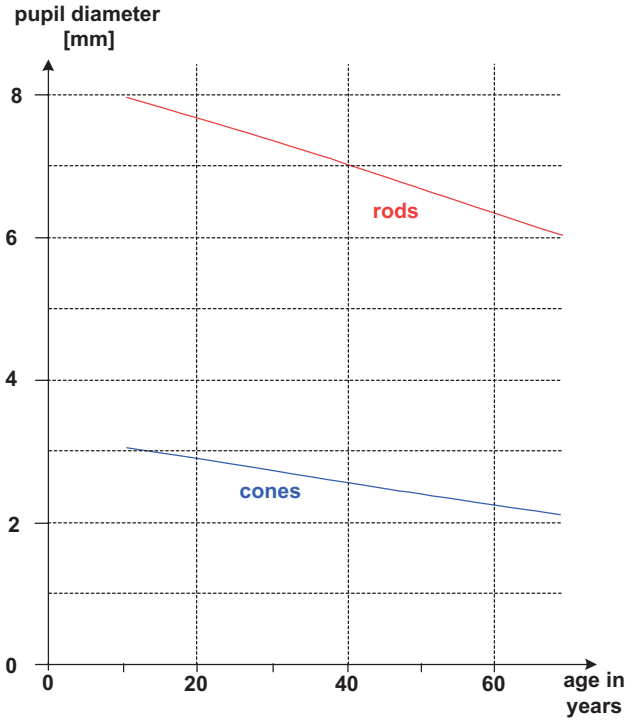

Figure 36-20: Effects of aging on the pupil size.

36.3.2
Adaptation

The variation in the pupil diameter D_{iris} with the radiance L can be approximately described by the following formula [36-9], [36-10]

$$\log_{10}(D_{\text{iris}}) = 0.8558 - 0.000401 \cdot \left[8.4 + \log_{10}(L)\right]^3, \tag{36-5}$$

where D_{iris} is measured in mm and L in cd m^{-2}. In fact the size of the pupil oscillates around a mean value, an effect known as Hippus.

In the eye, the pupil position lies between the location of the corneal refractive power and the lens. This is a location, which is particularly advantageous for the correction of coma and distortion.

If the pupil changes its size, the depth of focus changes between 0.1 dpt and 0.5 dpt. The adaptation of the iris diameter to the radiance entering the eye is shown in figure 36-21.

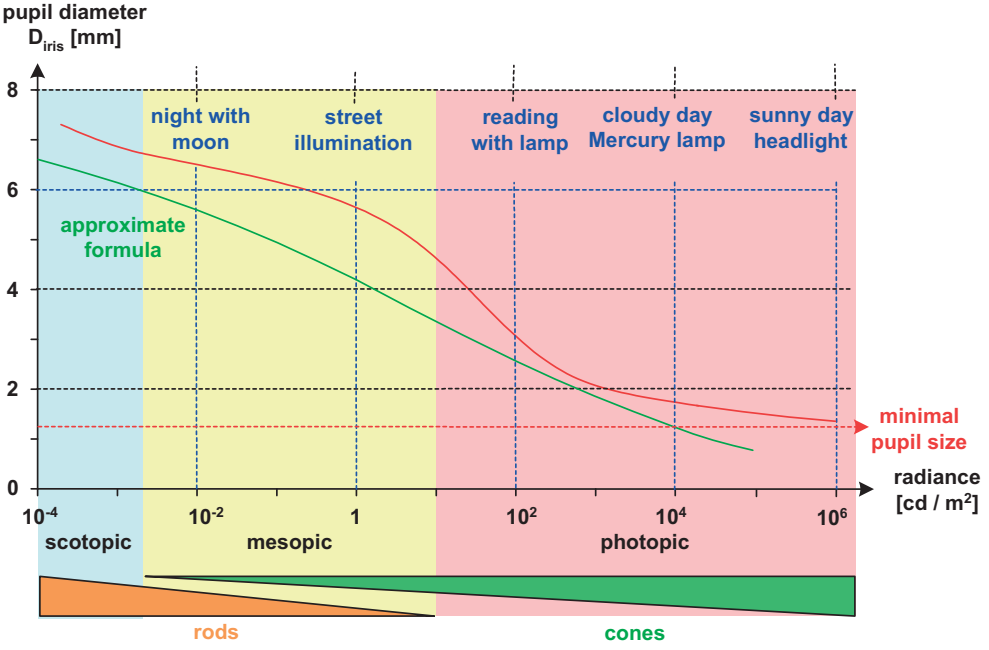

Figure 36-21: The size of the human pupil as a function of the radiance.

The cones are responsible for vision in a bright environment. If the radiance is higher than $L > 10$ cd m^{-2}, the eye only uses the cones; this is called photopic sight. The rods on the other side work in scotopic vision below $L < 5 \times 10^{-3}$ cd m^{-2}. In the range between these limits, both kinds of receptors are effective.

Table 36-5: Different effective receptors as a function of the radiance.

Scene	Vision	Receptor	Radiance
night vision	scotopic	rods	$L < 5 \times 10^{-3}$ cd m^{-2}
dim vision	mesopic	cones and rods	5×10^{-3} cd m$^{-2} < L < 10$ cd m^{-2}
day vision	photopic	cones	$L > 10$ cd m^{-2}

The change in vision from purely photopic detection with cones at daylight to scotopic vision with only rods in surroundings with very low radiance, results in a strong decrease in the resolution. The visus (see section 36.6.6) changes from 1 in the photopic case with 1′ angle resolution over a visus of 0.3 under dim light conditions to 0.1 in the scotopic case with only 10′ resolution. The influence of the radiance on the visual acuity is discussed in more detail in section 36.6.

36.3.3 Dark Adaptation

Dark adaptation is the special increase in the sensitivity of the eye to very dark scenes by means of chemical processes. This requires a longer time than does the change in the pupil size. In the first phase of approximately 7 minutes, new pigment is generated for the cones. By means of this process, the threshold sensitivity for the smallest detectable stimulus is increased by a factor of 50. In the second phase of 30 minutes duration, the rod pigment rhodopsin is produced. This increases the sensitivity of the retina by a factor of 1000. In the adaptation curves over time, which are shown in figure 36-22, these two phases are clearly separated by a kink, which is named after Helmholtz. As can also be seen in the figure, the ability of the eye to adapt decreases with increasing age.

There are two special cases of eye adaptation defects, which are also indicated in figure 36-22 [36-9]. If the rod pigment cannot be produced, the person suffers from night blindness during conditions of low radiance. If, on the other hand, vision is achieved only with rods and not the cones, monochromatic vision occurs.

The adaptation of the eye to increasing radiance takes place very quickly. In general, the adaptation effect is dominated by the rods and therefore is performed in the peripheral regions and not in the fovea.

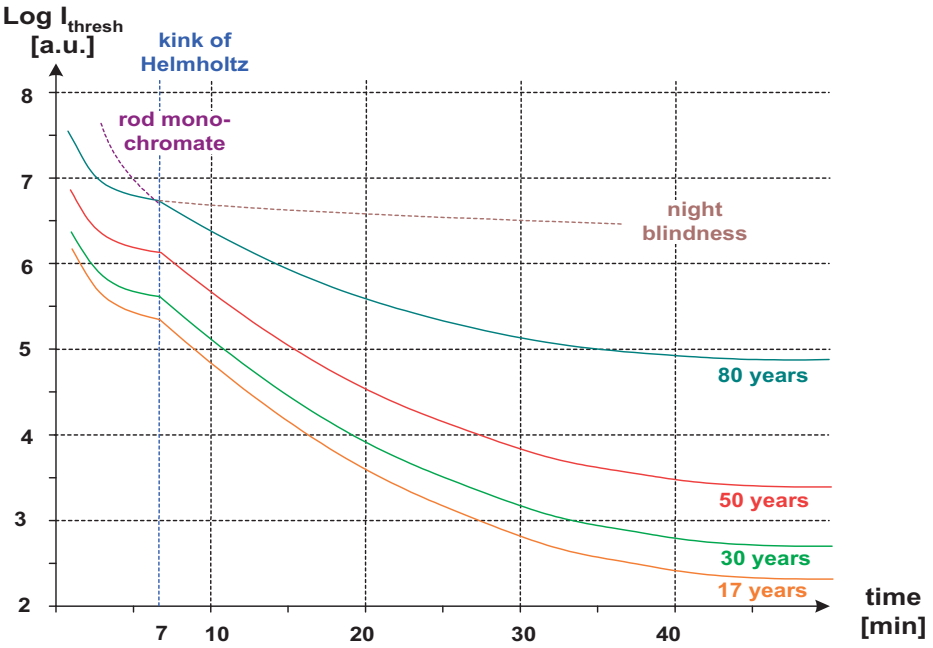

Figure 36-22: Adaptation of the eye to changing intensity with time. The smallest values of the stimulus that can be recognized are shown. The special effects for monochromatic rod vision and night blindness are indicated only on one of the curves, but are possible at all ages. The different curves indicate the change in adaptation capabilities of the eyes with increasing age.

36.3.4 Photometry of the Eye

The photometric properties of the human eye are complicated. This is due to the detection system.

If the duration of a signal is shorter than 100 ms, the eye summarizes the stimulus to a signal which is proportional to the time. This is Bloch's law.

The law of Weber–Fechner states that a signal is observed only as the logarithmic function of the signal strength

$$S = S_0 \cdot \log \frac{I}{I_0}. \tag{36-6}$$

In this equation, I_0 is the threshold value of the radiance, which corresponds to the smallest detectable stimulus.

According to Weber's law, the detection of differences in intensity is proportional to the absolute size of the mean intensity.

$$'' \; I = \text{const} \cdot I. \tag{36-7}$$

The validity of this equation is only be given for medium sizes of the radiance.

The behavior of the threshold radiance depends on the location of the image on the retina. In the fovea, according to Ricco, the product of the threshold radiance and the signal area A is constant

$$L_{\text{thresh}} \cdot A = \text{const.} \tag{36-8}$$

In the peripheral zones of the retina, Piper's law states that

$$L_{\text{thresh}} \cdot \sqrt{A} = \text{const.} \tag{36-9}$$

36.3.5 Dazzling

If the radiance of the scene is too great for retinal detection, the eye is dazzled. There are three different kinds of dazzling [36-11]:

1. Absolute dazzling, the radiance is too large and cannot be reduced sufficiently by adaptation.
2. Relative dazzling, there are large radiance differences inside the field of view. The hot spots in the object structure produce dazzling.
3. Adaptation dazzling, the reaction to adapt the eye is too slow and the temporal change in the radiance is too fast.

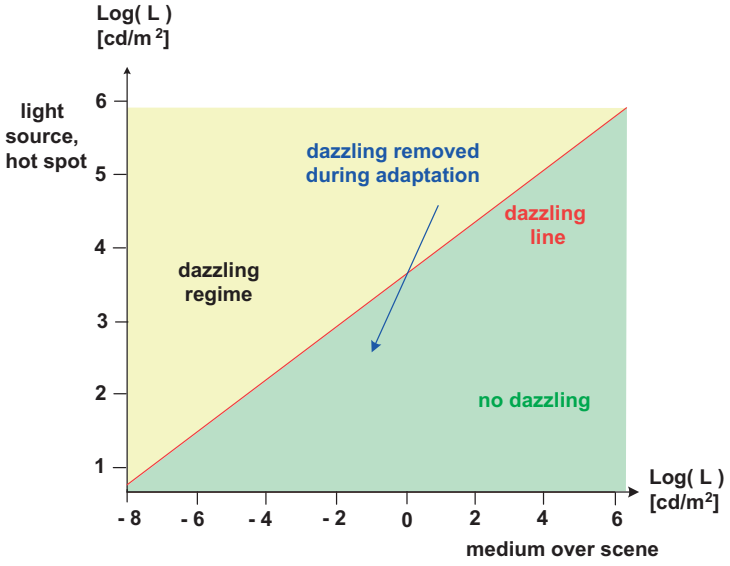

Figure 36-23: Dazzling of the eye.

If relative dazzling is considered, the irradiance of the complete scene and the radiance of a bright part of the scene must be distinguished. If the radiance of the whole scene is too great, the eye reacts by adaptation and also reduces the intensity of the light source. If this change reduces the radiance ratio correctly, the dazzling effect is removed. However, if the ratio between the radiance of the light source and the radiance of the medium for the complete scene remains too high, the dazzling effect remains. This is illustrated in figure 36-23.

36.3.6 Interpupillary Distance

The distance between the two pupil axes of the two eyes is called the interpupillary distance d_{IPD}. This is an important measurement and is responsible for binocular vision. Optical instruments with two separated binocular channels must be at the correct distance, otherwise the field of view will be reduced.

Figure 36-24 shows the geometry of the two eyes and their interpupillary distance.

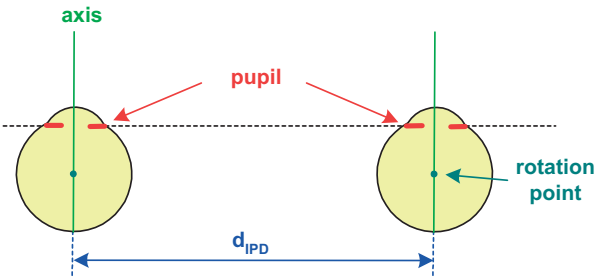

Figure 36-24: Interpupillary distance of the eyes.

The statistical spreading of the interpupillary distance over a large number of people gives a range of 56 mm to 72 mm. Figure 36-25 shows the statistical distribution of this measure, the mean values are $d_{\mathrm{IPD}} = 62.6$ mm for females and $d_{\mathrm{IPD}} = 65.0$ mm for males [36-11].

36.4 Schematic Optical Models of the Eye

36.4.1 Introduction

A large number of theoretical eye models can be found in the literature. Nearly all models have two versions of the data for the relaxed and the accommodated eye, respectively. All the models try to describe the paraxial data of the eye by the corresponding radii, distances and refractive indices. The complex shell structure of the

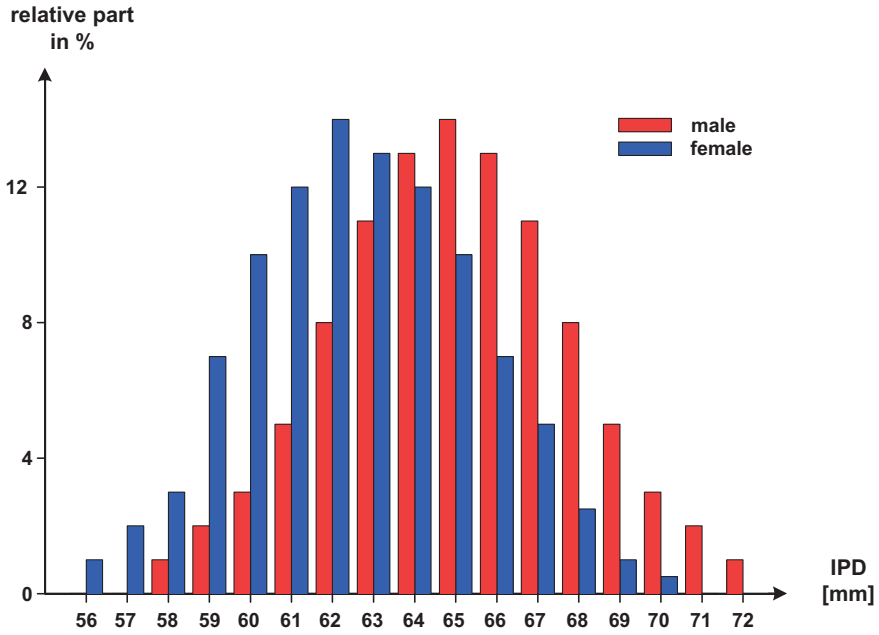

Figure 36-25: Statistical distribution of the interpupillary distance over a large number of people for males and females.

real human eye is simplified, therefore synthetic and effective values for the parameters are necessary in order to achieve this goal. The older models consist of spherical surfaces and their inventors use only refractive indices for one wavelength in the green. These attempts are not able to describe the complex behavior of the eye for finite field angles and other wavelengths. Furthermore, in most cases the models are good only up to a maximum diameter of the pupil. The more modern and sophisticated eye models describe these effects more or less effectively. Several refractive indices are available for the main wavelengths and the surfaces also have an aspherical shape [36-12]. In some cases, gradient index media are used to model the human eye in a more realistic way. The aspherical surfaces allow us to model the spherical aberration for various diameters of the iris to a good approximation.

It should be noted that there is not one eye model, which is accepted as the best in all cases. Furthermore it must be mentioned that the data for a real human eye are scattered around mean values in a broad statistical distribution. Therefore the idea of a perfect eye model seems attractive, but is not possible in practice.

In table 36-6, several eye models are listed and compared. The last three rows indicate which of the named aspects of the complete behavior of real eyes are correctly modeled.

Table 36-6: Comparison of the various schematic eye models.

Model	Aspherical for all diameters	Accommo-dation	Chromatic in the visible	Astigmatism in the field
Simple Gullstrand		yes		
Full Gullstrand		yes		
Simple Theoretical / LeGrand		yes		
Theoretical / LeGrand		yes		
Walker		yes		
Emsley reduced		no	yes	
Kooijman	yes			
Generalized reduced (chromatic, Indiana)	yes		yes	
Navarro extended	yes	yes	yes	yes
Liou–Brennan	yes		yes	yes

There have been several attempts in the literature to provide an accurate chromatic description of the eye within a schematic eye model [36-13], [36-14].

All the more sophisticated eye models describe the optical properties of the eye, but are not realistic anatomical models.

Table 36-7 shows some typical basic optical data of an eye. They correspond to the full Gullstrand eye [36-15], which is historically the most used model.

Table 36-7: Typical optical data of the Gullstrand eye. The locations are referenced to the anterior surface of the cornea.

		Relaxed	Accommodated
Parameter	**Notation**	**value**	**value**
Focal length object-sided	f [mm]	17.055	14.169
Focal length image-sided	f' [mm]	22.785	18.930
Refractive power	F [dpt]	58.636	70.57
Location entrance pupil	p [mm]	3.045	2.667
Location exit pupil	p' [mm]	3.664	3.211
Principal point object-sided	P [mm]	1.348	1.772
Principal point image-sided	P' [mm]	1.602	2.086
Nodal point object-sided	N [mm]	7.078	6.533
Nodal point image-sided	N' [mm]	7.332	6.847
Length	L [mm]	24.387	

36.4.2
Data of Some Schematic Eyes

In this section, the actual data of some schematic eyes are listed. The data are mostly with explicit refractive indices. Usually, and when not mentioned otherwise, they correspond to a wavelength of 587 nm.

1. Simplified Gullstrand eye

In the simplified Gullstrand eye, a simple pair of surfaces represent the lens. The refractive index for the lens is adapted appropriately to obtain the correct refractive power.

Table 36-8: Simple Gullstrand eye [36-15].

		Relaxed			Accommodated		
No	**Notation**	**Radius *r* [mm]**	**Thickness *d* [mm]**	**Index *n***	**Radius *r* [mm]**	**Thickness *d* [mm]**	**Index *n***
1	cornea	7.70	0.50	1.376	7.70	0.50	1.376
2	anterior chamber	6.80	3.10	1.336	6.80	2.70	1.336
3	crystalline lens	10.0	3.60	1.4085	5.33	4.0	1.426
4	vitreous humor	–6.00	17.187	1.336	–5.33	13.816	1.336
5	image	–17.2			–17.2		

2. Full Gullstrand eye

In the full Gullstrand model, the lens is made up of a kernel and a shell capsule. Therefore, the lens is represented by four surfaces. In the two versions with a relaxed and accommodated eye, the refractive indices are invariant and the change in the refractive power is caused only by variations in the radii and the distances.

Table 36-9: Full Gullstrand eye [36-3].

		Relaxed			Accommodated		
No	**Notation**	**Radius *r* [mm]**	**Thickness *d* [mm]**	**Index *n***	**Radius *r* [mm]**	**Thickness *d* [mm]**	**Index *n***
1	cornea	7.70	0.50	1.376		0.50	1.376
2	anterior chamber	6.80	3.10	1.336		2.7	1.336
3	front lens capsule	10.0	0.546	1.386	5.33	0.6725	1.386
4	crystalline lens	7.911	2.419	1.406	2.655	2.655	1.406
5	rear lens capsule	–5.76	0.635	1.386	–2.655	0.6725	1.386
6	vitreous humor	–6.00	17.185	1.336	–5.33	16.80	1.336
7	image	–17.2			–17.2		

It should be noted that, from a simple calculation of the Petzval formula, with the data above, a resultant radius of the Petzval sphere of $R_{ptz} = -17.34$ mm results from the Gullstrand eye. The radius of the eye-ball is in the range of $r = 12.5$ mm. A considerable flattening of the eye-ball in the region of the fovea as indicated in figure 36-2 leads to a curved image surface, which matches the Petzval sphere very well.

3. Theoretical eye of LeGrand

The theoretical schematic eye according to LeGrand corresponds to the simplified Gullstrand eye. Its parameters are listed in table 36-10 [36-15]

Table 36-10: Theoretical eye of LeGrand [36-15].

		Relaxed			Accommodated		
No	**Notation**	**Radius *r* [mm]**	**Thickness *d* [mm]**	**Index *n***	**Radius *r* [mm]**	**Thickness *d* [mm]**	**Index *n***
1	cornea	7.80	0.55	1.3771	7.80	0.55	1.3771
2	anterior chamber	6.50	3.05	1.3374	6.50	2.65	1.3374
3	crystalline lens	10.20	4.00	1.420	6.0	4.5	1.427
4	vitreous humor	–6.00	16.60	1.336	–5.5	14.23	1.336
5	image	–17.2			–17.2		

4. Simplified theoretical eye of LeGrand

In the simplified theoretical eye of LeGrand, which is also named after Listing, some approximations are made in comparison with the standard LeGrand model. The cornea is not modeled as a separate medium with finite thickness but is combined with the anterior chamber. The lens is assumed to have an ideal vanishing thickness.

Table 36-11: Simplified theoretical eye of LeGrand [36-15].

		Relaxed			Accommodated		
No	**Notation**	**Radius *r* [mm]**	**Thickness *d* [mm]**	**Index *n***	**Radius *r* [mm]**	**Thickness *d* [mm]**	**Index *n***
1	cornea, chamber	8.00	6.37	1.3374	8.00	5.78	1.3374
2	lens	10.20	0.0	1.4208	6.00	0.0	1.426
3	vitreous humor	–6.00	17.83	1.336	–5.5	16.15	1.336
4	image	–17.2			–17.2		

5. The model eye of Walker

The schematic eye of Walker is quite similar to the simple Gullstrand model [36-16]. The corresponding data are listed in table 36-12.

Table 36-12: Theoretical eye of Walker [36-16].

		Relaxed			Accommodated		
No	**Notation**	**Radius *r* [mm]**	**Thickness *d* [mm]**	**Index *n***	**Radius *r* [mm]**	**Thickness *d* [mm]**	**Index *n***
1	cornea	7.80	0.60	1.376	7.8	0.60	1.376
2	anterior chamber	6.40	3.0	1.336	6.4	3.0	1.336
3	crystalline lens	10.10	4.0	1.410	5.95	4.0	1.411
4	vitreous humor	–6.10	17.20	1.337	4.5	17.20	1.337
5	image	–12.5			–12.5		

5. Reduced eye of Emsley

The reduced eye of Emsley [36-17] is a somewhat simpler model with only one refracting surface to describe the behavior of the eye. The system is listed in table 36-13 and has a refractive power of 60 dpt. The eye is filled with water and an Abbe number of 50.23 is assumed. This corresponds to a simple dispersion, which can be described by the equation

$$n(\breve{\omega}) = a + \frac{b}{\breve{\omega} - c} \tag{36-10}$$

with the constants

$$a = 1.31848 \ , \ b = 0.006662 \ , \ c = 0.1292. \tag{36-11}$$

Table 36-13: Reduced eye of Emsley.

		Relaxed			Accommodated		
No	**Notation**	**Radius *r* [mm]**	**Thickness *d* [mm]**	**Index *n***	**Radius *r* [mm]**	**Thickness *d* [mm]**	**Index *n***
1	cornea	5.555	22.222	1.3333	4.2	15.6	1.3333
2	image						

6. Generalized reduced eye

The generalized reduced eye model is an extension of the early system of Emsley [36-3]. A pupil is introduced to obtain a more realistic description of the field effects, and the front surface is made aspherical. The dispersion relation is modified to obtain a better fit of the chromatic properties of the human eye:

$$a = 1.320535 \ , \ b = 0.004685 \ , \ c = 0.214102. \tag{36-12}$$

Various modifications of this type of model are due to Thibos [36-14] and are also called chromatic eye or Indiana eye models [36-13], [36-18].

Table 36-14: Generalized reduced eye.

		Relaxed			
No	**Notation**	**Radius *r* [mm]**	**Thickness *d* [mm]**	**Index *n***	**Aspherical κ**
1	cornea	5.55	2.75	1.3333	0.6325
2	iris		19.47		
3	image				

7. Kooijman eye

The eye model of Kooijman [36-19] consists of four aspherical surfaces. With the help of these degrees of freedom, the spherical aberration of the eye on-axis and the photometric properties can be modeled quite accurately.

Table 36-15: Theoretical eye of Kooijman.

		Relaxed			
No	**Notation**	**Radius *r* [mm]**	**Thickness *d* [mm]**	**Index *n***	**Aspherical κ**
1	cornea	7.80	0.55	1.3771	–0.25
2	anterior chamber	6.50	3.05	1.3374	–0.25
3	crystalline lens	10.20	4.0	1.420	–3.06
4	vitreous humor	–6.00	16.60	1.336	–1
5	image	–14.1			

8. Navarros chromatic wide-angle eye

Navarro et al. [36-20], have proposed a model of the eye which can be used to describe accommodation, chromatic behavior and spherical aberration as a function

of the iris diameter to a good accuracy. In an extended version [36-21], the wide-angle properties are also taken into account.

The dispersion of the eye is described by Herzberger formulas for all media. Furthermore, Navarro gives the data as a function of the accommodation [36-20]. This allows one to calculate the model for arbitrary distances and not only for the far and the near point. The influence of the accommodation A, measured in dpt, is given in an empirical way with the help of the following equations:

$$\begin{aligned} r_3 &= 10.2 - 1.75 \cdot \ln(A+1) \\ r_4 &= -6 + 0.2294 \cdot \ln(A+1) \\ d_2 &= 3.05 - 0.05 \cdot \ln(A+1) \\ d_3 &= 4 + 0.1 \cdot \ln(A+1) \\ n_3 &= 1.42 + 9 \cdot 10^{-5} \cdot (10A + A^2) \\ \kappa_3 &= -3.1316 - 0.34 \cdot \ln(A+1) \\ \kappa_4 &= -1 - 0.125 \cdot \ln(A+1). \end{aligned} \tag{36-13}$$

Table 36-16: Theoretical eye of Navarro for relaxed eye and 589.3 nm.

		Relaxed			
No	**Notation**	**Radius *r* [mm]**	**Thickness *d* [mm]**	**Index *n***	**Aspherical κ**
1	cornea	7.72	0.55	1.367	–0.26
2	anterior chamber	6.50	3.05	1.3374	0
3	crystalline lens	10.20	4.0	1.420	–3.1316
4	vitreous humor	–6.00	16.40	1.336	–1.0
5	image	–12.0			

9. Liou–Brennan eye

The eye model due to Liou–Brennan [36-22] uses aspherical surfaces, together with two gradient media to describe spherical aberration and astigmatism very precisely. The anatomic similarity to real eyes is great and the prediction of the aberrations is very good. The spectral properties are valid only in the visible range and cannot be extended into the ultraviolet and infrared regions. The dispersion curves are synthetic and give efficient values, which do not correspond to realistic dispersion dependencies. In the original paper, the iris diaphragm is assumed to be decentered and the fovea corresponds to a field angle of 5°.

Table 36-17: Theoretical eye of Liou–Brennan for relaxed eye and 589.3 nm.

		Relaxed			
No	**Notation**	**Radius *r* [mm]**	**Thickness *d* [mm]**	**Index *n***	**Aspherical κ**
1	cornea	7.77	0.50	1.376	–0.18
2	anterior chamber	6.40	3.16	1.336	–0.60
3	crystalline lens	12.40	1.59	gradient 1	–0.94
4		infinity	2.43	gradient 2	
5	vitreous humor	–8.10	16.27	1.336	+0.96
6	image				

The gradients are described by the formula

$$n(r,z) = n_0 + n_1 z + n_2 z^2 + n_3 r^2. \tag{36-14}$$

The constants can be found in the literature.

36.4.3 Sample Calculations

Figure 36-26 shows the optical system of the classical Gullstrand eye model. The prolate shape of the eye globe in the region of the retina has to be noticed. Figure 36-27 shows the corresponding spot diagrams for three colors and field positions for a pupil diameter of 2 mm.

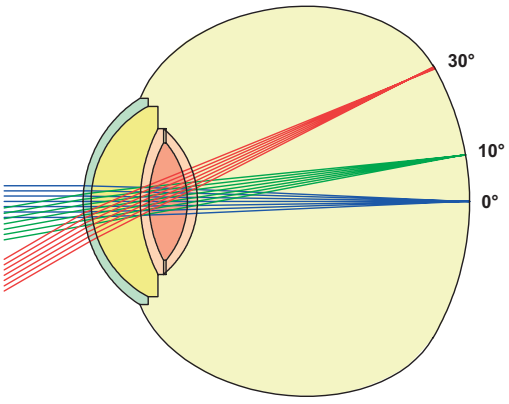

Figure 36-26: Gullstrand eye model.

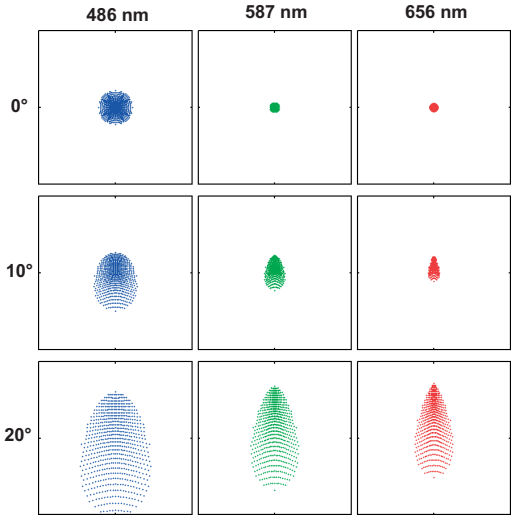

Figure 36-27: Spot diagram of the Gullstrand eye model for different colors and three field positions. The side length of the box is 0.1 mm. It has to be noticed, that in this representation, not the identical angles are chosen as in fig. 36-26.

Figure 36-28 shows the optical system of the Navarro eye model corresponding to the data of the previous section. This modern and rather good sample eye can be used to simulate the working of visual optical instruments together with the human eye. Figure 36-29 shows the spot diagram of this system for a pupil diameter of 3 mm, the axial and lateral chromatic residual aberrations can be easily recognized.

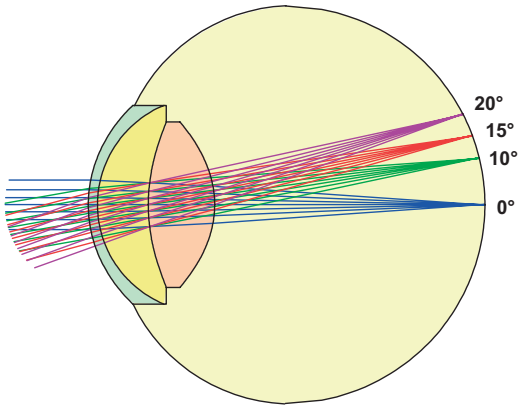

Figure 36-28: Schematic drawing of the Navarro eye model.

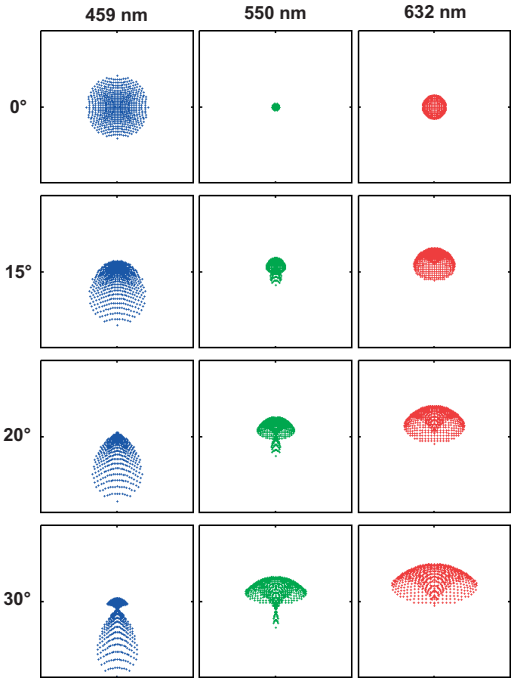

Figure 36-29: Spot diagram of the Navarro eye model for different colors and four field positions. The side length of the box is 0.1 mm. It has to be noticed, that in this representation, not the identical angles are chosen as in fig. 36-28.

Figure 36-30 shows the spot diagram of the Navarro model eye for various accommodations and four field angles. The diameter of the pupil is approximately 2.7 mm for all cases and the wavelength is 555 nm. The decrease in quality of the eye with accommodation and increasing field angle can be seen. In the upper left point for the relaxed eye and on-axis the spot size has almost the same diameter as the Airy circle.

Figure 36-31 shows the residual rms wavefront aberration for $\breve{\omega}$= 550 nm on-axis as a function of the pupil diameter for the Gullstrand and the Navarro eye models. The results are quite different for diameters of the iris larger than 2 mm. The results of the Navarro schematic eye are more likely to model the real human eye, as can be seen by a comparison with experimental values. It is clear that the performance of the eye decreases rapidly when the aperture is opened more than 3.5 mm in diameter.

Figure 36-32 shows the modulation transfer function at three field positions, a pupil diameter of 2.7 mm and a wavelength of 550 nm for the schematic eye models of Gullstrand and Navarro. The two lines correspond to tangential and sagittal line orientations, respectively. It can be seen that there are significant differences for the two models. In particular, the Gullstrand model is not able to describe the field effects properly and, even on-axis, 30% differences occur in the visibility.

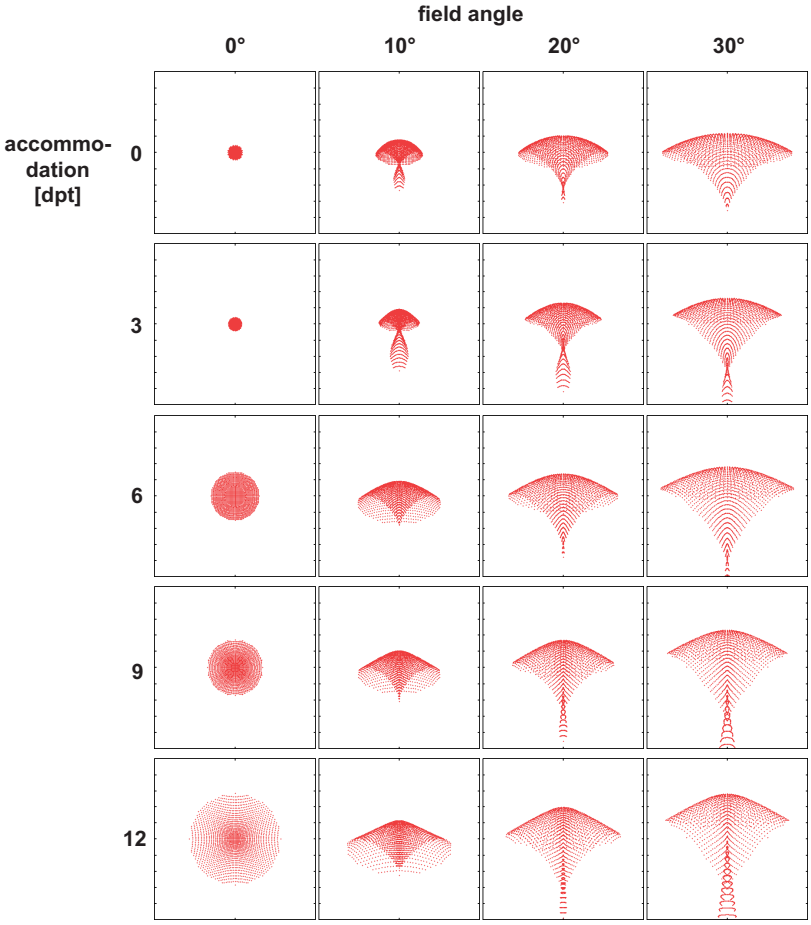

Figure 36-30: Spot diagram of the Navarro eye model as a function of the accommodation and the field angle. The aperture corresponds to an iris diameter of 2.7 mm and the wavelength is 550 nm. The side length of the box is 0.1 mm.

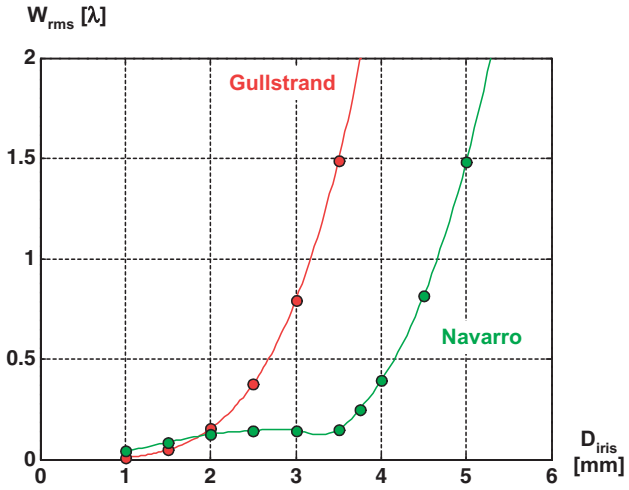

Figure 36-31: The rms value of the wavefront aberration for the Gullstrand and the Navarro eye model as a function of the pupil diameter.

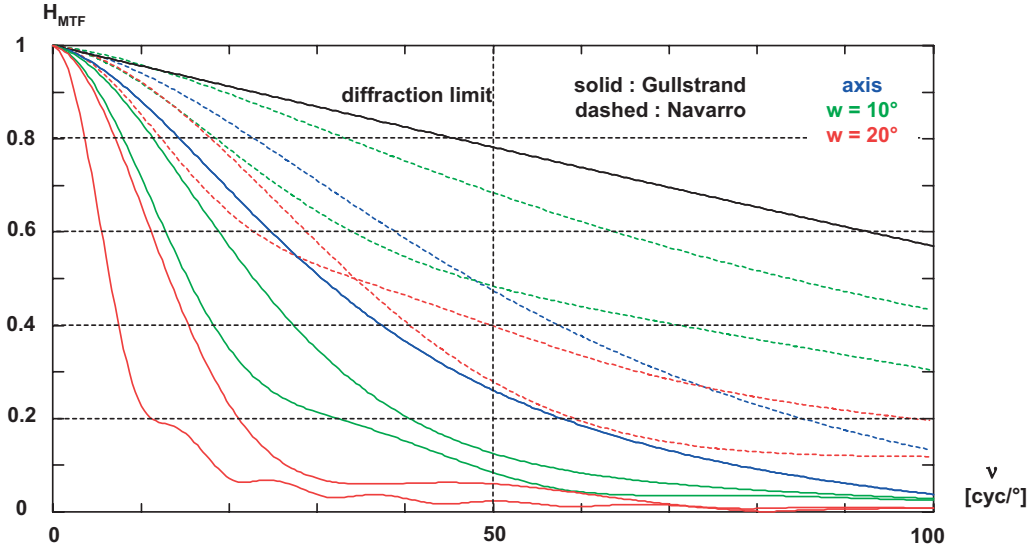

Figure 36-32: Modulation transfer function at three field positions, a pupil diameter of 2.7 mm and a wavelength of 550 nm for the Gullstrand and the Navarro eye models.

Figure 36-33 shows the theoretical eye of LeGrand. It is a model eye, which gives an especially good description of the chromatic properties of the eye. Figure 36-34 shows the chromatic variation of the image surfaces and the longitudinal chromatic aberrations on-axis.

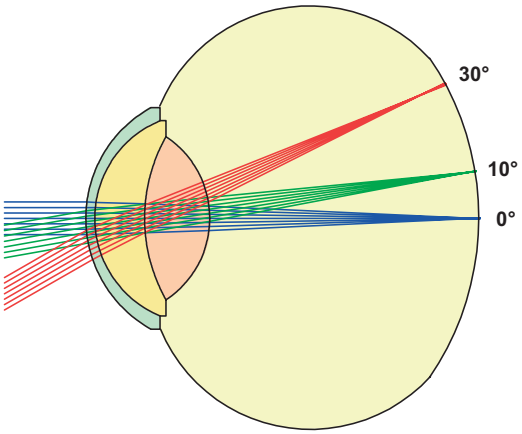

Figure 36-33: LeGrand theoretical eye model.

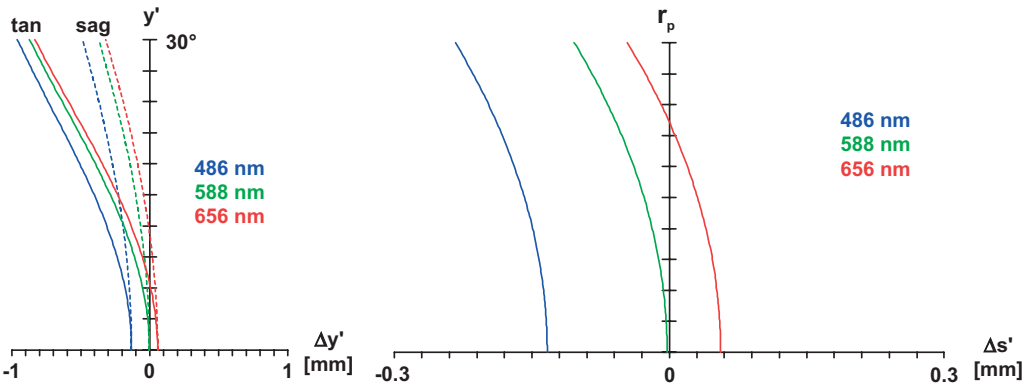

Figure 36-34: Chromatic image shells and longitudinal chromatic aberration of the LeGrand theoretical eye model.

Figure 36-35 shows the transverse aberrations of the generalized reduced eye due to Thibos [36-18] for several values of the aspherical parameter p, which is used here as originally defined by the inventor. The relation with the usual conical parameter is given by

$$p = \kappa + 1. \tag{36-15}$$

As can be seen from this figure, the asphericity of the cornea is only essential for pupil diameters larger than 4 mm.

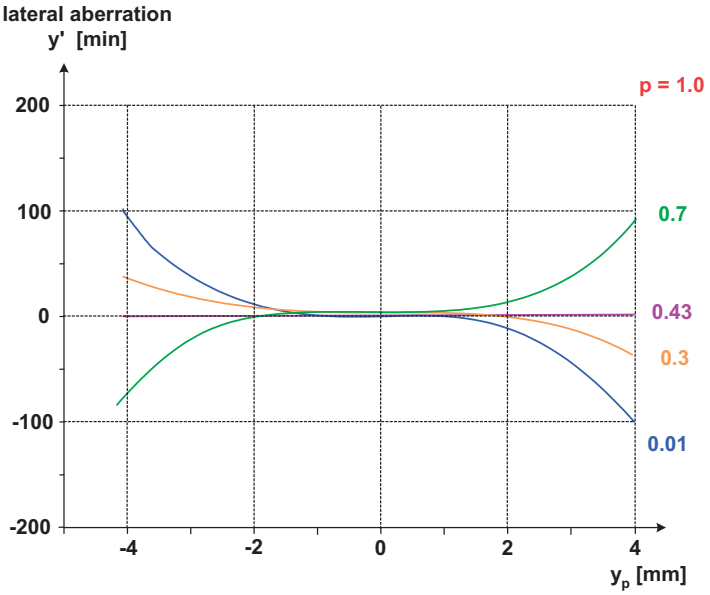

Figure 36-35: Transverse aberration of the generalized reduced eye for different values of the asphericity parameter $p = \kappa + 1$.

Figure 36-36 shows the tangential and the sagittal image surfaces for the generalized reduced eye as a function of the field height. The astigmatism can be clearly seen.

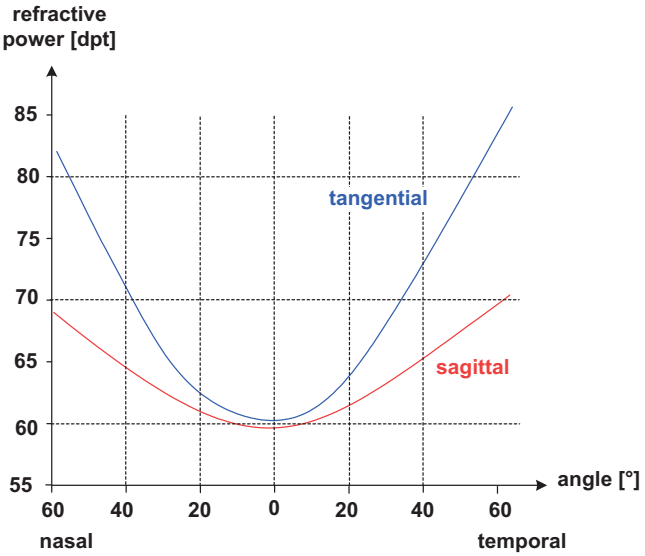

Figure 36-36: Tangential and sagittal image shells of the generalized reduced eye model.

36.5 Color Vision

Color vision has already been discussed in chapter 9 of the first volume of this book. For reasons of completeness, some of the details are reproduced here.

36.5.1 Spectral Sensitivity of the Eye

Rigorous physical approaches can explain the chromatic effect created by a particular radiation in an objective way. In the case of human sight, due to human sensory physiology, the actual color stimulus can only be described if additional aspects are considered. For example, different physical color stimuli can trigger the exact same chromatic sensation and therefore the same color values. This phenomenon of color sensation is called metamery.

The spectral sensitivity of the eye depends on brightness. Consequently, there are two different sensitivity curves for daylight vision (photopic vision mainly by the cones) and night vision (scotopic vision mainly by the rods) shown in figure 36-37. In daylight the maximum of the spectral sensitivity is at 555 nm, at night it is 507 nm. According to definition, the visible range of the spectrum lies between the wavelengths 380 nm (violet) and 780 nm (red).

The normalized sensitivity of the eye $V(\tilde{\omega})$ correlates to the photometrically scaled spectral sensitivity $\tilde{\omega}(\tilde{\omega})$ as

$$\tilde{\omega}(\tilde{\omega}) = 683 \frac{\mathrm{lm}}{\mathrm{W}} \cdot V(\tilde{\omega}). \tag{36-16}$$

Using this relation, $V(\tilde{\omega})$ can be converted into the physical-photometric quantity $\tilde{\omega}(\tilde{\omega})$. The unit is the lumen, lm (see chapter 6).

Investigating the circumstances more closely the curves are found to have a slightly different form depending on the brightness, i.e., comparing daylight vision with night vision. These small differences are clearly visible only in the logarithmic plot.

The phototopic curve for daylight vision as well as the scotopic curve for night vision are standardized under defined boundary conditions by the CIE (Commision Internationale de l'Eclairage, or International Commission for Illumination) [9-1], [9-2], [9-3].

All rods contain the same visual purple as the biological receptor for light and chromatic sensation. Therefore the rods cannot distinguish between different colors. They are simply brightness sensors.

In contrast, there are three types of cones with significant differences in terms of their spectral sensitivity. The combination of the reaction of these three cone types to the relevant visual stimuli leads to color vision. The activation of the different types of cones yields the chromatic tristimulus values registered by the eye.

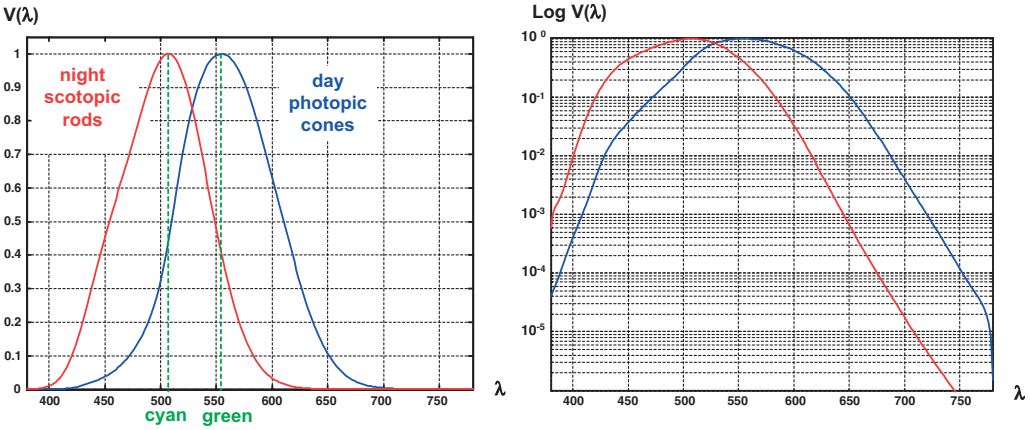

Figure 36-37: Spectral sensitivity of the human eye for daylight and night vision as a linear and a logarithmic plot.

The relative spectral sensitivity of rods and the three cone types l, m and s in the eye are shown in figure 36-38 as a linear plot and in figure 36-39 as a logarithmic plot.

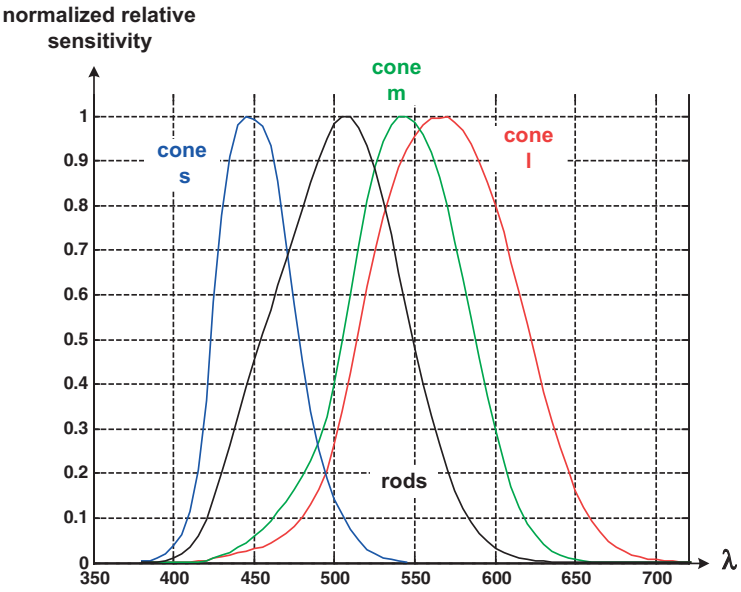

Figure 36-38: Normalized relative spectral sensitivity of the cones and the rods as a linear plot.

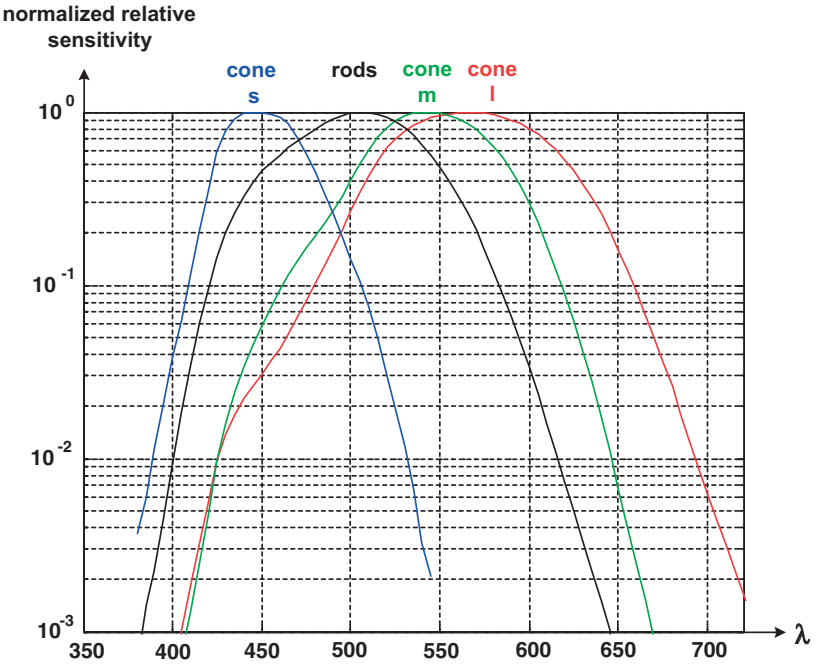

Figure 36-39: Normalized relative spectral sensitivity of the cones and the rods as a logarithmic plot.

The shift of the spectral sensitivity between daylight and night vision produces the Purkinje effect: Objects with different colors but with the same brightness in daylight appear to have a significantly different brightness at twilight or at night. The spectral sensitivity curves of the three cone types are given by the distributions $\bar{l}(\breve{\omega})$, $\bar{m}(\breve{\omega})$ and $\bar{s}(\breve{\omega})$. Then, for a chromatic stimulus $\varphi(\breve{\omega})$ the color components are calculated according to

$$L = \int_{380\text{nm}}^{780\text{nm}} \varphi(\breve{\omega}) \cdot \bar{l}(\breve{\omega})\, d\breve{\omega}, \tag{16-17}$$

$$M = \int_{380\text{nm}}^{780\text{nm}} \varphi(\breve{\omega}) \cdot \bar{m}(\breve{\omega})\, d\breve{\omega}, \tag{36-18}$$

$$S = \int_{380\text{nm}}^{780\text{nm}} \varphi(\breve{\omega}) \cdot \bar{s}(\breve{\omega})\, d\breve{\omega}. \tag{36-19}$$

Together they yield the chromatic values registered by the eye. So the three different types of cones define the LMS color system. The sensitivity curves given by nature form the color-value curves of the human eye. The integrals of the quantities $\bar{l}(\breve{\omega})$, $\bar{m}(\breve{\omega})$ and $\bar{s}(\breve{\omega})$ over $\breve{\omega}$are normalized for the visible spectral range.

36.5.2
Transmission of the Eye

In the eye the media of the lens and the vitreous body have spectral transmission functions independent of the receptors. They also influence the sensation of color. As shown in figure 36-40, the transmission approaches zero, especially for small wavelengths, at the blue end of the visible spectrum. A noticeable absorption between the cornea and the retina begins at about 600 nm.

Figure 36-41 shows the development of the transmission spectrum through the various parts of the eye when light enters the system. It can be seen that it is in particular the ultraviolet part of the incoming light which is blocked in the lens of the eye. The vitreous bodies before and after the lens absorb the infrared light components beyond 1300 nm. Therefore, the use of eye-save laser wavelengths at 1543 nm ensures that there is no damage to the eye at the corresponding applications for range finding.

The transmission curve of the eye already demonstrates a spectral dependence in the visible region. Therefore, for the determination of the LMS color system for the eye, these boundary conditions have to be taken into account. The exact curves and values are dependent on them. Among the boundary conditions are:

1. Consideration of the pure receptors of the retina or the spectral influence of the light passing into the eye through the cornea, anterior chamber, lens and vitreous humor.
2. Determination of the size of the image field in the fovea. Usual values for the image field are 2° and 10°.
3. Any strong color influences to which the eye has recently been subject, i.e., the effect of permanent color stimulus and contrast.

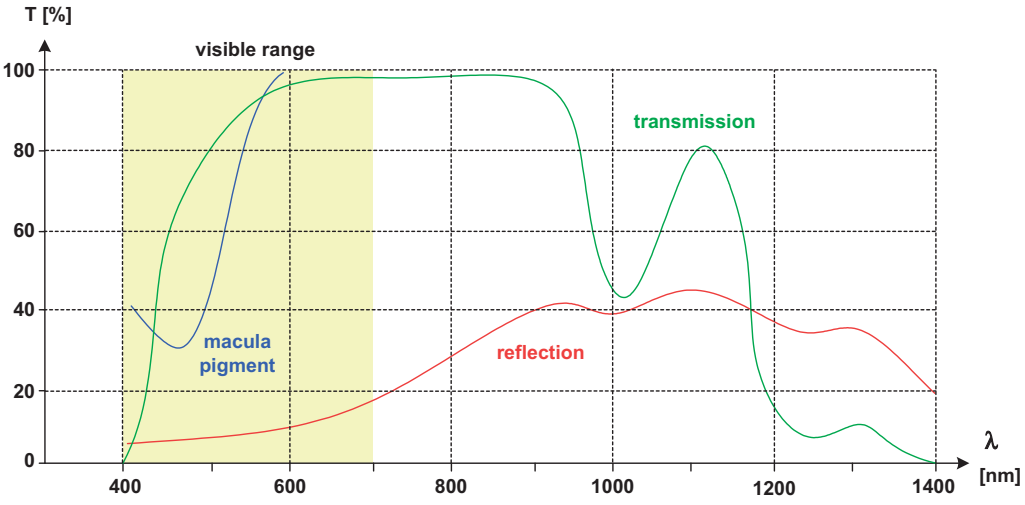

Figure 36-40: Spectral transmission and reflection curves of the eye.

4. The absolute value of the luminance of the radiation.
5. Environmental conditions, which also affect sensation, e.g., indirect lighting.

For in vivo conditions, the curves of the LMS color system are given in figure 36-42.

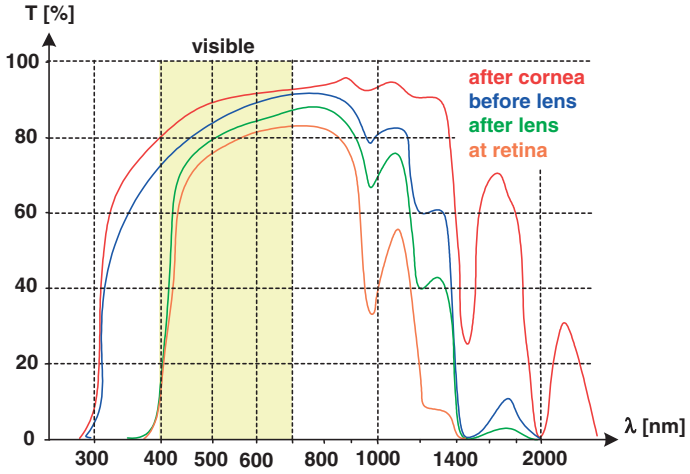

Figure 36-41: Spectral transmission curves at several depth locations inside the eye. The wavelength scale is not linear.

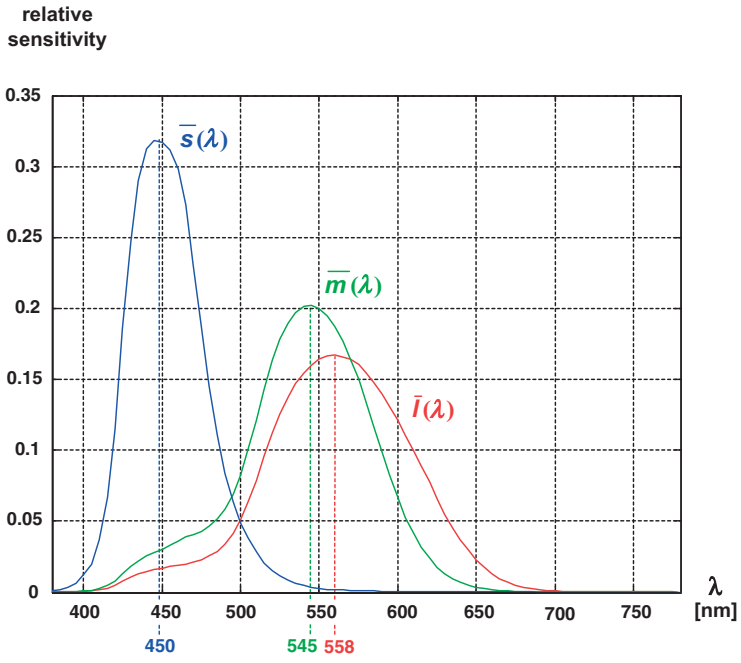

Figure 36-42: Curves for the color matching functions of the LMS color system based on the sensitivity of the eye.

36.6
Optical Performance of the Eye

36.6.1
Introduction

The quality of the optical system of the human eye can be considered in an objective way in analogy to usual optical systems. On the other hand, it can also be discussed in a subjective way, because the sensory influences of the human eye and the image processing capabilities of the brain are very large. In this section, the objective analysis is presented with the help of the criteria as discussed in chapter 30. A more subjective view of human vision can be found in section 36.6.9.

It must be taken into account, however, that the quality of the optical system of the eye depends on its adaptation and accommodation. Therefore a full description of the performance contains a two-dimensional set of data.

36.6.2
Point Spread Function

Figure 36-43 shows the diameter of the light spot on the retina for an emmetropic eye at $\tilde{\omega}$= 550 nm on-axis for a relaxed eye. It is calculated with the help of the Navarro schematic eye. The diffraction part and the size due to the residual spherical aberration and geometrical spreading are shown separately. It can be seen that the eye is diffraction limited up until the diameter of the iris diaphragm is approximately 3.5 mm.

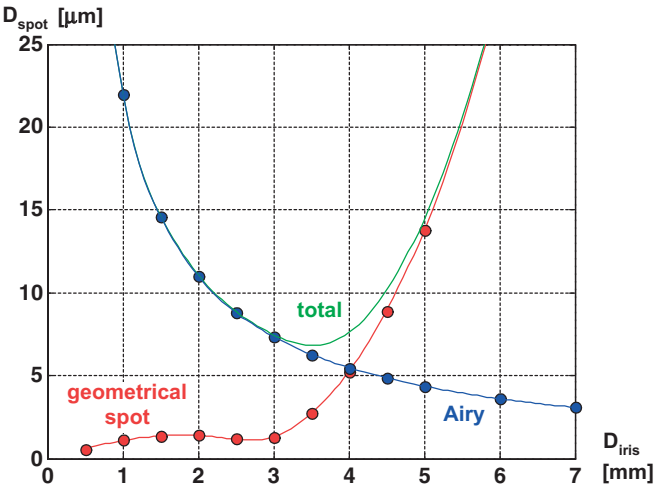

Figure 36-43: Spot diameter of the human eye as a function of the aperture diameter. The two parts due to diffraction and geometrical spreading are shown separately.

For a pupil diameter of 3 mm, the numerical aperture in the eye is NA = 0.0588 and the Airy diameter for $\breve{\omega}$ = 550 nm is D_{Airy} = 7.6 µm. The diameter and the pitch of the cones in the fovea lies in the range of 2.3 µm. Therefore, one object point illuminates approximately $(7.6 / 2.3)^2 \approx 10$ cones. The optical system of the eye limits the quality of image formation, but the resolution of detection on the retina is higher.

36.6.3 Field Aberrations

The cones are responsible for the high resolution imaging properties of the eye. Since the density of the cones decreases with increasing distance from the fovea, the range of the best imaging lies inside a field of view of $2w = 4°$. A second reason for the reduction of resolution with increasing distance to the centre of the fovea is neuronal signal processing. Far from the fovea, a large number of rod receptors are gathered in one ganglion, this also reduces the spatial resolution.

Figure 36-44 shows the behavior of this decrease in the highest resolvable spatial frequency $\breve{\varepsilon}$ as a function of the field angle. The exact curves of the decrease depend on both the wavelength and the brightness.

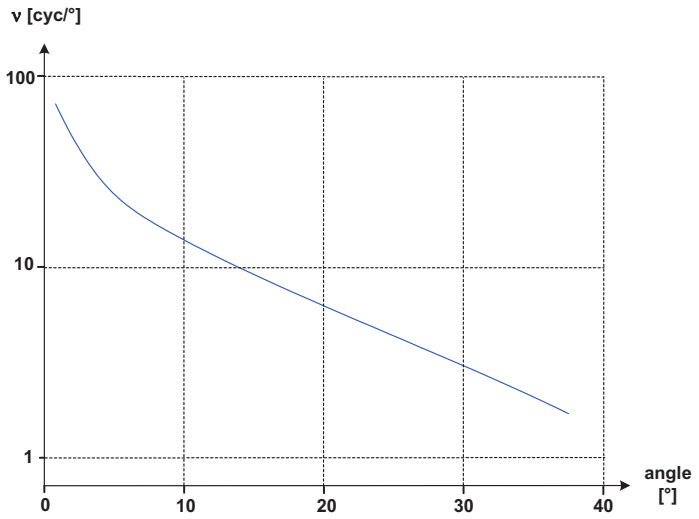

Figure 36-44: Reduction of the resolution with field angle.

If a light signal is very weak, only a small radiance enters the eye. The pupil therefore adapts and increases in size. In this case, the peripheral spherical aberration of the eye lens also reduces the quality and the resolution decreases.

If an object is imaged significantly outside the fovea at larger field angles, a residual astigmatism reduces the performance of the eye. This defect increases quadratically with the field of view. Figure 36-45 shows this growing astigmatism for two eye

model calculations and from measurements. This again shows the limited accuracy of the schematic eyes for larger field angles. Due to the eccentric location of the fovea, the curves are not symmetrical around the angle $w = 0$. The astigmatism is larger for field angles on the temporal side.

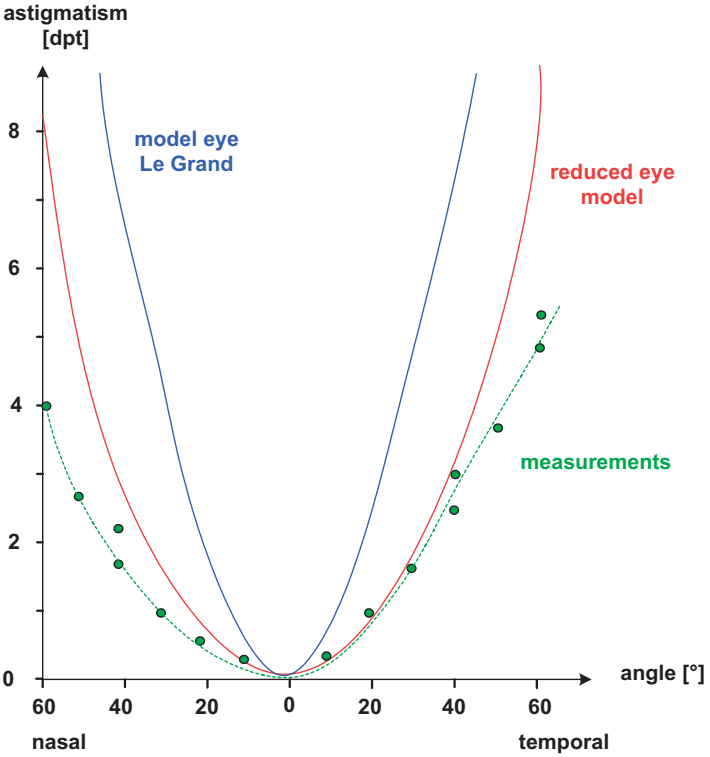

Figure 36-45: Astigmatism, measured and calculated for two model eyes.

36.6.4 Chromatic Aberrations

The natural dispersion of the media inside the system of the eye results in an axial chromatic aberration. This effect is also called a chromatic difference in the refraction of the eye. An image on the retina, which is sharply focused in the green range (550 nm) is myopic by –1 to –2 dpt in the blue range (480 nm) and +0.5 dpt hyperopic in the red (656 nm). This chromatic defect is especially large in the blue range. It can be recognized very easily. If the eye is accommodated on a green spot light, the blue light signals are blurred. The axial chromatic aberration shows only very small statistical distributions and is nearly constant for all people.

In the real eye, the worse imaging effects in the blue are partly suppressed by a yellow absorbing pigment in the macula and a lack of S-cones in the fovea. Figure 36-46 shows the axial chromatic aberration of the human eye [36-6].

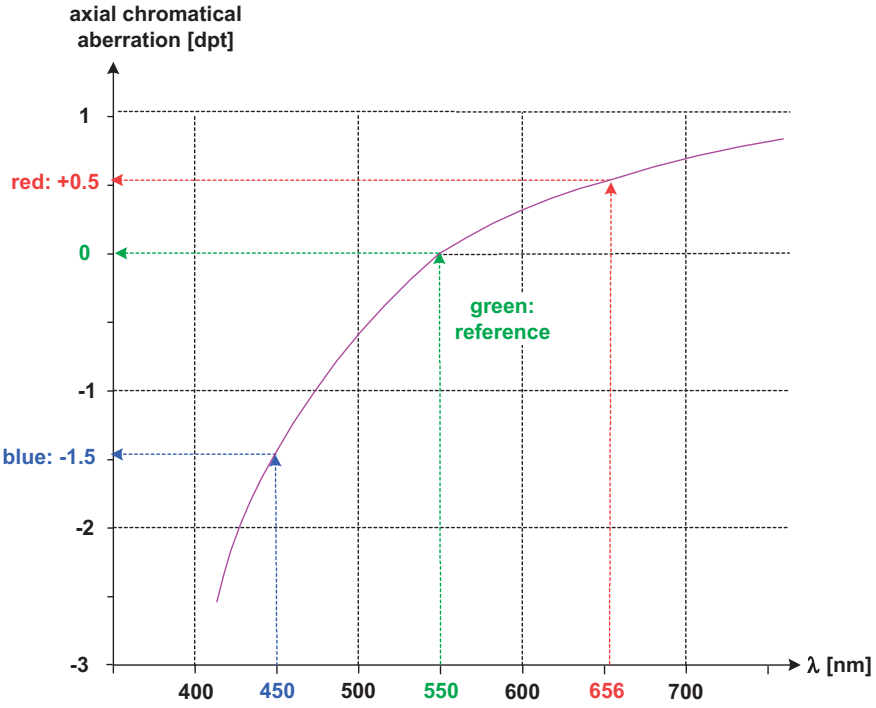

Figure 36-46: Axial chromatic aberration of the eye.

The residual axial aberration causes a considerable effect on the spectral intensity of the retina. If the eye is focused at $\tilde{\omega}$= 550 nm in the green, the defocusing in the red range has a value of +0.5 dpt and in the blue the image is defocused by –1.5 dpt. This spectral defocusing is illustrated in figure 36-47. This spectral effect always take place, independent of the spectral sensitivity of retinal detection.

Due to the special treatment of blue light and also due to the spectral sensitivity of the cones, axial chromatic aberration has almost no impact on the resolution of the eye.

The accommodation for far distant objects is done by the eye preferentially in the red range at 685 nm. This wavelength lies significantly far from the spectral sensitivity maximum. If the object is located nearer to the eye, shorter wavelengths are used to accommodate [36-11]. Figure 36-48 shows the change in the wavelength, which is used for accommodation setting as a function of the object distance. This distance is also measured here in diopters.

The lateral chromatic aberration generates colored stripes or fringes at the edges of an object. This effect can be already seen in the centre of an image due to the

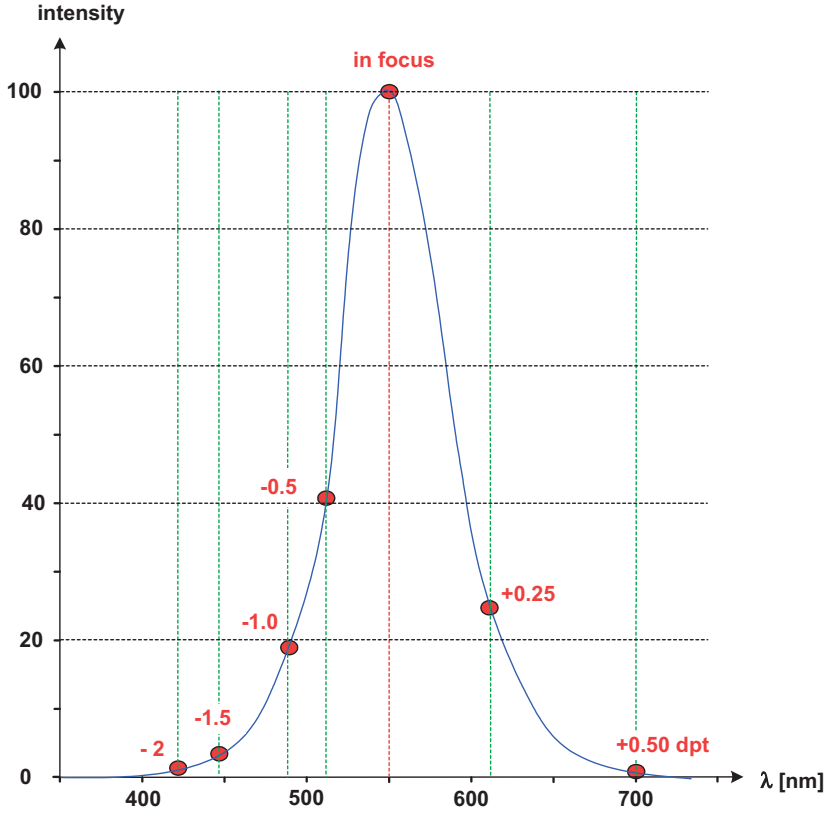

Figure 36-47: Spectral defocusing due to axial chromatic aberration.

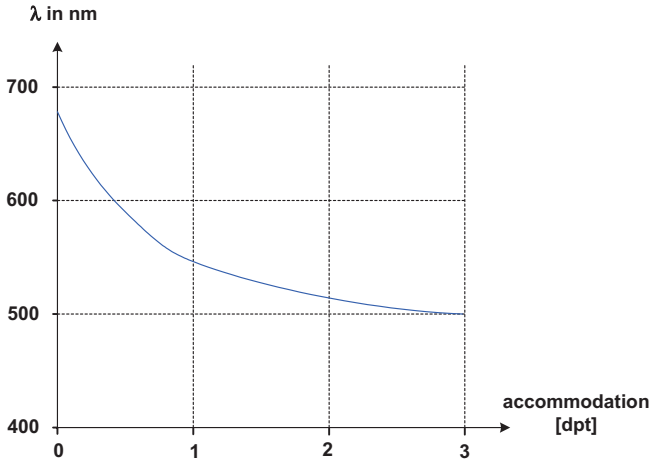

Figure 36-48: Change in the accommodation wavelength with the accommodation value.

off-axis use of the eye. In the fovea, this residual aberration has a size of approximately 36″ and therefore lies slightly beyond resolution.

The lateral chromatic aberrations depend on the height of the chief ray at the refracting surfaces, especially the outer cornea surface. In the human eye, the distance between the pupil and the nodal points of the eye determines this height. Values deviating from the nominal value of 5.7 mm cause an increase in the lateral chromatic color aberration with a slope of 0.037%/mm. Figure 36-49 shows the increase in the lateral chromatic aberration with the distance between the pupil location and the nodal point in the eye. This effect is called chromatic stereopsis and causes errors in the detection of object distances if, when using an instrument, the pupil of the system and the eye are not matched correctly. This effect also occurs if the pupil of the instrument forces a shift in the chief ray relative to the eye pupil position.

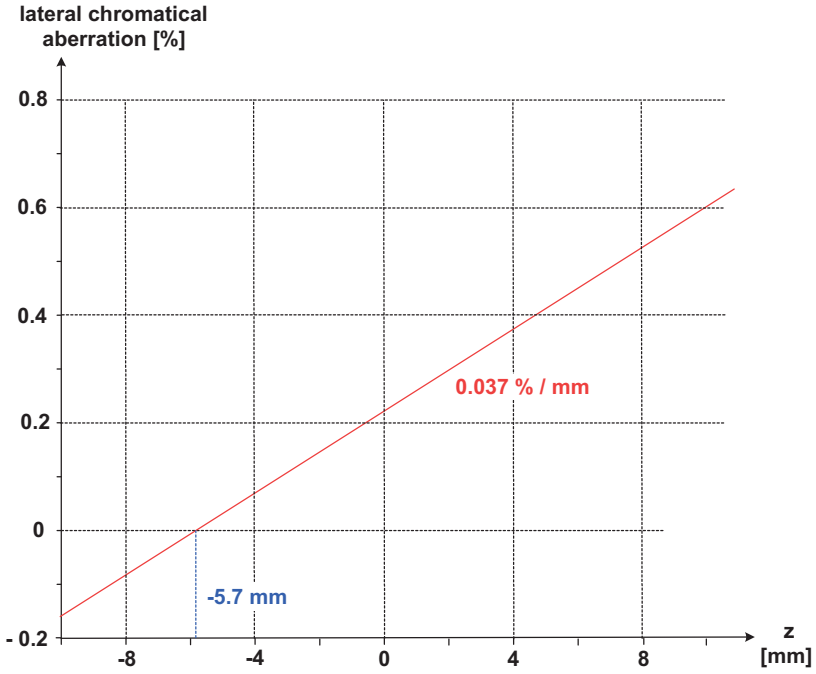

Figure 36-49: Lateral chromatic aberration of the eye as a function of the distance between the pupil location and the nodal point in the eye.

36.6.5 Modulation Transfer Function

If the modulation transfer function is used to describe the quality of the human eye, it is possible to incorporate the effects of the following:

1. The optical system.
2. Retinal detection.
3. The influence of neuronal signal processing.

Typically, the relaxed eye is accommodated for an object at infinity. Therefore the size of the field of view is scaled as an angle in degrees and the spatial frequency is measured in cycles per degree (cyc/°). According to the focal length of the eye and the fact that the image is situated in a medium with a refractive index of 1.336, the correspondence between this information and the real size of the retinal image is

$$10\ \text{cyc}/^{\circ} \ \leftrightarrow \ 33.3\ \text{Lp/mm}\,. \tag{36-20}$$

Under usual conditions in photopic vision with 3 mm pupil diameter, an emmetropic eye can resolve 100 Lp/mm on the retina at $\breve{\omega}$= 550 nm. The ideal value corresponding to the cone-pixel size is higher, but the statistical distribution of the cones and the residual aberrations and the diffraction reduce this to the above value. This normal vision corresponds to an angle resolution of 1′.

An empirical approximation of the modulation transfer function of the relaxed eye for $\breve{\omega}$= 550 nm as a function of pupil size and the field angle can be formulated as [36-23]

$$H_{\text{MTF}}(\nu) = (1 - C) \cdot e^{-A \cdot \nu} + C \cdot e^{-B \cdot \nu}. \tag{36-21}$$

In this equation, the spatial frequency $\breve{\varepsilon}$ is measured in cyc/° and the constants A, B and C depend on the pupil diameter and field angle, as indicated in tables 36-18 and 36-19 [36-24]. The parameters are optimized by fitting measured data and correspond to the mean contrast of the eye between the sagittal and tangential orientation of structures. Therefore, the data sets are not fully compatible. In principle, the parameters of the third row of table 36-18 and the first row of table 36-19 must coincide. This model of the modulation function contains the optical influences of the eye only; the properties of the retina sensors are not included.

Table 36-18: Dependence of the fit-parameters on the pupil diameter on-axis.

Diameter pupil [mm]	*A* [°]	*B* [°]	*C*
2.5	0.16	0.06	0.36
3	0.16	0.05	0.28
4	0.18	0.04	0.18
6	0.31	0.06	0.20
8	0.53	0.08	0.11

Table 36-19: Dependence of the fit-parameters on the field angle for a pupil diameter of 4 mm.

Field angle [°]	*A* [°]	*B* [°]	*C*
0	0.172	0.037	0.22
5	0.245	0.041	0.20
10	0.245	0.041	0.20
20	0.328	0.038	0.14
30	0.606	0.064	0.12
40	0.82	0.064	0.09
50	0.93	0.059	0.067
60	1.89	0.108	0.05

Figure 36-50 shows the monochromatic modulation transfer functions for a 4 mm pupil size for the relaxed case. If the eye accommodates to nearer object distances, the performance of the eye is reduced.

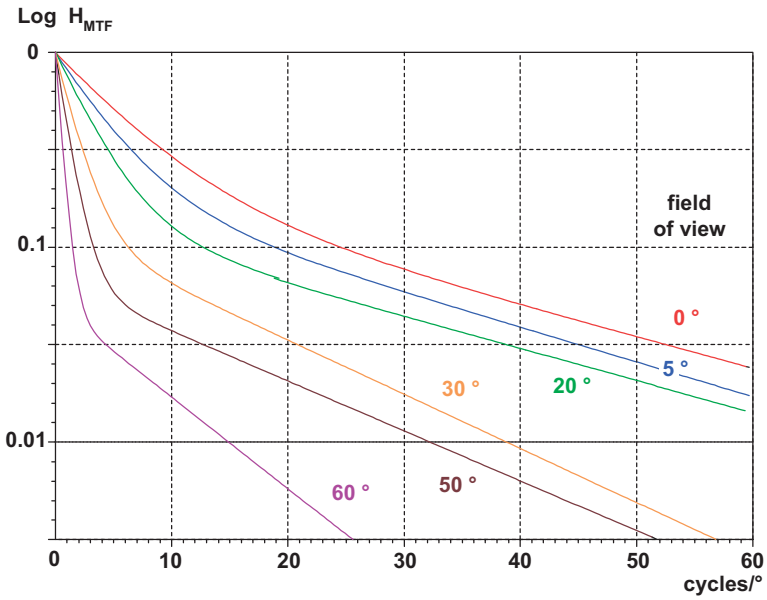

Figure 36-50: Monochromatic modulation transfer function of the human eye for different angles of the field of view for a pupil of 4 mm diameter.

Figure 36-51 shows the dependence of the visibility on the spatial frequency for the relaxed eye on-axis, white light, a pupil size of 2.5 mm and two object distances with the corresponding accommodation states on-axis. The diagram is generated by calculation with the help of the generalized relaxed eye model for polychromatic light.

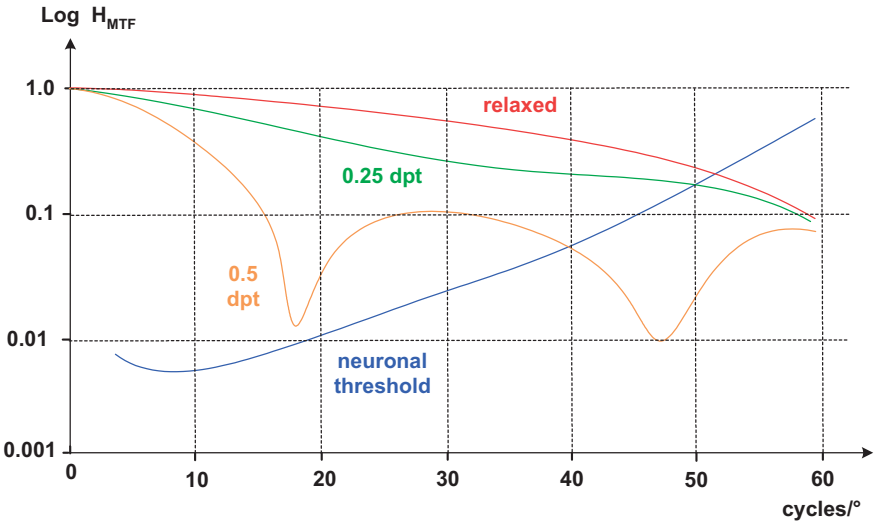

Figure 36-51: Polychromatic modulation transfer function of the human eye for different accommodation states.

The polychromatic modulation transfer function takes the lateral chromatic aberration into account. The behavior of this curve is different and shows a considerable impact of the field size on the performance due to the lateral color aberration. Figure 36-52 shows some modulation transfer functions incorporating the lateral color, calculated in the generalized reduced eye model [36-3].

It should be noted that there is a threshold visibility for the human retina, which depends on the brightness and the spatial frequency [36-25]. The corresponding curve is shown in figure 36-51. It is also called the aerial image modulation contrast (AIM) or is used as the reciprocal contrast sensitivity function (CSF). Higher spatial frequencies need a significantly higher contrast to be resolved. For the determination of the real modulation transfer this effect must be taken into account. It is only the difference between the optical contrast curve and the threshold contrast which is useful and which improves the visibility of details.

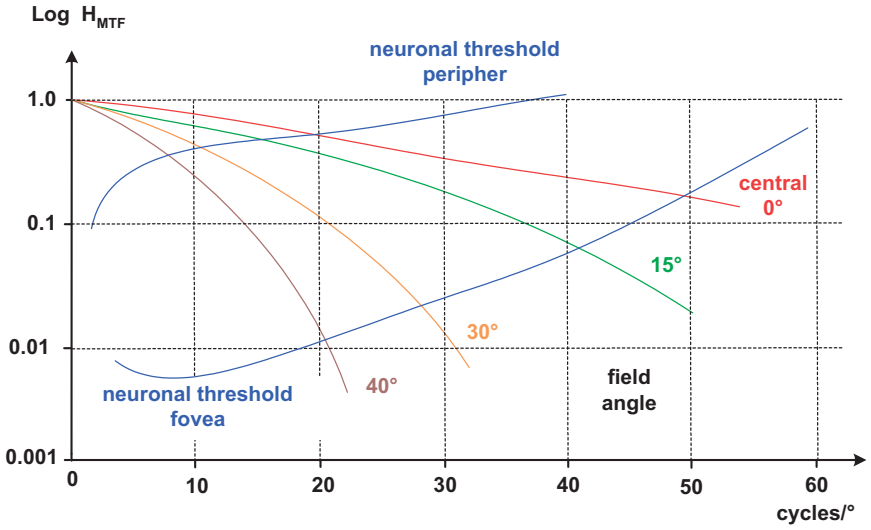

Figure 36-52: Polychromatic modulation transfer function of the human eye for different locations in the field of view.

If the pupil diameter is enlarged, the modulation transfer function changes dramatically. The performance of the eye decreases with increasing pupil width due to spherical aberration. This is shown in figure 36-53 for illustration.

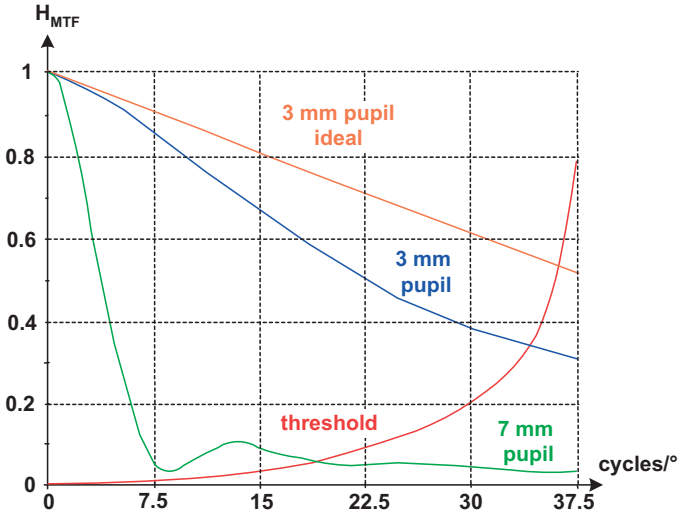

Figure 36-53: Monochromatic modulation contrast of the eye for $\breve{\omega}$= 550 nm and pupil sizes of 3 mm and 7 mm. For a 3 mm pupil size, the perfectly corrected case without spherical aberration is shown for comparison. The red curve shows the threshold contrast.

Figure 36-54 shows the combined effect of the discrete nature of the cone structure of the retina and the Nyquist limit of the neuronal Ganglion cells as a function of the field size. The pure optical performance is also indicated for comparison [36-3]. The resolution decreases with increasing field angle, since the pooling effect of the cone cells generates a lower Nyquist resolution limit for larger field angles. On the other hand, the detection limit of the cones due to the finite contrast sensitivity decreases only slightly with the field angle. Between these two limits, a broad zone of aliasing occurs. This shows that the resolution of the eye for finite field angles is primarily determined by the resolution of the detection and not by contrast sensitivity.

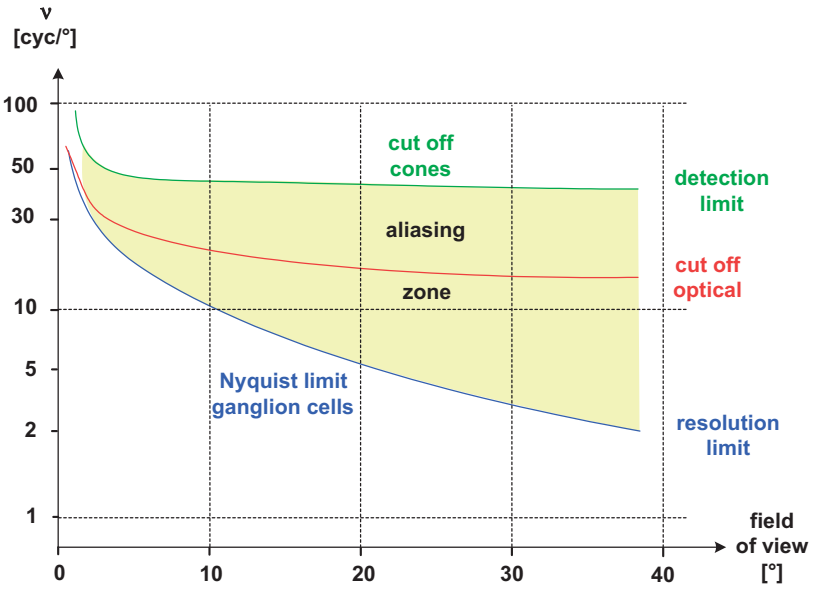

Figure 36-54: Neuronal, optical and retinal limits of the modulation transfer in the eye as a function of the field of view.

The limiting threshold contrast sensitivity of the eye depends on the brightness and the field position. This is due to the distribution of the rods and cones on the retina and a clustering of sensors dependent on the radiance. Figure 36-55 shows this threshold contrast as a function of the spatial frequency for various values of the radiance on-axis. Figure 36-56 shows the threshold contrast sensitivity as a function of the spatial frequency for photopic vision at several field positions according to [36-26].

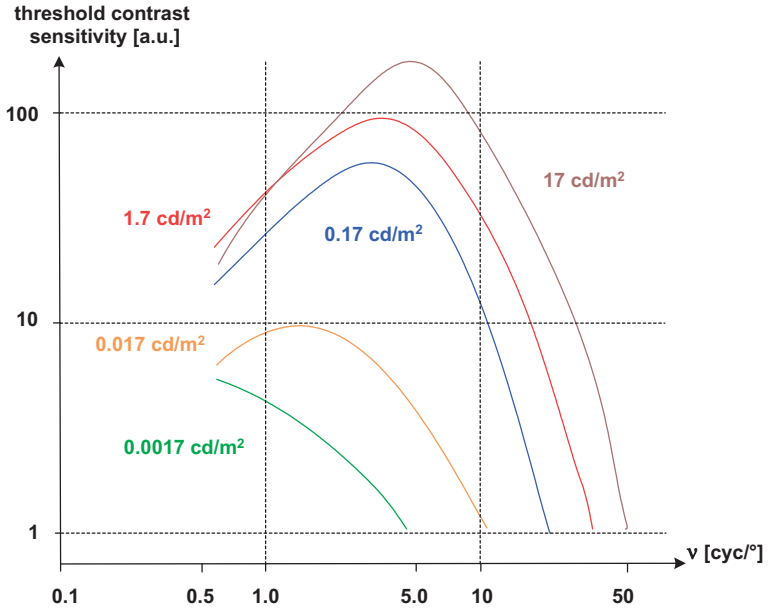

Figure 36-55: Threshold contrast sensitivity as a function of the spatial frequency for several values of the brightness on-axis.

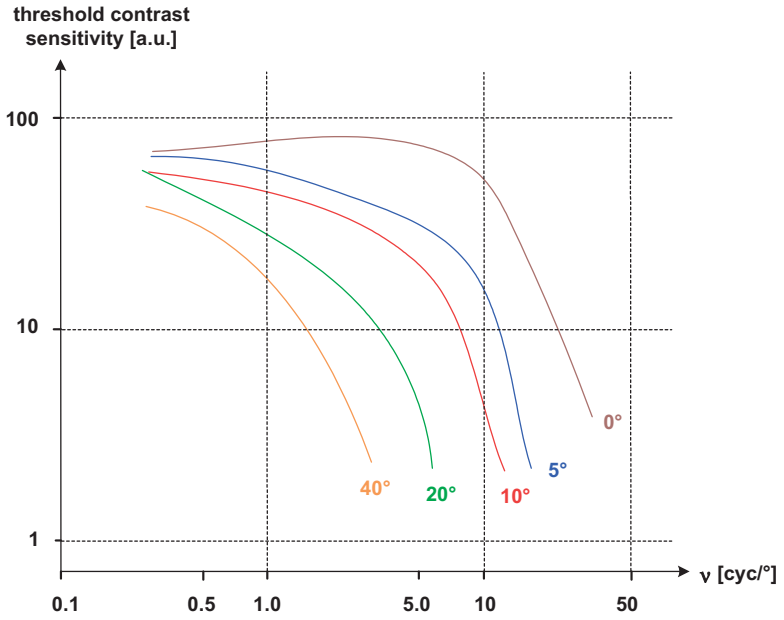

Figure 36-56: Threshold contrast sensitivity as a function of the spatial frequency for several values of the field angle for photopic vision.

36.6.6 Visual Acuity

The resolution of details in an object is called the visus or the visual acuity. The relative possibility to recognize object details of the angular size w by the eye defines the visus

$$V = \frac{1'}{w}. \tag{36-22}$$

For $\tilde{\omega}$= 550 nm, a typical object can be resolved by a healthy eye under bright illumination and observation in the fovea down to an angle size of approximately 1′. This corresponds to a visus of 1. All situations in which there are some problems with vision have a visus of $V < 1$.

In real life, the visus is determined by observing a standardized shape under normalized conditions for different distances z. Figure 36-57 shows two accepted symbols, which are used to measure the visus of patients. Part a) shows a ring shape with an opening according to Landolt. The ring is positioned with increasing distance to the observer and is rotated in the azimuth. If the resolution is poor, the patient cannot decide on the azimuthal angle of the gap. The corresponding distance allows a quantitative determination of the visus. This is a subjective measurement of the performance of the eye.

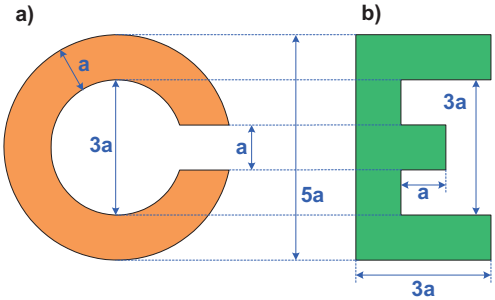

Figure 36-57: Geometry of a) the Landolt ring and b) the standard letter E.

The visus of 1 is measured in a standard situation corresponding to the data of figure 36-58. The block letter 'E' with a size of 8.9 mm is observed at a distance of 6.096 m, the size of the image on the retina is 25 µm. This corresponds to approximately 2 cones per length scale a of the letter structure.

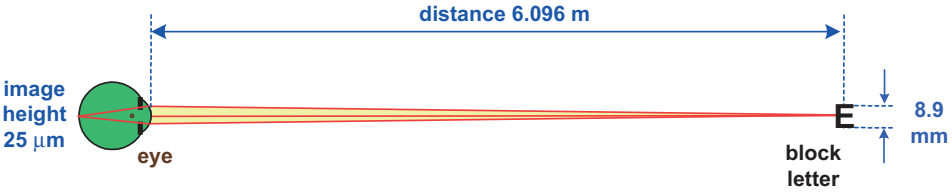

Figure 36-58: Definition of the visus 1 by observing the norm letter E under standardized conditions.

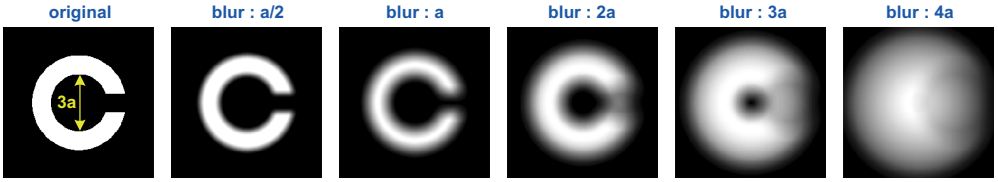

Figure 36-59: Image of the Landolt ring with increasing blur.

Figure 36-59 shows some examples of blurred Landolt rings. If the distance is too large, the finite quality of the eye produces a blurred shape. The size of the blur is scaled with the parameter a of the geometry. In the case of blur $2a$, the gab can still be seen, in the case of $3a$, it is not really possible, although an asymmetry can be recognized.

The visus is directly proportional to the distance of the object. A scaling of this criterion therefore satisfies the equation

$$V_{\text{norm}} = \frac{s_{\text{real}}}{s_{\text{norm}}} \cdot V_{\text{real}} \,. \tag{36-23}$$

An appropriate scaling is valid for larger angular fields of view. Generally, the visus is higher in binocular vision in comparison with monocular sight. Simulations of the retina image and an estimation of the corresponding visus can be found in the literature [36-27].

36.6.7 Resolution

A first consideration of the resolution of the eye uses the two-point resolution criterion. Figure 36-60 shows the corresponding geometry. It is simply assumed that two points can be resolved, if they fall onto different neighboring cones in the fovea. If a cone distance of 4 µm is assumed and the object is located at the normalized distance $s_0 = 250\,\text{mm}$, where the length $L = 22\,\text{mm}$ of the eye defines the limiting resolvable angle, we obtain

$$\hat{\imath}_c = \frac{\text{''}\, x'}{L} = 1'. \tag{36-24}$$

This corresponds to a separation of

$$\text{''}\, x'_c = s_0 \cdot \hat{\imath}_c = 75\,\mu\text{m} \tag{36-25}$$

of the two points at the normalized distance of 250 mm.

There are several different influences on which the visual acuity depends. These factors are, for example,

1. Geometry: Shape of the resolved details.
2. Physical: Radiance and color.
3. Optical: Quality of the image on the retina.

4. Anatomic: Age, conditions on the retina, other non-optical defects.
5. Physiological: Adaptation, status of the optical nerve.
6. Psychological: Attention, habitation and experience.

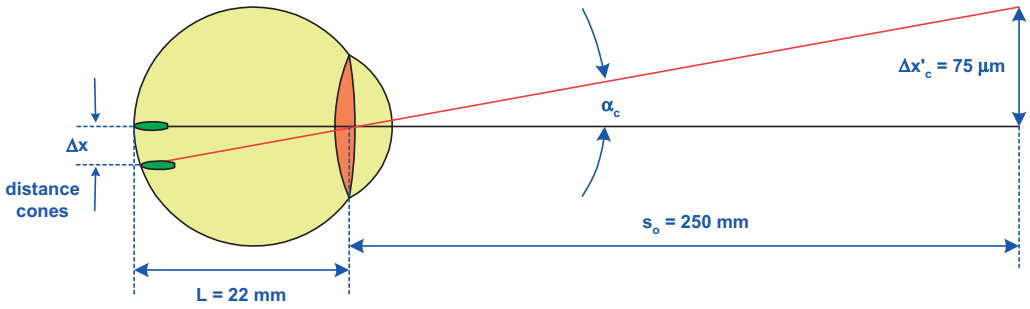

Figure 36-60: Explanation of the resolution of the eye. The angles are extremely exaggerated.

Generally, due to the optical system of the eye and the structure of retinal detection, the visual acuity decreases with increasing field of view. Furthermore, it depends on the color, the radiance and the accommodation of the eye.

There are some rather different conditions for human vision resolution, depending on the shape of the object.

a. **Pattern recognition**
   The human eye can resolve and recognize black letter shapes on a white background corresponding to a spatial frequency of 30 cyc/° or 5′.
b. **Grating resolution**
   Resolution of black-and-white bar patterns with rectangle or sinus-modulation. In the best case the eye can resolve 60 cyc/° corresponding to an angle of 2′.
c. **Two-point resolution**
   The human eye can resolve two black points on a white background, which are separated by 1′. If the colors are inverted, the resolution is half the size.
d. **Vernier or nonius acuity**
   The separation and resolution of two small parallel straight lines is possible up to a separation of 10″. This is a rather high value and lies below the structure size of the cones which is approximately 19″. This shows that the eye is able to determine the centroid of a corresponding light distribution over several cones very precisely.
e. **Stereoscopic resolution of depth**
   The angle resolution, which is necessary in order to get a stereoscopic impression of depth lies in the range of 5″. This is the binocular acuity and is the highest resolution which the eye possesses.

In figure 36-61, these different conditions of resolution are shown for illustration. The differences in the resolution limits are not easy to understand. One reason, which must be taken into account, is the mosaic structure of the retinal cone distribution. The sensoric elements therefore show a coarseness, which is similar to the discrete structure of an electronic detector.

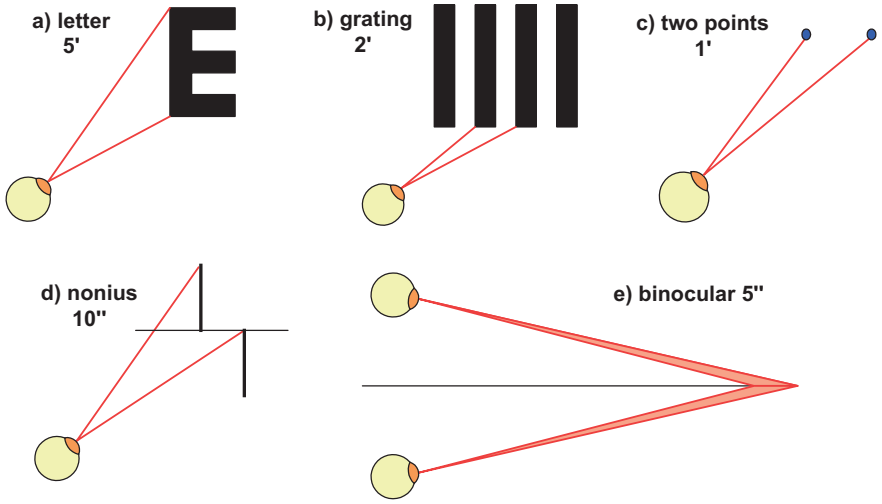

Figure 36-61: Different conditions for visual resolution.

As mentioned above, the visual acuity and the angle resolution depends on several parameters. Figure 36-62 shows four of these dependencies. In a) the increase in the acuity with contrast is shown. In b), it can be seen how the acuity reduces if the signals rapidly changes with time. In c), the dependence of the resolution on the radiance is shown: a brighter signal can be better resolved. In d), the reduction in the resolution with the age of the eye is shown. Several reasons contributing to the degradation of the whole system are responsible for this change. The acuity is drawn on a logarithmic scale. Since the curves are the results of measurements under slightly different conditions, the absolute values are not directly comparable [36-3].

The dependence of the angular acuity on the radiance is shown in figure 36-63 in more detail.

The structure of the retina with the various ranges of cone and rod detection and the blind spot causes a dependence of the angle acuity on the location on the retina. Figure 36-64 shows this behavior [36-6].

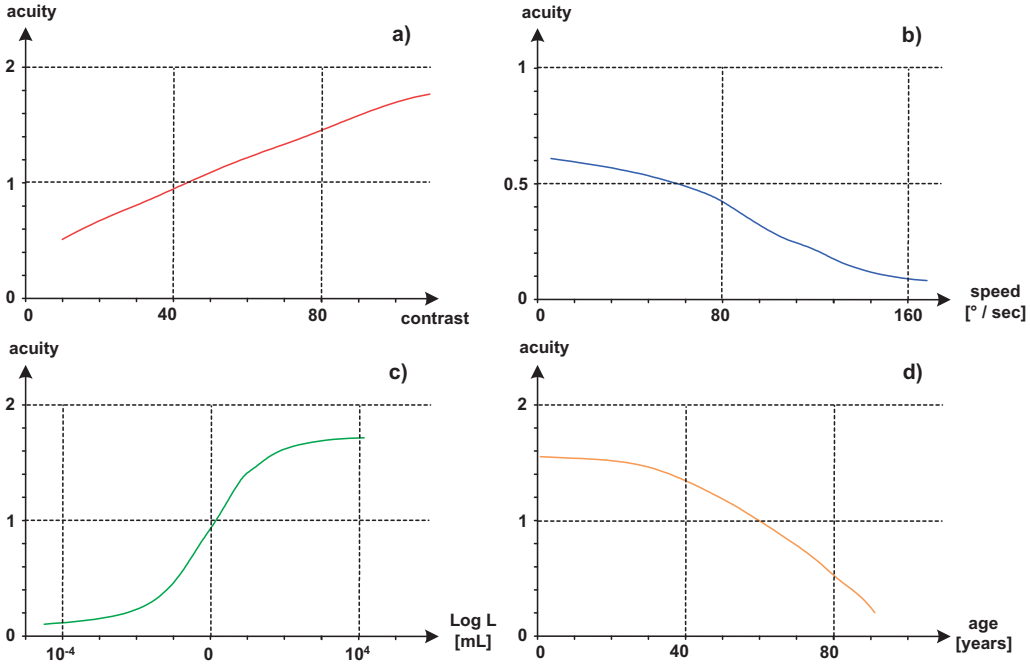

Figure 36-62: Various dependencies of the visual acuity *V*. Shown are the dependencies on the visibility a), the speed b), the radiance c) and the age d).

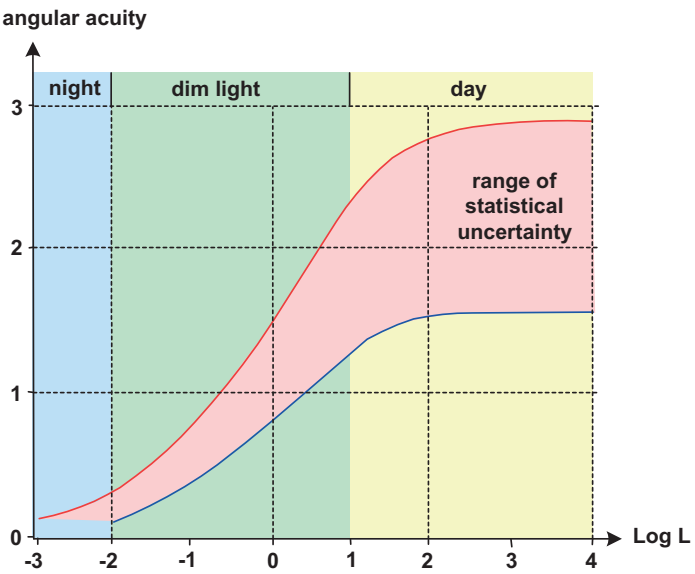

Figure 36-63: Acuity of the eye as a function of the radiance.

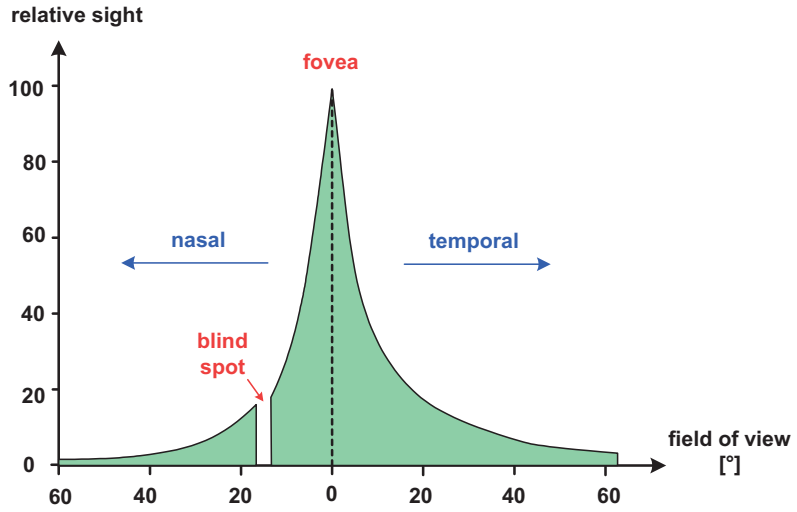

Figure 36-64: Change of relative sight as a function of the position on the retina.

36.6.8 Stray Light

Stray light inside the eye causes a reduction in the contrast and a decrease in the resolution. There are several reasons for the generation of stray light in the eye. The most important sources of stray light are as follows:

1. The outer surface of the cornea (contribution of approximately 25%).
2. Reflection at the retina (25%).
3. Scattering in the structure of the crystalline lens. This effect is particularly pronounced when a cataract is present.
4. Volume scattering effects in the anterior chamber or in the vitreous humor.
5. Residual transmission in the outer zones of the iris diaphragm.

Typically, due to aging effects in the media, the stray light level increases during a lifetime by a factor of 2 to 3.

36.6.9 Measuring the Performance of the Eye

There are several methods which are used to measure the standard of performance of the eye.

In the more subjective methods, the patient must give his impression of the particular resolution or quality of the perceived object. Test charts with normalized patterns are presented at different distances and conditions. The resolution of the details is analyzed by discussion and subjective information. Usually, the defects of the eyes are compensated by Phoropter systems which measure only the residual errors.

In the objective methods, several different concepts are used to analyze the optical quality using external instruments such as ophthalmometers, refractometers or sciascopes.

The most important basic techniques used by these instruments are listed in the following:

1. Psycho-physical measurement of the visibility:
   A sinus grating is projected onto the retina and the visibility is detected.
2. Ophthalmoscopic double-pass method:
   A point object is projected onto the retina. The spot on the retina is imaged back using a detection system outside of the eye. The external measured point spread function is used to analyze the wavefront, which passes the eye.
   The problem with this method lies in the consideration of the double pass, where the asymmetrical aberrations are cancelled and the complicated scattering behavior of the retina has an impact on the result. Due to the layered structure of the retina, the origin of the back-scattered light comes from different depth locations and therefore has partially coherent properties. The circumstances are more convenient when the illumination used to generate the spot has a small numerical aperture and the total aberration comes mainly from the back-directed light with the full numerical aperture of the eye.
3. Measuring the wavefront:
   This is very similar to method 2. The light of the spot on the retina is analyzed by a wavefront-measuring technique. For example, a Hartmann–Shack sensor can be used to detect the quality of the outcoming wavefront.

36.7 Binocular Vision

36.7.1 Introduction

If both eyes are used, we have so-called binocular vision. There are three types of binocular vision, which can be distinguished.

1. Without fusion:
   Both eyes produce a separate impression.
2. With fusion:
   Both eyes produce a separate picture, but both pictures, although slightly different, are merged in the brain to form a common impression.
3. With fusion and 3D impression:
   In addition to 2., the brain uses the common information to form an impression of depth. This is called stereopsis and provides additional information.

Figure 36-65, shows the principle of binocular vision. Both eyes are rotated towards one another, which is the so-called vergence. Therefore, the object point is

seen by both eyes, but from a slightly different angle. This angle difference produces the impression of distance, the basis for which is the interpupillary distance. As can be seen in figure 36-66 [36-16], the field of view of both eyes is also different with a significantly overlapping part. Binocular stereoscopic vision is only possible in this common part of the field of view, which has a size of approximately 140° in the horizontal direction.

The fusion of the two images from the right and left eye channel can only be achieved if the region of overlap is large enough and the difference between the two separated images is not too great. If the two images are quite different, the common image disintegrates and no stereoscopic effect occurs. As a rule of thumb, the lateral deviations of the object detail should not exceed 1/30 of the total width of the image. Differences within this range can be integrated by the brain into a common image.

Stereoscopic vision can also be generated synthetically by the images produced by two cameras. If both channels show the same differences as those obtained in natural observation, a stereoscopic impression will be produced.

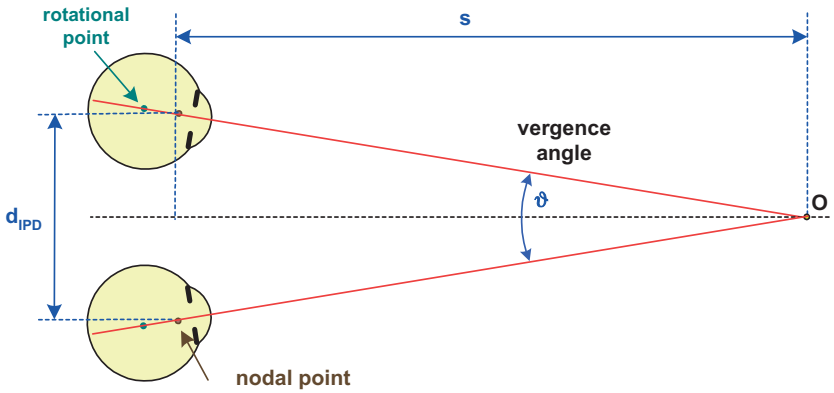

Figure 36-65: Principle of stereoscopic vision and vergence of the eye axis.

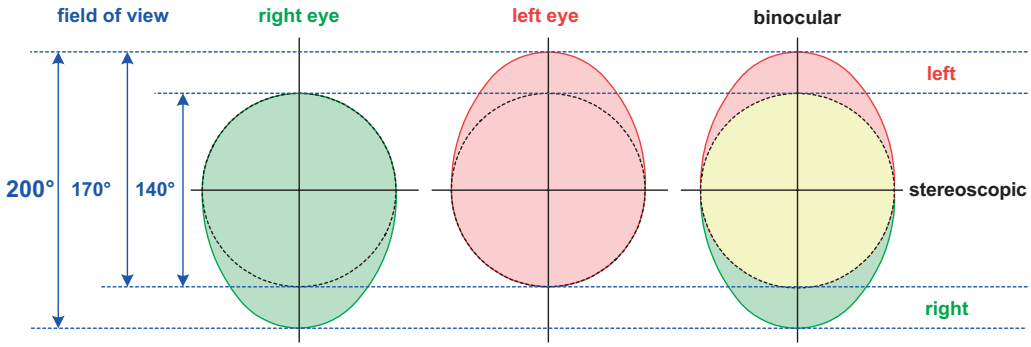

Figure 36-66: Field of view in binocular sight.

36.7.2 Convergence

For binocular vision, the axes of both eyes are not parallel. There are three types of movement of the eye and corresponding axis directions which can be distinguished.

1. If the axes are rotated inwards in the horizontal cross-section, both eyes are oriented towards a common object point. This is called vergence and is necessary for binocular stereoscopic vision.
2. If both axes are moved outwards in the horizontal cross-section, the position is called divergence.
3. If both eyes are moved in the vertical direction with reversed sign, they produce a dipvergence.

Figure 36-67 illustrates these different cases of axis orientation.

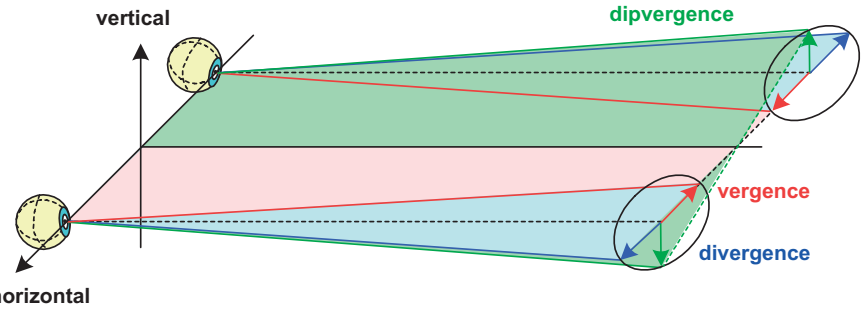

Figure 36-67: Principle of stereoscopic sight.

During a short time period of approximately 0.2–0.6 seconds, the eyes adjust the right vergence angle to focus on a distant object. The angle corresponds to the distance of the object respective to the pupillary distance of the eyes. Therefore the accommodation and the vergence are coupled. Figure 36-68 shows the relationship between these two measurements [36-3]. If the vergence angle is too large or too small, the difference between the right and the left image is too large and no stereoscopic vision is possible. The necessary vergence angle depends on the pupillary distance. The corresponding lines in the distance–convergence diagram of the figure are called the lines of Donders. In the orange zone, a fusion of the images is possible. However, in the yellow ranges, the images suffer from blur and are disintegrated. This relates to the fact that stereoscopic vision is only possible over a certain range of distances. If the distance is too large, the difference between the two images is too small. If the distance is too small, the differences between the images is too large.

A certain object distance may be given and the corresponding vergence of the eye is adjusted. The points of the field of view, which allow fusion of the images, are called correspondent and they are located on the so-called horopter surface. All other points with too large transverse deviations outside this region are called disparate.

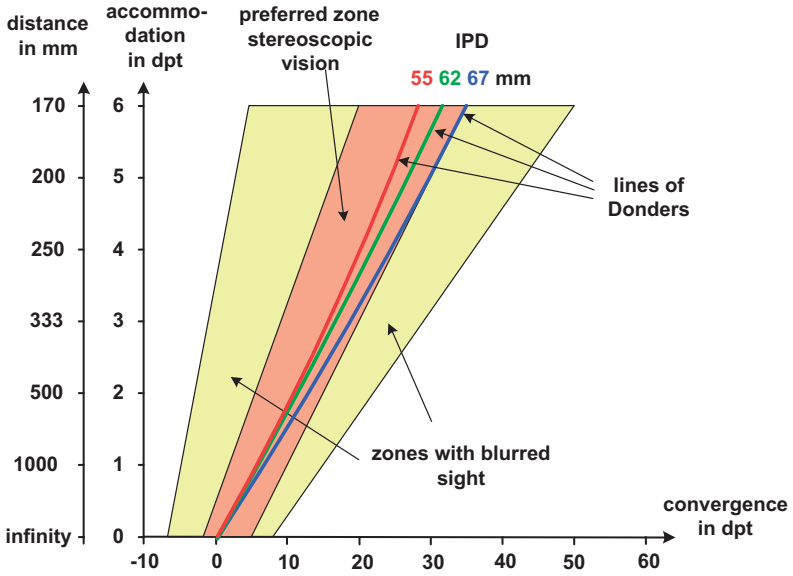

Figure 36-68: Distance–convergence diagram. The colored lines correspond to the ideal values and are called the lines of Donders. Stereoscopic vision can be achieved in the orange region.

There are two different types of region for vertical and horizontal disparate points. Usually, due to the position of the eyes, only the horizontal direction allows for depth discrimination. Figure 36-69 shows an illustration of the region of possible

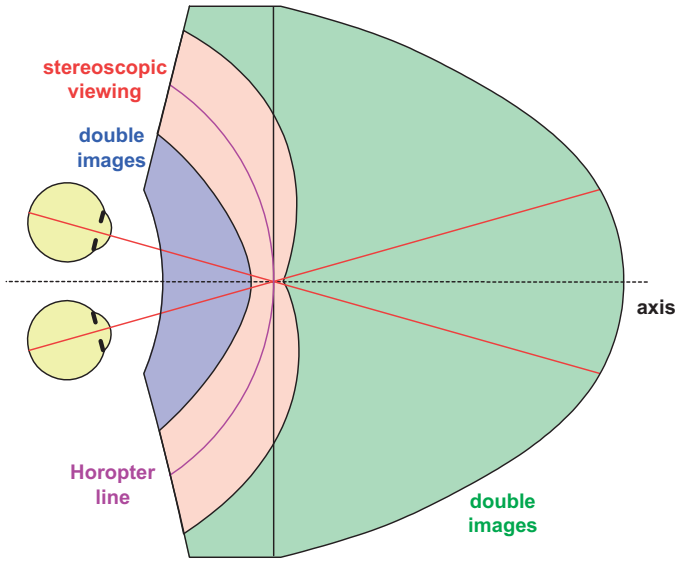

Figure 36-69: Region of stereoscopic vision.

stereoscopic vision. On a hypothetical surface in front of the eyes, the images lies on corresponding points of the fovea. The intersection of this surface with the horizontal plane is called the horopter line. Around this line, the so-called panum region allows for stereoscopic vision. For points with greater distance, the difference between the images is too small, for points with a smaller distance, the difference between the images is too large for successful fusion. The corresponding regions are indicated in figure 36-69 by different colors.

36.7.3 Stereo Vision and Depth Discrimination

The resolution of depth information in stereoscopic vision is only possible due to the difference between the two images from the right and the left eye channels. A small lateral deviation occurs, which allows the brain to separate the information. If s is the distance from an object, the angle of convergence is given by

$$\vartheta = \frac{d_{\mathrm{IPD}}}{s}\,. \tag{36-26}$$

The corresponding geometry is shown in figure 36-70.

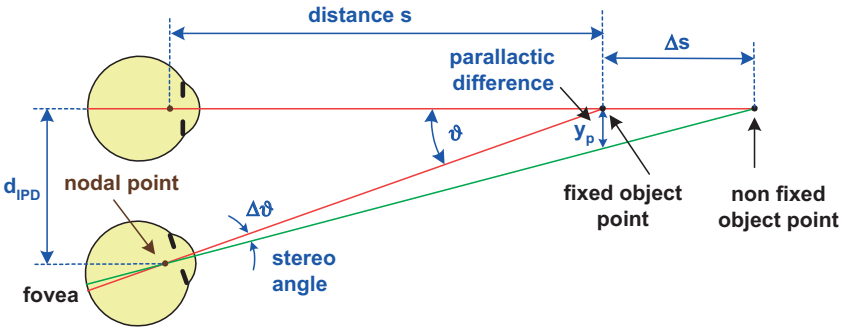

Figure 36-70: Principle of stereoscopic vision.

If the lateral deviation is given by y_p and the depth difference is small compared with the absolute distance s $s \ll s$, the relation

$$\vartheta = \frac{y_p}{s} \tag{36-27}$$

is valid. The smallest stereo angle which can be resolved and which allows stereoscopic vision is called the stereo resolution limiting angle. It lies in the region of 10″ under appropriate conditions. The limiting difference of the stereoscopic angle corresponds to

$$\vartheta_{\min} = \frac{y_p}{s}. \tag{36-28}$$

From these equations, we get the relation

$$''\vartheta_{\min} = \frac{d_{\mathrm{IPD}} \cdot ''s}{s^2} \tag{36-29}$$

from which the resolvable depth can be determined. If, for example, a distance of $s = 1$ m is considered and a limiting angle resolution of $''\vartheta = 10''$ is assumed, we get a depth of $''s = 0.8$ mm, which can be resolved.

This critical angle depends on the radiance. The corresponding function is illustrated in figure 36-71.

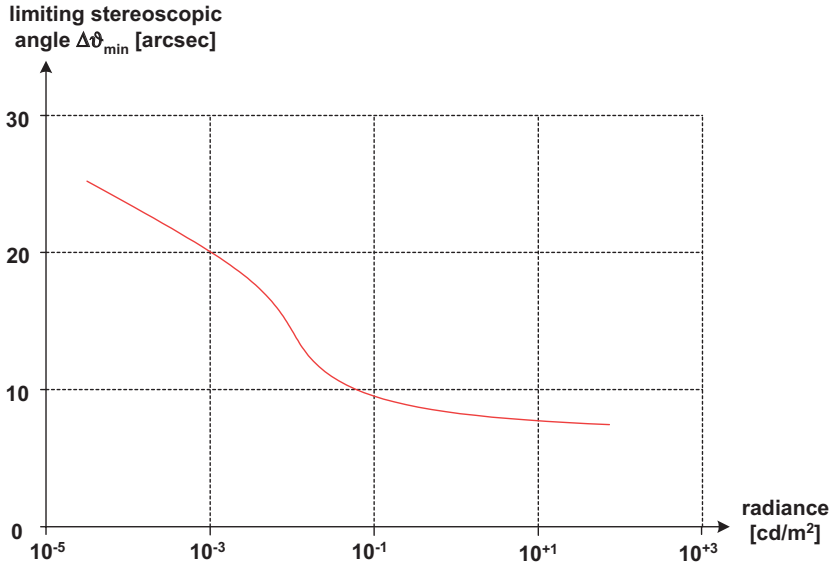

Figure 36-71: Dependence of the critical angle of stereoscopic vision on the radiance.

Stereoscopic vision gives an impression of depth. If the conditions are appropriate, stereoscopic vision results in a depth resolution. There are several aspects which contribute to the impression of depth. The following list contains various aspects which assist in the discrimination of depth and which are also present for monocular vision without fusion of the images:

1. Geometrical perspective.
2. Sharpness of contour lines.
3. Distribution of light and shadow.
4. Coverage of objects.
5. Parallax of movement.
6. Impulse of convergence of the eye.
7. Impulse of accommodation of the eye.
8. Size of images and experience.

36.8
Eye Defects

36.8.1
Introduction

There are several different causes of eye disease which may involve either the optical system of the eye or retinal detection.

Figure 36-72 compares some typical cases. In a) a typical refraction aberration is shown. This is the main problem for which spectacles are used. A simple myopic or hyperopic eye, spherical aberration or astigmatism fall within this area. In b) the visual impression produced by glaucoma is shown. Here the field of view is reduced due to a degeneration of the macula. As a special phenomenon, in c), particular defects of the retina produce black areas in the field of view and a decrease in resolution and contrast within the visible parts. If the eye has a cataract, a strong scattering and absorption effect reduces the contrast of the imaging. The appearance of the image in this case is shown in part d) .

In this chapter, the discussion of eye defects concentrates on refraction errors. An eye is called emmetropic, if the vision is good and without defects. This means that the far point is at infinity, there is no abnormal color impression and there is no astigmatism or stronger defect of refractive power or spherical aberration. In particular there is no conic-like topography of the outer corneal surface, known as keratoconus. If the eye does have one or more of these defects, it is called ametropic. All of these defects are quantitatively described by modern more sophisticated schematic eye models.

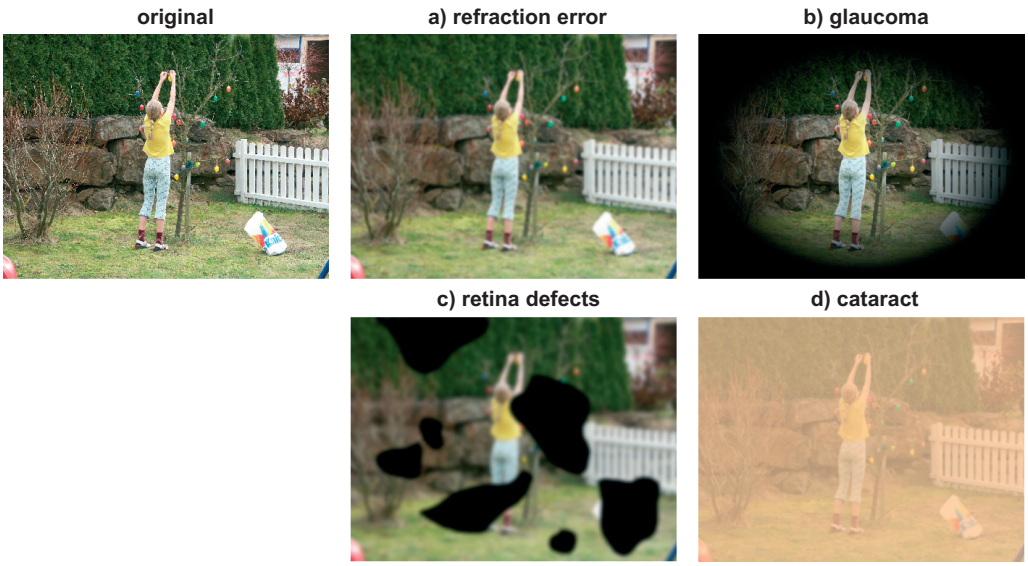

Figure 36-72: Original object and four different examples a) to d) of eye diseases.

36.8.2
Myopia

If an eye is myopic, only close objects can be seen sharply and with good resolution. Accommodation fails to adjust for more distant objects. The reason for this effect can be an eye-ball which is too long, too short a radius of curvature of the cornea, or an eye lens with a very short focal length. Figure 36-73 shows these three cases of myopia. The correction of this problem can be by means of spectacles with a negative refractive power.

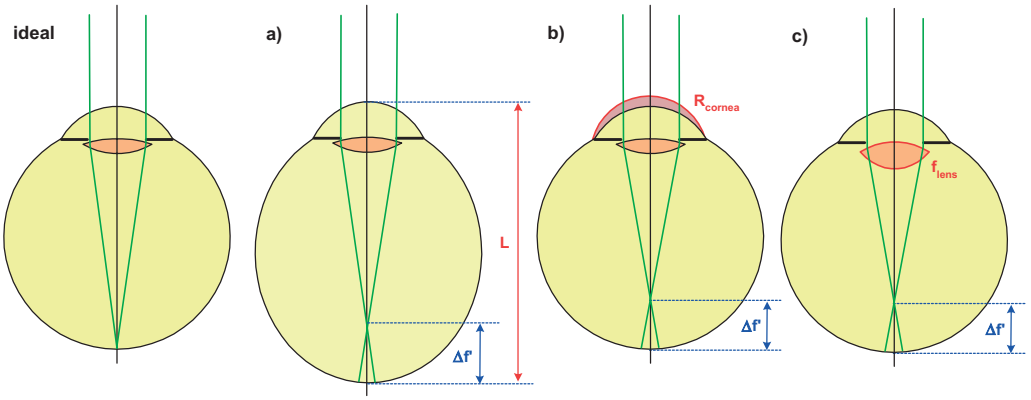

Figure 36-73: The three most important reasons for myopia. In case a) the eye-ball is too long, in case b) the curvature of the cornea is too large, and in case c), the refractive power of the eye lens is too large. The first diagram shows an ideal eye.

Since natural accommodation results in a shorter focal length of the eye lens, myopia can therefore be corrected with the help of an additional lens. Due to the sign of the effect it is not possible to compensate for myopia by accommodation. If no correction lens is used, the accommodation reduces the visus of the eye as can be seen in figure 36-74.

If the radiance is low for scotopic vision, a natural myopia of the eyes due to adaptation occurs. The reasons for this night-myopia are the immobile position under low radiance and the chromatic shift of the best accommodation.

36.8.3
Hyperopia

An eye is called hyperopic, if only far distant object can be seen sharply. The eye-ball may be too short, the refractive power of the eye lens too small or the cornea has a radius of curvature, which is too large. Figure 36-75 shows these cases for illustration.

If the eye is accommodated, this refraction error can be compensated. But the dynamic range of the accommodation is reduced in this case.

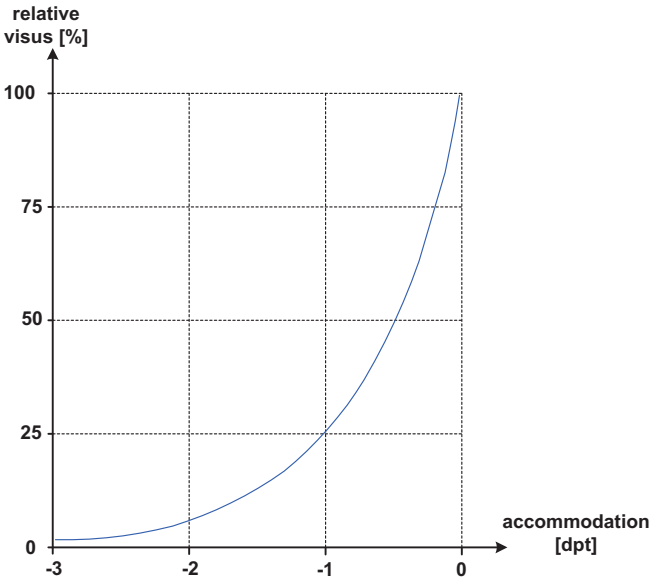

Figure 36-74: Reduction of the visus performance of the eye due to accommodation or defocus.

This type of refraction error in principle occurs in higher ages automatically, since the refractive power of the eye lens is reduced. This effect is called prespyopia.

The correction of hyperopia is possible with a positive lens, which helps to shift the far point correctly.

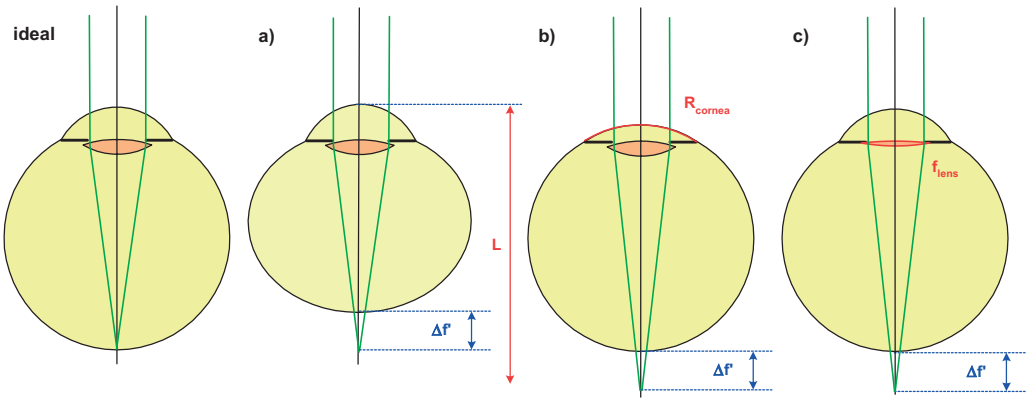

Figure 36-75: The three most important reasons for hyperopia. In case a) the eye-ball is too short, in case b) the curvature of the cornea is too small, and in case c) the refractive power of the eye lens is too small. The first diagram shows an ideal eye.

36.8.4 Astigmatism

If the refractive power of the eye is different in the horizontal and the vertical cross-section, this is known as astigmatism. In most cases this defect results from different radii of the cornea. Usually the refractive power is larger in the vertical section. The correction of this aberration is only possible with a toric lens. For the description of this refractive error, the amount of astigmatic difference and the location of the azimuth are necessary. It is also possible to correct the astigmatism of the cornea by using hard contact glasses which force the cornea to adjust the radii of curvature. Only a small residual error due to a tear film usually remains.

36.8.5 Aniseikonia

If two eyes have different focal lengths, the magnification will be different. This results in two different sizes of the image and causes problems in binocular vision. A problem of this type is called aniseikonia.

The correction of this effect is possible with quite thick meniscus-shaped spectacles.

36.8.6 Color Aberrations

There are three major cases of chromatic problems with the human eye. They are:

1. Anomal trichromasy
   In this case, one of the cone receptors are weak, there is a perturbation of the equilibrium of the three color perceptions. The overall color impression is somewhat strange in this case, but is not registrated by the individual due to a lack of comparison.
2. Partial color blindness, dichromasy
   In this case, the eye is completely blind to one of the main colors. This kind of problem is quite rare.

   A particular variation of this problem is red-green blindness. The patient cannot distinguish between these two colors. Figure 36-76 shows a test chart for this kind of defect. With correct vision, the word 'ARMEE' is seen, in the case of red-green blindness, the reader sees the word 'ZIVIL'.
3. Monochromasy
   If the eye has no ability to distinguish any colors, the person is completely color blind. For genetic reasons, this effect only occurs in males.

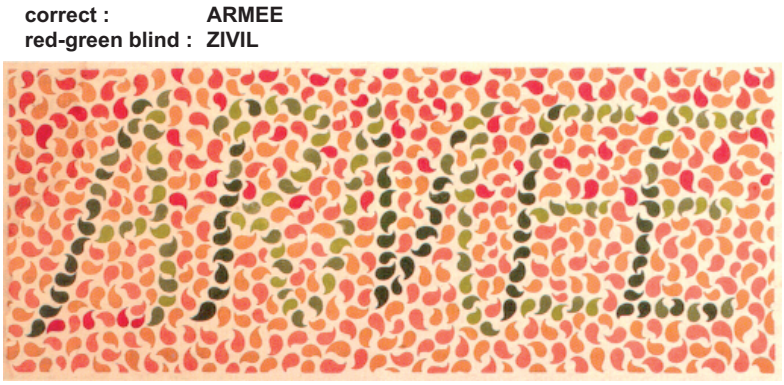

Figure 36-76: Demonstration of red–green blindness.

36.8.7 Spreading and Aging Effects

The optical performance of the human eye usually shows a statistical distribution and decreases with increasing age.

Figure 36-77 shows the ametropic distribution for spherical aberration over a large population [36-3]. It can be seen that a negative refraction error is more probable than a positive one. Figure 36-78 shows the corresponding diagram for the probability of astigmatism.

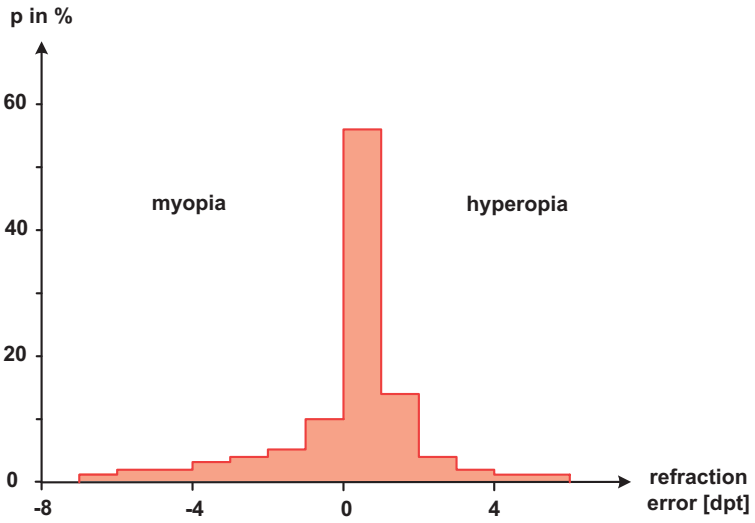

Figure 36-77: Probability distribution for the occurrence of spherical aberration.

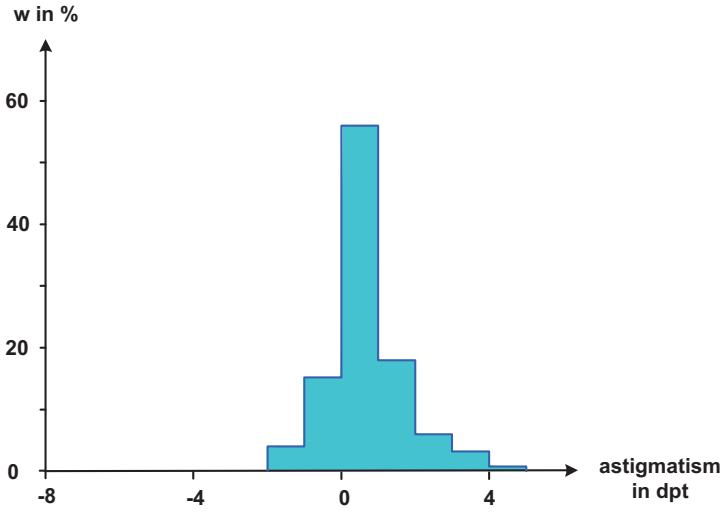

Figure 36-78: Probability distribution for the occurrence of astigmatism.

The ability of the human eye to accommodate changes during a lifetime and therefore older people usually require spectacles in order to observe close objects. This presbyopia effect occurs slightly earlier for females. The corresponding statistics can be seen in figure 36-79.

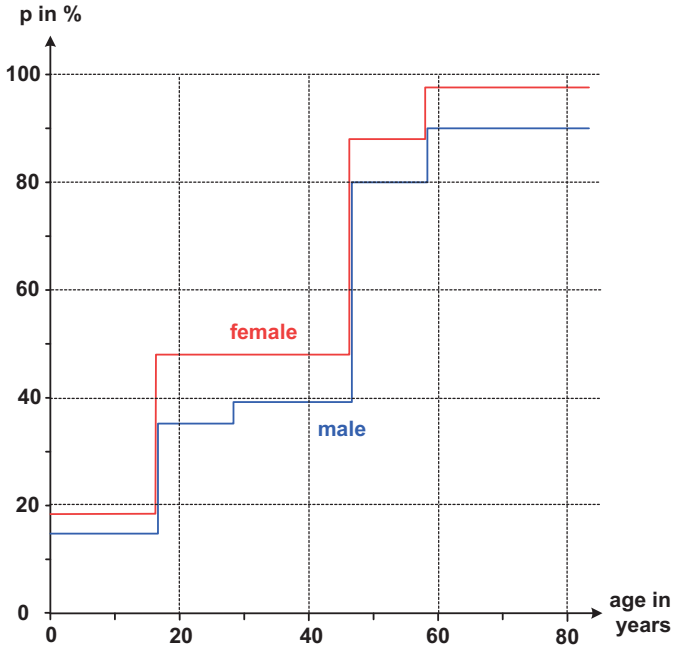

Figure 36-79: Probability for the use of refractive correction with age.

36.8.8
Cataract

An eye which has a cataract will suffer from strong scattering inside the eye lens due to cloudy effects. This causes low transparency and a reduction in the contrast and resolution. The only possible way of overcoming the problem in this case is the removal of the lens.

Figure 36-80 shows two pictures of a moderate and a dense cataract. In the extreme case, the eye is effectively blind.

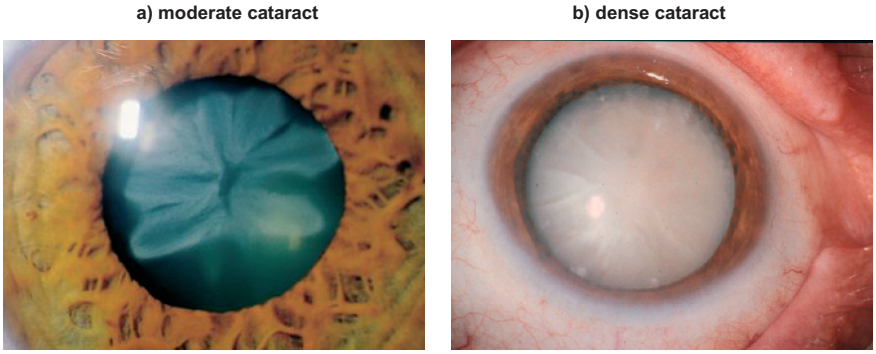

Figure 36-80: Eyes with cataracts.

36.9
Correction of Eye Aberrations

36.9.1
Correcting Refraction by Spectacles

Simple spectacles are the oldest and most widely used method to correct eyes with refractive defects. In the case of myopia, a negative lens helps to increase the total focal length. This case is shown in figure 36-81.

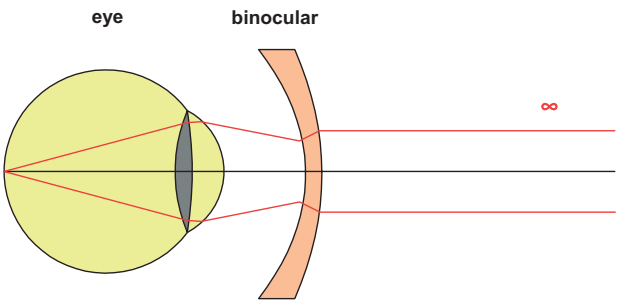

Figure 36-81: Correction of myopia by a spectacle lens with negative power.

The opposite case is hyperopia, where a spectacle lens with positive power is necessary to reduce the focal length of the complete system. This case is shown in figure 36-82.

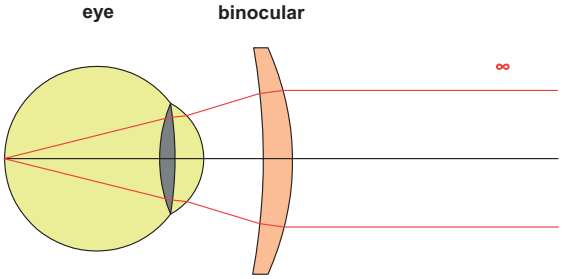

Figure 36-82: Correction of hyperopia by a spectacle lens with positive power.

Most ophthalmic lenses have a meniscus shape with the concave side oriented towards the eye. If the optometrist indicates that spherical correction is required, only power correction is needed. A real correction of higher aberration orders, such as spherical aberration is possible, but not usual. The tolerance of the power correction of an ametropic eye is typically 0.06 dpt.

For a correct adaptation of a spectacle lens, there are several aspects which must be considered. These are as follows:

1. Centering both lenses at the correct interpupillary distance.
2. Adjusting the height position of the lens for a correctly centered passage through the axis of the eye.
3. Obtaining the correct distance of the lenses form the cornea. Typically, a distance of 14 mm is chosen.
4. Finding the correct tilt of the lenses for near distances to obtain a comfortable reading position.

For the correct determination of ophthalmic lenses, the following terms for characterizing the axial powers of the lens are used.

1. The surface powers of the radii of curvature for the front surface with index 1 and the rear surface towards the eye with index 2 are

$$\breve{o}_1 = \frac{n-1}{r_1} \quad , \quad \breve{o}_2 = -\frac{n-1}{r_2} \, , \tag{36-30}$$

where n is the refractive index of the glass.

2. The equivalent power is the overall power of the lens

$$\breve{o}_e = \breve{o}_1 + \breve{o}_2 - \frac{t}{n} \cdot \breve{o}_1 \cdot \breve{o}_2 \, , \tag{36-31}$$

which results from the simple paraxial formula for the power of two lenses at a distance t.

3. The back vertex power of the lens with thickness t is defined as the refractive power as it is effective for a location reference at the back surface. It is given by

$$\breve{o}'_v = \frac{\breve{o}_1}{1 - \frac{t}{n} \cdot \breve{o}_1} + \breve{o}_2 = \frac{\breve{o}_e}{1 - \frac{t}{n} \cdot \breve{o}_1} \tag{36-32}$$

and obtained easily, if the reference of the focal length is changed form the principal plane to the back vertex plane. Since the principal planes are not measurable directly, the term $\breve{o}'_v$ is easier to use. It corresponds to the radius of curvature of the bent outgoing wave for an incoming plane wave.

4. All the equations so far are concerned with a far point or an object at infinity. If the lens must correct for an object at a finite distance s, by using the lens-makers' formula, this case can be obtained by

$$\breve{o}'_v = \breve{o}_2 + \frac{\breve{o}_1 + 1/s}{1 - \frac{t}{n} \cdot (\breve{o}_1 + 1/s)} = \breve{o}'_{v\infty} + \frac{m^2 \cdot \breve{o}_1}{1 - \frac{t}{n} m \breve{o}_1} . \tag{36-33}$$

The last expression indicates that a refractive power must be added to the relaxed case in order to design a suitable lens for a finite object distance.

Figure 36-83 shows the geometry of the eye with a spectacle lens. The distance of the glass from the cornea vertex is denoted by a. The distance between the lens and the pupil plane is denoted by p.

In practice, the choice of the thickness t of the lens is optimized by being of light weight but having a thicker edge, which is not too small. The greatest problem concerns the thickness, when designing positive glasses.

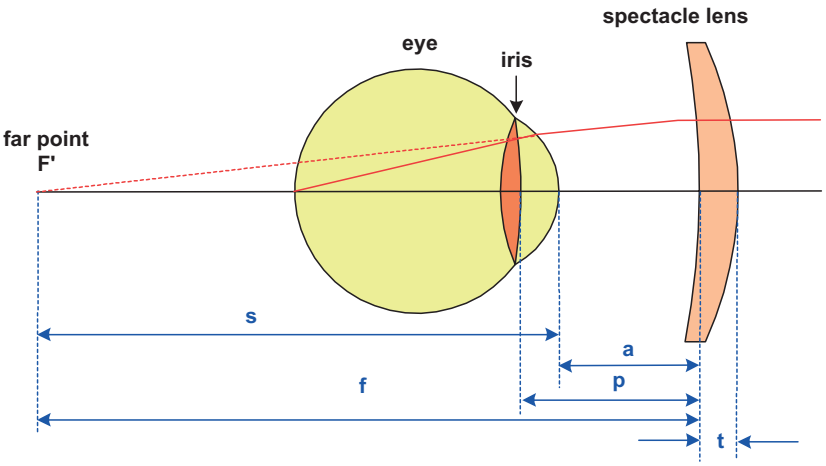

Figure 36-83: Correction of a refraction defect by a spectacle lens.

An ophthalmic lens changes the magnification of the retinal image. The equation

$$m = \frac{1}{1 - p \cdot \tilde{\sigma}} \tag{36-34}$$

gives the magnitude of this effect, where $\tilde{\sigma}$ is the desired correction of the refractive power. Figure 36-84 shows the influence of the refractive power on the magnification for the usual distance of $a = 14$ mm, corresponding to $p = 17$ mm.

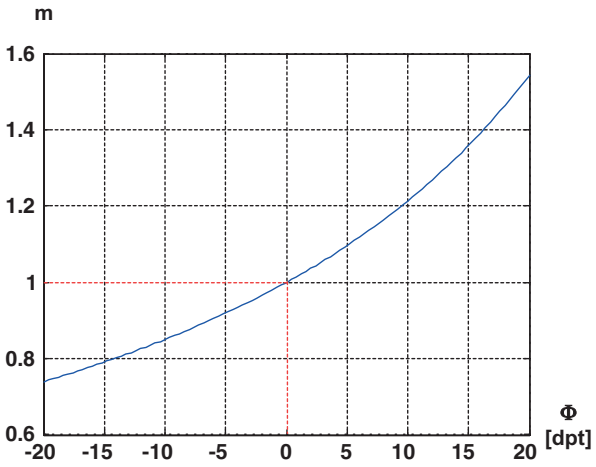

Figure 36-84: Change in the magnification by the correction of a refraction defect with a spectacle lens.

If the binoculars are not centered relative to the axis of the eye, a prismatic effect is produced. If a is the distance of the back vertex of the glass to the eye and S'_∞ is the back vertex power of the lens for relaxed vision, according the rule of Prentice, the deviation of the angle due to the decentration c of the glass is given by

$$\tilde{\omega} = c \cdot \frac{S'_\infty}{1 - a \cdot S_\infty} \tag{36-35}$$

which results from the simple approach of the declination angle of a dispersing prism.

36.9.2 Binoculars with Corrected Oblique Astigmatism

Usually the eye rotates when a moving object is observed. The brain tries to fix the object detail in the fovea in order to obtain the best possible resolution. The rotation of the eye around the rotation point causes different heights and angles for the axis bundle of the eye through the spectacle lens. This geometry is illustrated in figure 36-85.

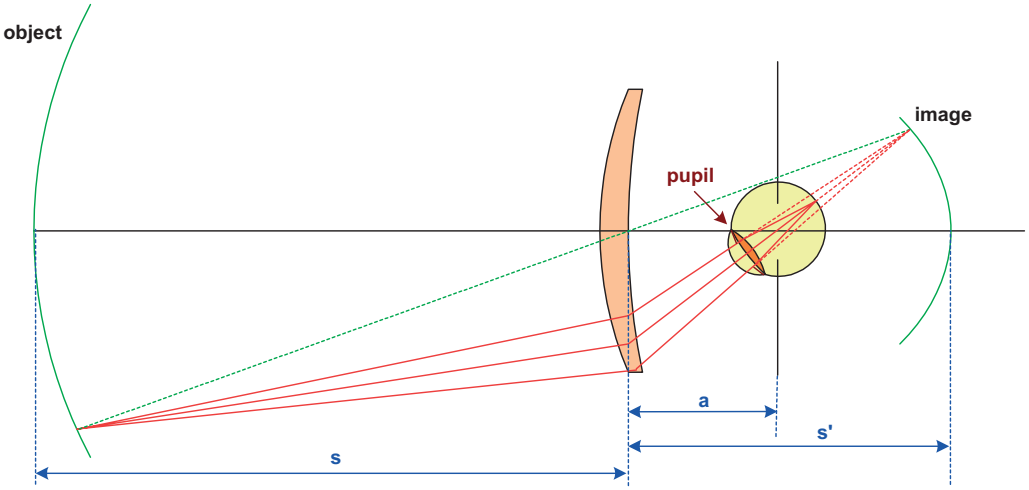

Figure 36-85: Geometry of an eye with a correcting spectacle lens and a rotating eye-ball.

If the eye is rotated, field dependent aberrations will occur. These are lateral color, distortion and curvature of field, which cannot, in principle, be removed by the two surfaces. Lenses with positive refractive power show a pincushion distortion, while negative lenses have a barrel-type distortion. Furthermore, astigmatism is caused by the oblique passage of the rays in the field. This type of aberration can be corrected under certain circumstances by the bending of the lens.

According to the Coddington equations, for the refractive power in the sagittal cross-section we have

$$\frac{1}{s} = \frac{n\cos i'_1 - \cos i_1}{r_1} + \frac{n\cos i'_2 - \cos i_2}{r_2} \tag{36-36}$$

and analogously for the tangential case

$$\frac{1}{t} = \left(\frac{n\cos i'_1 - \cos i_1}{r_1 \cdot \cos^2 i'_1} + \frac{n\cos i'_2 - \cos i_2}{r_2 \cdot \cos^2 i_2}\right) \cdot \frac{\cos^2 i_2}{\cos^2 i'_2}. \tag{36-37}$$

In the small-angle approach and the thin-lens approximation $d \approx 0$, one obtains the refractive powers of the front and the rear surface of the glass by

$$\ddot{o}_1 = \frac{n-1}{r_1} \quad , \quad \ddot{o}_2 = \frac{1-n}{r_2} \tag{36-38}$$

and the complete lens has the power

$$\ddot{o} = \ddot{o}_1 + \ddot{o}_2 . \tag{36-39}$$

Here r_1 and r_2 are the radii of curvature and n is the refractive index. If s is the intersection length of the object position and a is the distance from the back vertex

of the lens to the point of eye rotation, then from the above equations in third-order expansion, the following condition for vanishing astigmatism $s' = t'$ can be obtained

$$(n+2)\cdot \breve{o}_2^{\,2} + \left[2(n^2-1)\left(\frac{1}{a}-\frac{1}{s}\right) - (n+2)\breve{o}\right]\cdot \breve{o}_2 + \left[\left(n\breve{o} - \frac{2(n-1)}{a}\right)\cdot\left(\frac{1-n^2}{s}+\breve{o}\right) + \frac{n(n-1)^2}{a^2}\right] = 0\,. \qquad (36-40)$$

This is the equation of an ellipse, which is named after Tscherning. If the lens of the spectacle glass is curved, the distribution of the refractive power between the front and the rear surface will change. If the size of $\breve{o}$ as the necessary correction of the refraction is fixed, there are two possible solutions for a spectacle glass without astigmatism. The distance from the glass to the eye influences the solution indirectly due to the size of the distance a. It should be mentioned that this anastigmatic solution is only valid in third order. The condition of zero astigmatism is valid for all image field sizes y. An example is shown in figure 36-86 with parameters $a = 28.5$ mm and $n = 1.525$ and the object in infinity.

The two solutions are named after their inventors Ostwald and Wollaston. The Wollaston solution has a strong curvature of the lens, but has the advantage of a weak dependence of the solution on the desired object distance s. This is shown in figure 36-87. The case of the Ostwald solution has the advantage of a small curvature, but has a strong dependence on the object distance. For extreme values of the necessary refractive power $\breve{o}$, there is no solution of the quadratic equation (36-40), an astigmatism-free glass does not exist. This case happens approximately for $\breve{o} > 7$ dpt and for $\breve{o} < -22$ dpt. In these cases, only a curvature with minimal astigmatism can be chosen, which is given by the equation [36-28]

$$\breve{o}_2 = \frac{\breve{o}}{2} - \frac{n^2-1}{n+2}\cdot\left(\frac{1}{s}+\frac{1}{a}\right). \qquad (36\text{-}41)$$

The location of these solutions is also indicated in figure 36-87 by straight lines.

If for practical reasons, the curvature is reduced in order to ensure comfort during the wearing of the spectacles, there will be a remaining astigmatism. Figure 36-88 shows the residual astigmatism together with the astigmatism-free solution lines.

The same consideration as for spherical eye-glasses can be made in the practical requirements regarding thickness, finite field of view, aspherical surfaces and varying stop position. In this case, the solution curves become more complicated and can be solved only numerically [36-29].

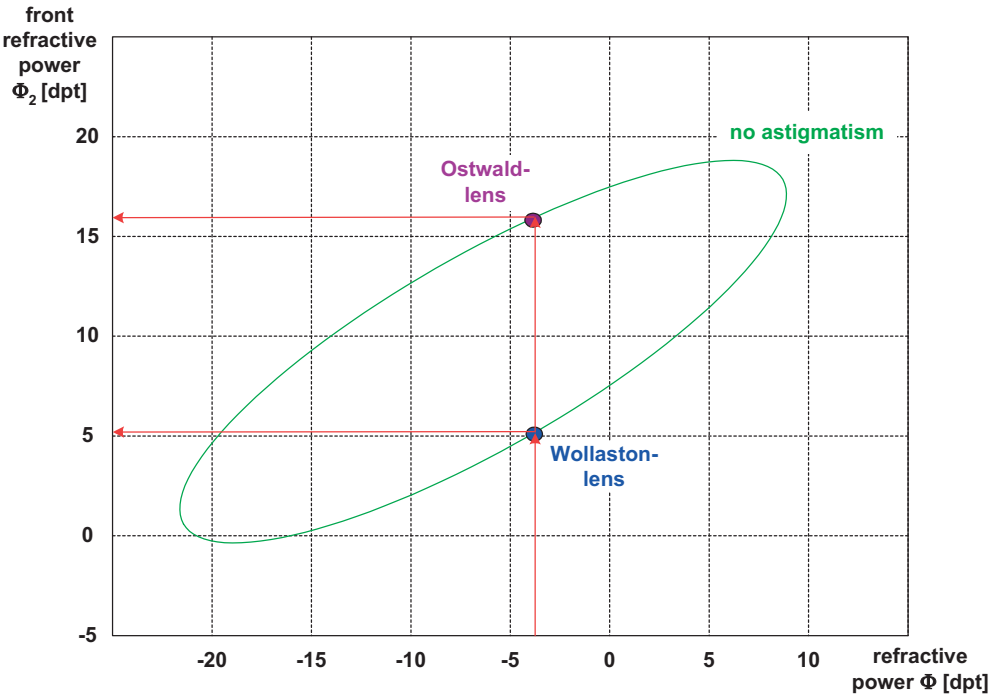

Figure 36-86: Solutions for the power distribution with corrected astigmatism.

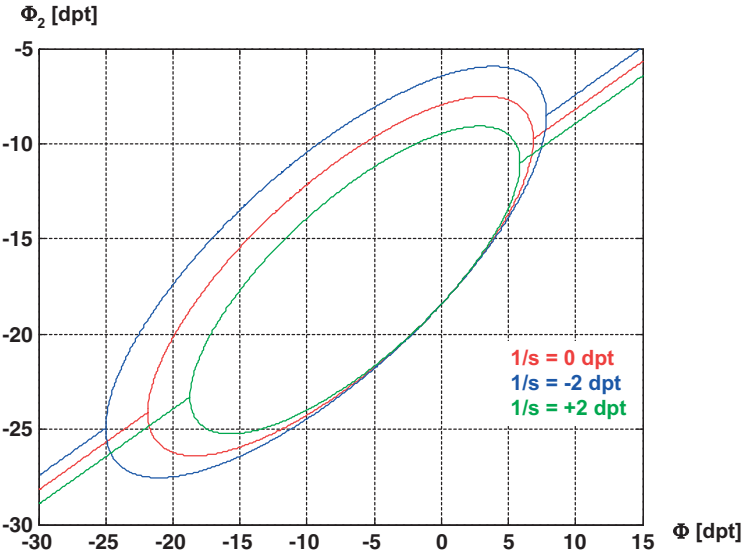

Figure 36-87: Solutions for the power distribution with corrected astigmatism for three different values of the object distance *s*.

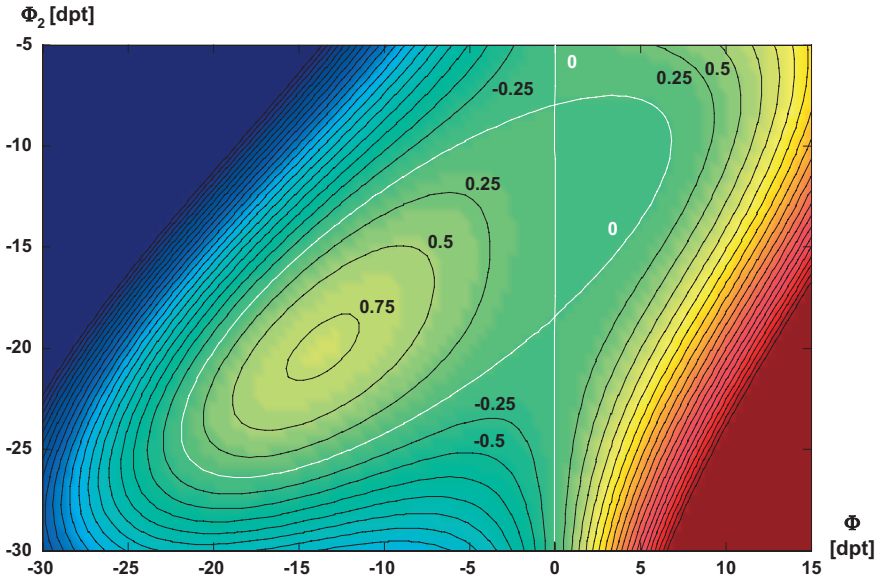

Figure 36-88: Values of the residual astigmatism for all possible values of the curvature.

36.9.3 More Complicated Spectacle Shapes

In reality, more complicated requirements are often needed to correct for the combined defects of an eye. The surfaces must be toric to correct astigmatism or aspheric to correct defects of higher order. Usually this reduces the field of view considerably.

One particular requirement is a combination of different corrections in different parts of the lens. This type of spectacle lens uses free-formed surfaces to guarantee smooth transitions between the different parts. One important case, for example, is a far-sight vision in the upper zone and a near-sight vision in the lower part of the lens.

Figure 36-89 shows the refractive power of this type of spectacle lens for illustration. Usually it is not possible to correct for astigmatism and the transition zones as well. This means that there are regions of the glass which are not usable and do not permit good vision.

To avoid these large unusable regions of the lens, it is possible to separate defined areas using different corrections. For example, figure 36-90 shows a spectacle lens with an inserted part for near vision. The problem with this kind of lenses is a sharp step at the boundary of the areas. This kink in the surface slope causes a jump in the field of view. This is illustrated in the figure too.

If the axes of each of the eyes are not aligned, binocular vision can be disturbed. In this case a prismatic correction can help to align them. This can be done using regular spectacle glass, which shows a lateral offset. The optical axes of the spectacle lenses have a distance which is different from the interpupillary distance in this case.

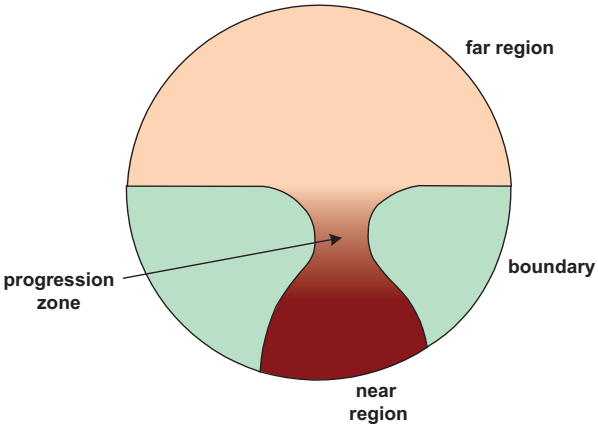

Figure 36-89: Regions of a free-formed binocular glass.

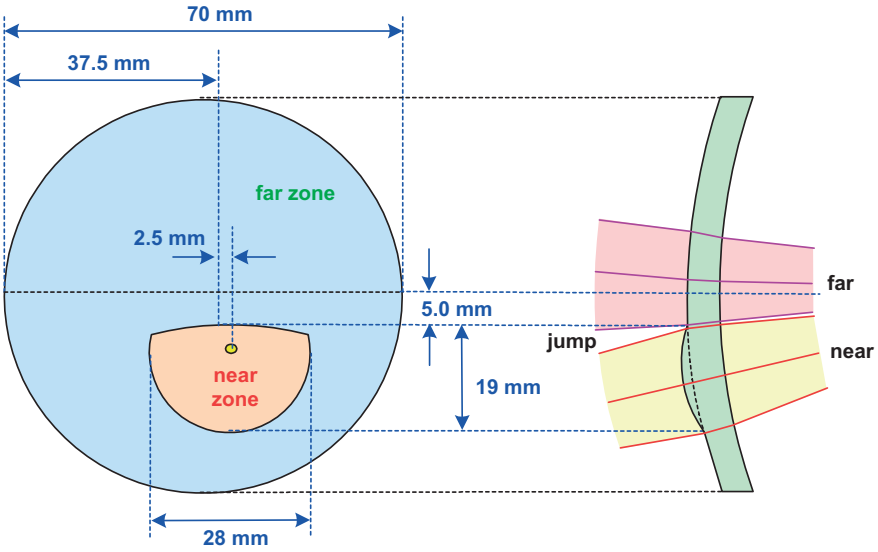

Figure 36-90: Ophthalmic lens with two correction sections.

36.9.4
Contact Lenses

Contact lenses are another means used to correct human vision. In contrast to conventional spactacles, contact lenses are located directly on to the cornea. In reality, a small tear film is generated by the eye and lies between the plastic lens and the eye itself. Figure 36-91 shows an eye with a contact lens.

There are two different types of contact lenses. In the first kind, the size of the glass diameter is smaller than the cornea and only the smaller inner region is

included in the correction. In the second case, the diameter is larger than the cornea and the contact glass is also fitted to the outer zones, which are not optically transparent. These lenses, which are of the sclera type, are more secure.

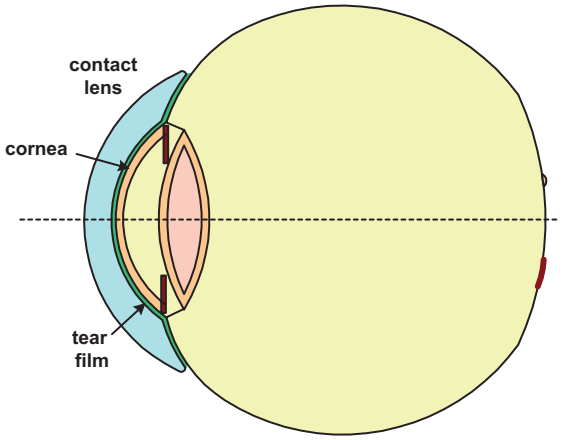

Figure 36-91: Eye with contact lens.

Contact lenses are usually made of plastics with a refractive index of approximately $n = 1.44–1.49$. They rest on a thin tear film, which acts as a lens, if the radii are not perfectly matched. It is absolutely necessary, for the material of the contact lens to be biocompatible and remain stable in wet surroundings.

If contact lenses are used for the correction of eye defects, there are some fundamental differences in comparison with the use of spectacle lenses.

1. The lenses are in direct contact with the cornea, therefore there is almost no additional distance between the refractive power of the cornea and the contact lens.
2. The inner radius of curvature must be adapted to the cornea radius. Therefore there is only one degree of freedom to correct the refractive defect. If astigmatism must be corrected, this can be done very easily by means of a toric surface.
3. The contact lens follows the movement of the eye. Therefore, there are no problems with oblique astigmatism for finite field sizes.
4. If the contact lens is made of a hard material, the shape remains constant and the topology of the gap between the glass and the cornea is filled with tear liquid. This helps to compensate for astigmatic shapes of the cornea and a corrugated structure of the cornea surface. If the difference in the radii is too large and the tear gap is too wide, problems occur because the contact lens can be easily lost.
5. If the refractive astigmatic difference to be corrected is too large, the contact lens will be of an uncomfortable shape and thickness. Problems with the weight occur and the astigmatism at the outer surface is not negligible.

Contact lenses, which are set directly upon the cornea, are not only used to correct the vision of the eye, but also can be used for diagnostic purposes. If a contact lens is placed onto the eye, there is no total reflection for rays below larger incidence angles. Furthermore, the rotating position of the eye is fixed. These conditions are desirable for several observation modes in the ophthalmic diagnostic. There are some special types of contact lenses, which are used for diagnostic observations. For example, figure 36-92 shows a Goldman contact lens, which is used to view the corner of the anterior chamber of the eye [36-12].

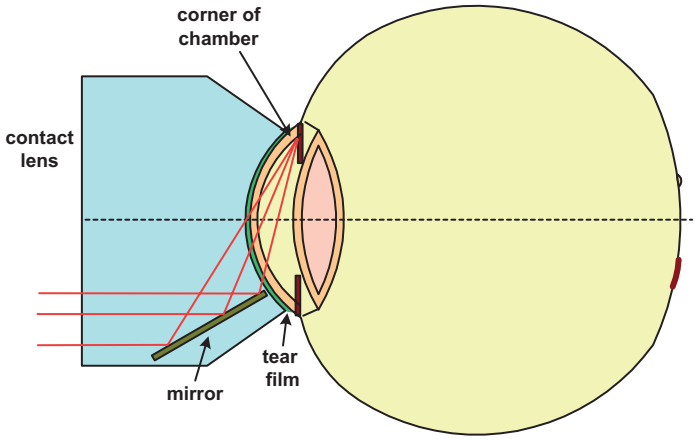

Figure 36-92: Eye with a Goldmann contact lens for observation of the anterior chamber or peripheral zones of the retina.

36.9.5 Intra Ocular Lenses

If an eye suffers from a dense cataract, the eye lens must be removed. There is no other way to restore vision and transparency in this case. The refractive power of the lens must now be changed to ensure correct vision. This can be done with an aphakic contact lens or by inserting a plastic lens inside the eye. These intra ocular lenses replace the natural eye lens at a fixed refractive power.

There are several possible ways to fix an artificial lens into the eye using small legs. The relative position of the lens and the iris diaphragm require different solutions in practice. The new lens can be inserted inside the intact residual capsule or in the anterior chamber or else in the posterior chamber position. The pre-calculation of the shape of the intra ocular lens is very important. It can be done, for example, with the help of the Navarro schematic eye [36-30].

36.9.6 Corneal Surgery

One possible method of correcting an eye with a wavefront deviation is direct surgery of the corneal front surface [36-27]. This shaping of the cornea topology is critical, and can only be done within a certain range of refractive aberration. Considering the remaining mechanical stability of the cornea, corrections in the region of 10 dpt myopia and 4 dpt hyperopia are possible. The shaping can be performed with an excimer laser ablation. One advantage of this procedure, which is sometimes called photorefractive keratectomy or LASIK is the possibility of ensuring a correct centration of the correction relative to the eye.

A disadvantage of this kind of correction is the non-reversible change in the eye. Usually the performance of the eye changes with age and therefore the correction cannot be done once for all time. Furthermore, the physical problems involved in changing the mechanical stabilization of the eye are critical.

In recent years a special version of the direct surgery of the cornea has been proposed. This technique uses ultra short laser pulses and removes some material from the cornea inside the finite thickness. This offers the advantage to leaving the surface undamaged.

Since the ablation of the corneal material is not reversible, the pre-calculation of the necessary correction has to be done with care. The correction can be predicted by a wavefront measurement of the eye or by using a schematic eye model [36-31]. The necessary correction can be determined by the simple relation

$$z(r) = \frac{W(r)}{n_c - 1}, \tag{36-42}$$

where $n_c = 1.377$ is the refractive index of the cornea and r is the transverse radius in the centered system of the eye. If R_I is the initial radius of curvature of the cornea and R_D the desired value, the equation

$$z(r) = \sqrt{R_I^2 - r^2} - R_I - \sqrt{R_D^2 - r^2} + R_D \tag{36-43}$$

is a first approximation for the geometry. In a more exact consideration, the difference in the height along the optical axis and normal to the surface must be distinguished. It is also possible to incorporate a non-spherical correction with this method [36-32]. In particular, keratoconus defects can only be treated in this way.

36.10 Literature

36-1 Y.-J. Liu, Z.-Q. Wang, L.-P. Song and G.-G. Mu, An anatomically accurate eye model with a shell-structure lens, Optik **116**, 241 (2005).

36-2 M. A. Rama, M. V. Perez, C. Bao, M. T. Flores-Arias and C. Gomez-Reino, Gradient-index crystalline lens model: A new method for determining the paraxial properties by axial and field rays, Opt. Commun. **249**, 595 (2005).

36-3 P. Mouroulis, Visual Instrumentation (McGraw Hill, New York, 1999).

36-4 A. Valberg, Light Vision Color (Wiley, Chichester, 2005).

36-5 M. Jüttner, Physiological Optics, in T. G. Brown (Ed.), The Optics Encyclopedia (Wiley-VCH, Berlin, 2004), Vol. 4, p. 2511.

36-6 G. A. Fry, The Eye and Vision, in: R. Kingslake, Applied Optics and Optical Engineering, Vol II, Chapter 1 (Academic Press, New York, 1965).

36-7 D. A. Atchison, A. Joblin and G. Smith, Influence of the Stiles–Crawford effect apodization on spatial visual performance, JOSA **A 15**, 2545 (1998).

36-8 A. Popiolek-Masajada and H. Kasprzak, Model of the optical system of the human eye during Accommodation, Ophthal. Physiol. Opt. **22**, 201 (2002).

36-9 G. Wyszecki and W. S. Stiles, Color Science (Wiley Interscience, New York, 2000).

36-10 S. G. de Groot and J. W. Gebhard, Pupil size as determined by adapting luminance, JOSA **42**, 492 (1952).

36-11 H. Goersch, Handbuch für Augenoptik (Maurer Verlag, Geislingen, 1992).

36-12 W. Lotmar, Theoretical eye model with asperics, JOSA **61**, 1522 (1971).

36-13 E. R. Villegas, L. Carretero and A. Fimia, Le Grand eye for the study of ocular chromatic aberration, Ophthal. Physiol. Opt. **16**, 528 (1996).

36-14 L. N. Thibos, M. Ye, X. Zhang and A. Bradley, The chromatic eye: a new reduced-eye model of ocular chromatic aberrations in humans, Appl. Opt. **31**, 3594 (1992).

36-15 Y. Le Grand and S. El Hage, Physiological Optics (Springer, Berlin, 1980).

36-16 B. H. Walker, Optical Engineering Fundamentals (McGraw Hill, New York, 1995).

36-17 G. Smith and D. A. Atchison, The Eye and Visual Optical Instruments (Cambridge University Press, Cambridge, 1997).

36-18 L. N. Thibos, M. Ye, X. Zhang and A. Bradley, Spherical aberration of the reduced schematic eye with elliptical refracting surface, Optom. Vision Sci. **74**, 548 (1997).

36-19 A. Kooijman, Light distribution of the retina of a wide-angle theoretical eye, JOSA **73**, 1544 (1983).

36-20 R. Navarro, J. Santamaria and J. Bescos, Accommodation-dependent model of the human eye with aspherics, JOSA **A 2**, 1273 (1985).

36-21 I. Escudero-Sanz and R. Navarro, Off-axis aberrations of a wide-angle schematic eye model, JOSA **A 16**, 1881 (1999).

36-22 H.-L- Liou and N. A. Brennan, Anatomically accurate, finite model eye for optical modeling, JOSA **A 14**, 1684 (1997).

36-23 P. Artal and R. Navarro, Monochromatic modulation transfer function of the human eye for different pupil diameters: an analytical expression, JOSA **A 11**, 246 (1994).

36-24 R. Navarro, P. Artal and D. R. Williams, Modulation transfer of the eye as a function of retinal eccentricity, JOSA **A 10**, 201 (1993).

36-25 P. G. Barten, Contrast Sensitivity of the Human Eye (SPIE Press, Bellingham, 1999).

36-26 M. S. Banks, A. B. Sekuler and S. J. Anderson, Peripheral spatial vision: limits imposed by optics, photoreceptors and receptor pooling, JOSA **A 8**, 1775 (1991).

36-27 J. F. Bille, C. F. Harner and F. H. Loesel (Eds.), Aberration-Free Refractive Surgery (Springer, Berlin, 2003).

36-28 H. Diepes and R. Blendowske, Optik und Technik der Brille (Optische Fachveröffentlichung GmbH, Heidelberg, 2005).

36-29 D. Malacara and Z. Malacara, Handbook of Optical Design (Marcel Dekker, New York, 2004).

36-30 E. R. Villegas, L. Carretero and A. Fimia, Optimum bending factor of intraocular lenses in pseudophakic eyes with high myopia, J. Mod. Opt. **44**, 941 (1997).

36-31 D. Cano, S. Barbero and S. Marcos, Comparison of real and computer-simulated outcomes of LASIK refractive surgery, JOSA **A 21**, 926 (2004).

36-32 J. R. Jimenez, R. G. Anera, L. Jimenez del Barco and L. Carretero, J. Mod. Opt. **47**, 1587 (2000).